UNIVERSITY OF CALIFORNIA

Los Angeles

Dark Matter as a Consequence of Catastrogenesis

A dissertation submitted in partial satisfaction of

the requirements for the degree

Doctor of Philosophy in Physics

by

Anna Simpson

2023

ABSTRACT OF THE DISSERTATION

Dark Matter as a Consequence of Catastrogenesis

by

Anna Simpson

Doctor of Philosophy in Physics

University of California, Los Angeles, 2023

Professor Graciela B. Gelmini, Co-Chair

Professor Alexander Kusenko, Co-Chair

Pseudo-Nambu Goldstone bosons (pNGBs), such as axion-like particles (ALPs), are a compelling candidate for cold dark matter. In the following thesis, I will discuss two separate ALP models of cold dark matter. In both models, a spontaneously bro-ken approximate global U(1) symmetry results in the formation of an interlocking network of 1- and 2-dimensional topological defects that is stable unless a bias term is present in the Lagrangian. The annihilation of this system results in the production of ALPs, gravitational waves, and possibly primordial black holes (PBHs). We dub this process "catastrogenesis", from the Greek word $\kappa\alpha\tau\alpha\sigma\tau\rho\phi\acute{\eta}$, meaning "annihilation." The first model I will discuss assumes that the ALPs are stable and therefore constitute some or all of the dark matter. In this case, if produced at temperatures below 100 eV gravitational waves could be detected by future cosmological probes for ALP masses anywhere between 10^{-16} and 10^{6} eV. The second possibility I discuss is that ALPs could decay into Standard Model products that then thermalize, in which case ALPs do not make up any of the dark matter. However, if PBHs are produced during the last stages of string-wall annihilation they could themselves constitute up to 100% of the dark matter. In addition, produced gravitational waves could be detectable by future interferometers.

The dissertation of Anna Simpson is approved.

Edward L. Wright

E. T. Tomboulis

Graciela B. Gelmini, Committee Co-Chair

Alexander Kusenko, Committee Co-Chair

University of California, Los Angeles 2023

To my high school counselor, who told me I couldn't do it.

Contents

List of Figures

VITA

2015-2019	B.S. (Physics), College of William and Mary.
2019-2023	Teaching Assistant, Physics Department, UCLA.

PUBLICATIONS

Gravitational waves from axion-like particle cosmic string wall networks. Physics Letters D, 2021.

Catastrogenesis: DM, GWs, and PBHs from ALP string-wall networks. Journal of Cosmology and Astroparticle Physics, 2023.

Primordial black hole dark matter from catastrogenesis with unstable pseudo-Goldstone bosons. Journal of Cosmology and Astroparticle Physics, 2023.

CHAPTER 1

Introduction

1.1 Dark Matter

It is widely accepted that the best explanation for several key results in astrophysics and cosmology is the presence of a significant amount of matter in the universe that is not directly detectable via photon detection. Despite strong evidence for its existence, none of the possible candidates for dark matter that have been put forward by theorists during the past few decades have been directly detected.

The observational evidence for dark matter is, at present, overwhelming. For example, the observed mass-to-light ratio in our solar neighborhood yields a cosmological matter density parameter $\Omega_m \simeq \rho_m/\rho_c$ of approximately 0.01 [Zwi33], where ρ_m is the energy density of matter, $\rho_c \simeq 10.5\ h^2$ keV/cm^3 is the critical density at present, and $h \simeq 0.7 \times 100$km/(Mpc sec^3) is the reduced Hubble parameter. On the

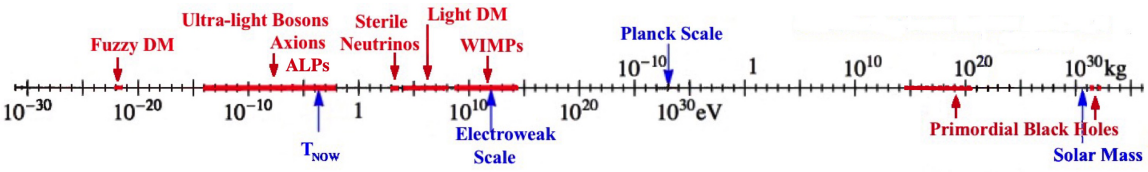

Figure 1.1: A summary of current dark matter candidates discussed in chapter 1.1 in the order of the mass of a single particle. The mass ranges of each variety of candidate are shown in red, and are compared to the present temperature of the photon background T_{now}, the electroweak scale, the Planck scale, and the solar mass $M_\odot$, which are labelled in blue.

scale of binaries and groups of galaxies, however, this number rises to 0.1, and on the scale of clusters this number becomes approximately 0.3 [FG79]. More recent results, such as from the PLANCK telescope [Agh20], have suggested that the density of baryonic matter is around 0.04, and therefore the density of dark matter is around 0.24. The presence of dark matter is required to resolve this discrepancy. One can also appeal to observations of velocity curves of galaxies [PSS96], which according to the virial theorem suggest a higher amount of matter present than is visible to optical telescopes. The X-ray emissions of hot gas from elliptical galaxies also provide evidence for dark matter [WBH13]. The rate of emission of X-rays from galaxies such as M87 [WBH13] and others of different morphological types [LM02] suggests that their visible mass makes up only 1% of the total mass present within their volumes.

Gravitational lensing also presents straightforward evidence for the existence of dark matter [TVW90]. The amount of lensing experienced by light at redshifts between 1 and 3 is a function of the mass density of the medium, and can be compared to the visible luminosity. Strong lensing, which involves the splitting of the image of a galaxy into multiple images, suggests that Ω_m is also on the order of 0.3-0.4 [BN92]. Meanwhile, weak lensing, which involves the distortion of the images of background galaxies, also predicts a value for Ω_m of around 0.3 on scales above that of galactic clusters [Mel99]. Weak lensing can also determine the amount of cosmic shear [WMR01] and can predict the existence of dark clusters, which do not have a significant amount of visible matter within them [UF00].

At supergalactic scales, Ω_m can also be estimated by observing the peculiar velocities of galaxies and clusters [DFB87]. These show that the total value of $\Omega = \Omega_m + \Omega_\Lambda$ is very close to 1, where Ω_Λ is the contribution to the density from dark energy, which could be due to a cosmological constant. Observations of the CMB

anisotropy have helped to differentiate these two values. Fitting to the observed power spectrum [Lee01, Net02, Hal02] has produced values of Ω_m and Ω_Λ consistent with a total density of 1 and a value for Ω_m of around 0.3 as well. These have also shown that the density of baryonic matter Ω_b is less than 0.05. The difference between this and the total Ω_m is an indicator of the presence of a contribution due to dark matter $\Omega_{DM} = \Omega_m - \Omega_b$ [Abr02].

In addition to the observational evidence, there is also good theoretical evidence for the existence of dark matter. For example, in the absence of inflation the Standard Model of cosmology requires that the dimensionless curvature of the universe $\hat{k} \simeq k/(R^2 T_0^2)$ where k is the curvature of the universe, T_0 is the photon temperature at present, and R is the scale factor, be constant and small, around the order of 10^{-58} [LR99]. This is known as the "curvature problem", and is resolved in inflationary models, which require that k approach 0 and therefore Ω approach 1 during inflation. Inflation also produces density perturbations that are adiabatic and lead to anisotropies in the CMB [Pre80, Zel72]. As indicated first by the COBE results [Wri92], the current magnitude of these anisotropies is too small for the formation of galaxies to have been produced by the presence of baryonic matter alone. Instead, the presence of dark matter at matter-radiation equality leads to small-scale perturbations which then grow into larger-scale perturbations [BES80] that can then lead to the growth of visible galaxies like we observe (and reside in!) today. A more comprehensive overview of the experimental evidence for dark matter can be found in [Oli03].

The full list of possible dark matter candidates is impossibly large. However, all theoretical candidates are subject to stringent theoretical and experimental constraints [M 08]. For example, we know based on experimental observations [Ber00] that the density of the dark matter in the universe $\Omega_{DM} h^2$ is about equal to 0.12,

and therefore any model of dark matter production should not produce an energy density greater than this. In addition, the dark matter present in the universe was "cold", i.e. non-relativistic when dwarf galaxy-size inhomogeneities were first encompassed by the horizon at a temperature of $\simeq 1$ keV. In cosmologies with cold dark matter (CDM), the structure of the universe grows from the "bottom up", i.e. from initial clumps smaller than dwarf galaxies which then coalesce into larger and larger structures [Pee82]. With "hot" dark matter, which is relativistic at $T \simeq 1$ keV, structure formation would happen from the top down, with superclusters forming first and then fragmenting off into smaller structures like the ones we see today [BST82]; HDM models are largely rejected by simulations of structure formation. Dark matter is said to be "warm" when it becomes nonrelativistic at $T \simeq 1$ keV; examples include sterile neutrinos [BPP82] and gravitinos [BST82]. Currently, CDM and WDM models are the ones in agreement with the large-scale structure of the universe [BD06]. Therefore, this thesis will focus exclusively on models of CDM.

There are many existing proposals for DM candidates, many of which are listed in [G 05] and [Lin19]. They can be classified by the upper or lower bound on the mass of a single object as shown in figure 1.1. The lightest candidates, at masses on the order of 10^{-20} eV, are referred to as fuzzy dark matter [HBG00]. These are CDM candidates which persist in the form of a cold Bose-Einstein condensate and which prevent the overabundance of dwarf galaxies predicted by other CDM models. Next are axions, which are pseudo-Goldstone bosons associated with the breaking of a U(1) global symmetry and which must be very light if they are also to be viable dark matter candidates (< 0.01 eV) [DB09]. The bounds on the coupling of axions to photons as a function of their mass are shown in figure 3.2. These include the QCD axion as well as other axion-like particles known as ALPs.

At higher masses are sterile neutrinos [S 93b], whose mass is expected to range

from 1-10 keV. These are particles that behave like Standard Model neutrinos but are not coupled with it through weak interactions. These could include right-handed Standard Model neutrinos as well as other, similar particles whose mass is larger than that of left-handed neutrinos due to the breaking of a global symmetry such as flavor. Another proposal is light scalar dark matter [LW77], which could be non-interacting or could be associated with e.g. the mass hierarchy between different flavors in the Standard Model [FN79]. The mass range of these particles is extensive depending on their mechanism of production, but most candidates fall between 10 keV and 100 MeV.

Sitting within three orders of magnitude on either side of the electroweak scale, i.e. 1 TeV, are weakly interacting massive particles, also known as WIMPs. Per the name, these particles interact with the Standard Model solely via gravity and another force weaker than the weak force. These are often produced in supersymmetric theories; SUSY WIMP candidates include neutralinos, sneutrinos [T 94], gravitinos [J 03], and axinos [S 93a].

In addition to fundamental particles, there is also the possibility of the production of light primordial black holes (PBHs), which are a hypothetical variety of black hole formed by the gravitational collapse of large stars in the early universe via processes such as an early phase transition. These were first proposed by Zel'dovich and Novikov in 1966 [ZN66], Hawking in 1971 [Haw71], and Carr and Hawking in 1974 [Haw74a], and could explain the existence of dark matter [ZN66, Haw71, Haw74a, Car75, CKS20, CK22]. The masses of viable PBH candidates range from 10^{15} to 10^{20} kg as well as around the order of a single solar mass. The viability of PBHs as dark matter candidates is supported by the fact that the DM has not been observed to interact with matter in any other way except gravitationally [BHS05, DBD17]. DM PBHs should also evaporate slowly enough as

to survive until the present day [CKS10, Haw74b, Haw75, BC19b, DG19, CMP21]. They must also avoid current constraints from microlensing [Tis07, Nii19b, Nii19a] as well as numerous other bounds collected in e.g. [Kav20]. As indicated above, the window of PBH masses for which they could constitute all of the DM is between 10^{-16} and 10^{-10} $M_{\odot}$, i.e. roughly the mass of a typical asteroid. A necessarily incomplete list of proposed formation scenarios for PBHs in the asteroid-mass range includes density perturbations in the early universe [Car75, Yok95, GLW96, BT18] , bubble collisions [HMS82, LV20], the collapse of cosmic strings [Haw89], scalar field dynamics [KMZ85, CK17], long-range interactions [FK21], and the collapse of domain walls [GVZ16, DGV17] or vacuum bubbles [DV17, KSS20] in multi-field inflationary scenarios.

Dark matter, as indicated by observations, is electromagnetically transparent, i.e. any charged dark matter candidate should have a charge small enough that it remains invisible to current optical searches. In addition, the presence of dark matter should also be consistent with the relative abundances of elements produced during Big Bang nucleosynthesis. In particular, structures such as topological defects could survive until recombination; if so, their contribution to the number of neutrino degrees of freedom N_{eff} should be less than current experimental observations, which predict a value of ΔN_{eff} of less than 0.5 [Agh20]. Other limits include stellar evolution [Raf99], self-interaction constraints, bounds from direct detection, constraints from gamma-ray astrophysics, and model-dependent astrophysical bounds, all of which are discussed in much greater detail in [M 08]. Presently undetectable theoretical signatures from dark matter can also guide the direction of future experiments and observations. More details can be found in [Lin19].

1.2 Nambu-Goldstone Bosons

The focus of this thesis is on models of axion-like particles, or ALPs, which are a variety of pseudo Nambu-Goldstone boson (pNGB). In general, Nambu-Goldstone bosons (NGBs) are massless bosons that are associated with the spontaneously broken global symmetry of a theory at some given energy scale. To illustrate, consider a complex scalar field ϕ whose Lagrangian is invariant under a global U(1) symmetry. In 3+1 dimensions the most general renormalizable Lagrangian for this field contains terms proportional to $|\partial\phi|^2$ and $|\phi|^n$ where $n \leq 4$. For illustrative purposes, we will focus on the case where only even-numbered terms show up. The Lagrangian then becomes

$$\mathcal{L} = |\partial\phi|^2 - V(\phi) \tag{1.2.1}$$

where

$$V(\phi) = \frac{\lambda}{4}(|\phi|^2 - V^2)^2 \tag{1.2.2}$$

is the corresponding potential. Because ϕ is complex, we can write it as

$$\phi(x) = \rho(x)e^{i\theta(x)}. \tag{1.2.3}$$

In terms of the field amplitude $\rho(x)$ and the phase $\theta(x)$, the Lagrangian becomes

$$\mathcal{L} = \frac{1}{2}\partial_\mu\rho\partial^\mu\rho + \frac{1}{2}\rho^2\partial_\mu\theta\partial^\mu\theta - \frac{\lambda}{4}(\rho^2 - V^2)^2. \tag{1.2.4}$$

In general, this does not help us when it comes to calculating the dynamics of these fields. However, we notice that the potential we have constructed has a minimum at $\rho_{min} = V$. When the total mean energy of the field is low enough (for example, if the temperature of the vacuum is small) then the value of the field ρ will tend to remain in the neighborhood of V. We can expand the potential about this value to determine the dynamics near V, which is often referred to as the "true vacuum" (i.e. where the potential energy is at a global minimum). However, we also see that at this minimum the second term in equation (1.3.1) becomes

$$\mathcal{L}_{kin} = \frac{1}{2} V^2 \partial_\mu \theta \partial^\mu \theta, \tag{1.2.5}$$

which is the kinetic term of the Lagrangian of a massless particle $a = V\theta$. This is not a coincidence; in fact, Goldstone's theorem [Gol61] tells us that if the ground state (where the potential is minimized) is not invariant under a global symmetry of the Lagrangian, massless particles known as Nambu-Goldstone bosons (NGBs) will appear. In the U(1) example, the NGB in question is the field a. In general, one NGB will appear per generator of the spontaneously broken global symmetry. Quantum mechanically, this means that near the ground state the field ρ picks up an expectation value of $\langle \rho \rangle = V$. Note that regardless of which symmetry is broken ρ ought to be a scalar field, since a spinor or vector field having a vacuum expectation value would violate Lorentz invariance.

In many cases, the global symmetry of the Lagrangian is only approximate, i.e. it is explicitly broken at some smaller energy scale; this could be for various reasons, although we expect all global symmetries to be explicitly broken by quantum gravity at high enough energy scales regardless (see e.g. [GS89]). If this is the case, then the associated NGB will be massive. NGBs that are associated with a spontaneously

broken symmetry at a given energy scale that is then explicitly broken at a lower energy scale are known as pseudo-Nambu Goldstone bosons, or pNGBs for short.

Examples of U(1) pNGBs postulated in physics beyond the standard model (SM) are numerous. Famously, the axion is associated with a global U(1) symmetry that is then explicitly broken by the QCD phase transition [PQ77]. The original axion model was proposed to explain why the neutron electric dipole moment, and therefore the amount of CP violation in the quark sector of the SM, was so small [VS00, Wei78, Wil78]. The dipole moment is smaller than 10^{-26} e cm [Bak06], which implies that the θ-parameter in the QCD Lagrangian must be very small ($< 10^{-10}$), when it could in principle be of order 1. The solution to this problem, proposed by Roberto Peccei and Helen Quinn [PQ77], is to promote the θ parameter to a dynamical field a/f_a, whose dynamics then relax it to a small value. This field is known as the axion field a, and it is in fact a pNGB due to the associated U(1) symmetry being broken at the QCD energy scale $\Lambda \simeq 200$ MeV. The motivation for the existence of the axion is reviewed in more detail in [Bac21b] and [Hoo].

The original axion was rejected experimentally soon after it was proposed [DGN20a], leading to the development of so-called "invisible axion" models. These propose an axion that is much lighter than the original model due to symmetry breaking at a higher scale $V \gg \Lambda_{QCD}$ [Kim79a, SVZ80b, DFS81a, Zhi80b]. Invisible axions are also commonly referred to as QCD axions. These axions are referred to as "invisible" due to the weakness of the coupling between the axion and the SM, which is proportional to $1/V$. Examples of invisible axion models include the Kim-Shifman-Vainshtein-Zakharov (KSVZ) model and the Dine-Fischler-Srednicki-Zhitnisky (DFSZ) model. In KSVZ models, the PQ symmetry is broken by a quark pair with PQ charge, and the interactions between the axion and the SM do not happen at tree level [Kim79b, SVZ80a], while in DFSZ models the normal Higgs is replaced by two Higgs

doublets which carry PQ charge, and the resulting axion interacts with the SM at tree level [DFS81b, Zhi80a].

Majorons are another example of U(1) pNGBs. These are hypothetical bosons that accompany the violation of global U(1) lepton number [CMP81, SV82]. The Majoron mass is expected to come from gravitational interactions. Another set of pNGBs associated with an SM mass hierarchy are "familons" which result from the spontaneous breaking of the symmetry between each of the quark-lepton families in the SM (see e.g. [Wil82, Rei82, GNY83a]). In the case where this symmetry is only between the leptons, these particles are referred to as "flavons" [FN79]. The spontaneous breaking of flavor symmetry leads to the pronounced hierarchy between the masses of leptons and quarks of each successive generation, while the masses of the flavons and familons are once again expected to be generated by gravitational interactions.

An example of pNGBs known to exist in the SM are the pions, which are associated with the spontaneous breaking of the chiral flavor symmetries during the QCD phase transition, which happens at scales larger than the explicit breaking due to the quark masses [LMO47]. Other hypothetical pNGBs include familon models involving SU(2) [WZ79] and SU(3) symmetries [Chk80]. pNGBs also show up in theories outside of particle physics. Examples include theories of phonons [FK18], Cooper pairs in superconductors [BCS57], and magnons [Blo30].

U(1) pNGBs that are not coupled to QCD but behave similarly to the QCD axion are known as axion-like particles, or ALPs. When the spontaneous symmetry breaking (SSB) scale is much higher than the explicit breaking scale, these are viable DM candidates [JR10]. ALPs show up in models of cosmic strings [VS00] as well as in proposed solutions to the transparency of the universe to TeV photons [DRM07, DMP09]. They are associated with an approximate U(1) symmetry that is broken

into a discrete Z_N symmetry by effects that are expected to come from gravitational interactions. For more examples, see [SW06, ADD10, ABK10, DFK11, JR10].

The stability of heavy ALPs depends on their mass and on their couplings. ALPs with a coupling to photons are probed up to masses of several hundred MeV by beam-dump experiments [Ber85, Rio87, Dol17, Blu91, Ban20] and supernovae [JMR18, HS23, Luc20, CRV22a, Cap22, CRV22c, Dia23a], and neutron star mergers [Dia23b], while cosmological observations can reach up to $\sim$1 TeV for very small couplings [CR12, DHS21]. Colliders can exclude masses up to the TeV scale [Kna17, BNT17], though only for large couplings. (Note that this implies an open window for the high-quality QCD axion [HKL20].) Assuming that ALPs couple to leptons also leads to bounds from beam dumps [BNT17] and astrophysical observations [CRV22b, FMM22], although the parameter space is largely unconstrained above the GeV scale. Heavy majorons are similarly probed by cosmology [KSZ21], supernovae [FRV22], and laboratory searches [Ber18, Gou20, Brd20], which again leave ALPs of masses above 1 GeV largely unconstrained.

1.3 ALP Cosmology

The Lagrangian for a U(1) ALP should capture both SSB at a high energy scale V and explicit symmetry breaking at some lower scale v. In the case of the QCD axion, the explicit breaking is associated with a term that is a periodic function of $N\theta$, where θ is the phase of the complex scalar field and N is a model dependent parameter that determines the number of true vacua present in the theory. For example, in KSVZ models N is the number of fermions that carry QCD charge [SVZ80a]. In the case of ALPs, N is a parameter of our choosing, and we incorporate this phenomenon by introducing a term in the Lagrangian proportional to $\cos(N\theta)$.

Thus, the potential term in the Lagrangian for the field Φ whose phase $\theta = a/V$ is proportional to the ALP field a includes the terms (see e.g. [HKS10] and references therein)

$$\mathcal{L} \supset -\frac{\lambda}{4}(|\Phi|^2 - V^2)^2 - \frac{v^4}{2}(1 - \frac{|\Phi|}{V}\cos(N\theta)) \tag{1.3.1}$$

The sources of evidence for the existence of ALP dark matter we will focus on are cosmological. The cosmology of these simple models, in which an approximate U(1) symmetry is spontaneously broken, is surprisingly rich. To build a model of large-scale axion dynamics, we make the usual assumption that the universe is homogeneous and isotropic to all relevant scales. The most generic nonreducable metric that obeys these requirements is

$$ds^2 = dt^2 - R^2(t)d\vec{x}^2 \tag{1.3.2}$$

where s is the proper time, t is the cosmic time, and $R(t)$ is a time-dependent scale factor. Plugging this into the Einstein field equations gives the Friedmann equations for $R(t)$ [Fri79]. Assuming that there is no spatial curvature, these are

$$H^2(t) = \left(\frac{\dot{R}}{R}\right)^2 = \frac{8\pi G}{3}\rho + \frac{\Lambda}{3} \tag{1.3.3}$$

$$\frac{\ddot{R}}{R} = -\frac{4\pi G}{3}(\rho + 3P) + \frac{\Lambda}{3} \tag{1.3.4}$$

where ρ and P are the density and pressure of the matter and radiation in the universe, Λ is the cosmological constant, and $H(t) = \dot{R}/R$ is known as the Hubble parameter. During the early universe, the Λ term is negligible.

For any metric that is a solution to these equations, all lengths are scaled by a redshift factor $R(t)/R(t_0)$. To calculate this explicitly, we will assume that the universe is radiation-dominated (RD) during the timescales of interest, meaning that the dominant contribution to the Friedmann equations is due to the energy density of photons and relativistic particles, and that all other contributions can be ignored. From thermodynamics, we can derive the relations $P_{rad} = \rho_{rad}/3$ and

$$\rho_{rad}(T) = \frac{g_*(T)\pi^2}{30} T^4 \tag{1.3.5}$$

where $g_*(T)$ is the effective number of degrees of freedom of all relativistic particles at temperature T. Plugging this into our equations and setting the present scale factor $R(t_0) = 1$ gives the result that $R(t) \sim t^{1/2}$ and $H(t) = 1/(2t)$. We may also write the Hubble parameter as a function of temperature,

$$H(T) = \sqrt{\frac{8\pi^3 g_*(T)}{90}} \frac{T^2}{M_P} \tag{1.3.6}$$

where $M_P = 1/\sqrt{G}$ is known as the Planck mass. In natural units, $M_P = 1.22 \times 10^{19}$ GeV. In a RD universe, combining equations (1.3.3) and (1.3.5) as well as recognizing that the cosmological constant is negligible in the early universe and that $H(t) = 1/2t$ gives us a relationship between the temperature T and the cosmic time t, which is

$$T(t) = \left(\frac{45}{16\pi^3 G g_*(T)}\right)^{1/4} t^{-1/2} \ . \tag{1.3.7}$$

The U(1) symmetry of the first term in the potential in equation (1.3.1) is spontaneously broken at a temperature $T_b \simeq V$, after which different volumes corresponding to different correlation lengths will have different values of the phase θ. At this point, topological defects will form where a rotation of 2π around a point

in real space can be mapped to a phase rotation of 2π in the phase space of the field Φ [Kib76]. The centers of these loops become 1-dimensional topological defects known as cosmic strings. If the phase transition happens before inflation, then these inhomogeneities will be inflated away, and the entire universe will be at a single value of θ. This thesis focuses on the case where SSB happens post-inflation.

1.4 Cosmic Strings

The dynamics of the cosmic strings mentioned above very quickly approach a regime known as the "scaling regime" in which the length scale of the strings remains on the order of the horizon scale t. To illustrate why, we will follow the argument outlined in [VS00]. Dimensionally, we expect the energy density of the string network ρ_s to be $\rho_s = \mu/L^2$, where L is some characteristic length scale and μ is the mass per unit length of the strings. The energy in some volume V is just ρV. The main mechanism by which strings lose energy is through the formation of loops due to collisions with other strings. A string should collide once per characteristic length L it travels in a characteristic volume L^3, and therefore the rate of collision per unit time per unit volume is then L^{-4}. If the length scale of loops formed by string collisions is also approximately L, then the total amount of energy lost due to collisions per unit time in some volume V is then $\mu L V \times L^{-4}$. This plus the contribution due to redshift gives a rough expression for the rate of change of the total energy of the string network

$$\dot{E} \approx \frac{\dot{R}}{R} E - \frac{\mu V}{L^3}. \tag{1.4.1}$$

Meanwhile, because the string energy density $\rho_s \sim L^{-2}$ and quantities with dimensions of length L in an FRW metric should redshift as $L(t) = L_0 R/R_0$, the string

energy density redshifts as R^{-2}. Just as with equation (1.4.1), rate of change of the string energy density is due to this redshift along with energy loss due to decaying loops, i.e.

$$\dot{\rho}_s \approx -2\frac{\dot{R}}{R}\rho_s - \frac{\rho_s}{L}. \tag{1.4.2}$$

To see how quickly L approaches the horizon scale t, we define a new variable γ such that $L = \gamma t$. Plugging this into equation (1.4.2) and applying the assumption that the universe is RD gives

$$\frac{\dot{\gamma}}{\gamma} \approx -\frac{1}{2t}(1 - \gamma^{-1}). \tag{1.4.3}$$

This equation can actually be solved explicitly for $\gamma(t)$; the result is a solution that approaches 1 at a rate proportional to $t^{-3/2}$. In other words, a string network will approach the horizon scale within a time comparable to the Hubble time. Once it has reached the horizon scale, it is in the scaling regime.

For strings in the scaling regime, the energy density of the string network is about equal to $\xi\mu/t^2$, where ξ is the number of strings per horizon volume and can be found via simulations. The calculation of μ in terms of our given model parameters is discussed in full in [VS00], but we will still outline it here. Once symmetry breaking occurs, we know that the stable field solution is

$$\Phi(x) = Ve^{i\theta(x)}. \tag{1.4.4}$$

Furthermore, we know that for this configuration we expect $\theta(x) \approx n\phi$, where n is the winding number of the string. The explicit symmetry breaking part of the potential

is still small, so for a string with winding number 1 the energy of this solution is

$$E = \int d^3r |\vec{\nabla}\Phi|^2 = \int d^3r \frac{V^2}{r^2} \tag{1.4.5}$$

Finding the mass per unit length, then, is just a matter of integrating this over a plane normal to the string. To do so, we note that in any given plane there are ξ strings per unit area t^2, so our maximum cutoff length should be $r_{max} = t/\sqrt{\xi}$. Furthermore, our minimum cutoff length should be the Compton wavelength of the radial component of the field; choosing a scale such that the value of λ from equation (1.3.1) is 1, this is $r_{min} = (\sqrt{2}V)^{-1}$. Altogether, we find that

$$\mu \approx 2\pi V^2 \ln\left(\frac{\sqrt{2}tV}{\xi}\right). \tag{1.4.6}$$

1.5 Cosmic Walls Bounded by Strings

Let us now consider the effects of the explicit symmetry breaking. As mentioned previously, the broken U(1) symmetry is associated with a pNGB $a = V\theta$. The dynamics of this field at some given point in space $\vec{x}_0$ can be derived from the Lagrangian in equation (1.3.1); the associated Euler-Lagrange equation is

$$\ddot{a} - 3H\dot{a} + \frac{dV(a)}{da} = 0, \tag{1.5.1}$$

where H is the Hubble parameter and $V(a)$ is the second term in equation (1.3.1). The latter term becomes dynamically important when the field approaches the nearest minimum of the potential in field space. Close one of of these minima, we can

expand $V(a)$ for small changes in θ to find

$$\frac{v^4}{2}(1-\cos(N\theta) \approx \frac{v^4}{2}\frac{N^2V^2a^2}{2} \simeq \frac{1}{2}m_a^2a^2 \ . \tag{1.5.2}$$

In other words, the ALP picks up a mass

$$m_a = \frac{Nv^2}{\sqrt{2}V}. \tag{1.5.3}$$

In the case of the QCD axion, the axion mass is temperature-dependent due to couplings with the SM. We assume, however, that the couplings between the ALP field a and the SM are small enough that any temperature dependence may be neglected. The equation for the dynamics then becomes

$$\ddot{a} - 3H\dot{a} + m_a^2 a = 0. \tag{1.5.4}$$

The oscillatory term in this equation dominates over the damping term at a time $3H(t_w) = m_a$. In terms of our parameters, this happens at a time

$$t_w = 2.12 \text{ GeV}^{-1} \left(\frac{V}{NGeV}\right)\left(\frac{v}{GeV}\right)^{-2} \tag{1.5.5}$$

and temperature

$$T_w = 7.4 \times 10^8 \text{ GeV} \left(\frac{g_*(T_w)}{10}\right)^{-1/4}\left(\frac{V}{NGeV}\right)^{-1/2}\left(\frac{v}{GeV}\right). \tag{1.5.6}$$

After t_w, different regions of space reside in different vacua. The boundaries between these regions are occupied by structures called domain walls [VS00], which correspond to where values of the field Φ interpolate between different vacua. As

shown in figure 1.2, closed paths along which the field interpolates between each of the N different vacua in turn will also have a cosmic string in their center, and hence a total of N walls will attach to each string, forming a network of domain walls bounded by cosmic strings. The energy density of domain walls is equal to $\rho_w \simeq A\sigma/R$ where σ is the energy per unit area of the walls, A is a dimensionless, order 1 parameter known as the area parameter which can be found via numerical simulations, and R is the characteristic length scale of the walls.

We can determine how σ depends on our parameters by integrating the domain wall solution for $\theta(x)$ in the case where the approximate symmetry is U(1). The field equation for θ near one of the true vacua is [HKS13]

$$V^2 \partial_\mu \partial^\mu \theta + \frac{v^4}{2} N \sin(N\theta) = 0 \ . \tag{1.5.7}$$

The domain wall solution interpolates between two adjacent vacua and is symmetric along two spatial axes and stable over time. In this case, these conditions are satisfied by

$$\theta_w(z) = \frac{2\pi k}{N} + \frac{4}{N} \arctan(\exp(m_a z)) \tag{1.5.8}$$

where z is the axis normal to the domain wall, k is an integer ranging from 0 to $N-1$, and m_a is the mass of the ALP given in equation (1.5.3). The energy density per unit area of the wall σ is then given by

$$\sigma = \int_{-\infty}^{\infty} dz V^2 \left(\frac{d\theta}{dz}\right)^2 = \frac{8 m_a V^2}{N^2} = \frac{8 v^2 V}{N\sqrt{2}} \tag{1.5.9}$$

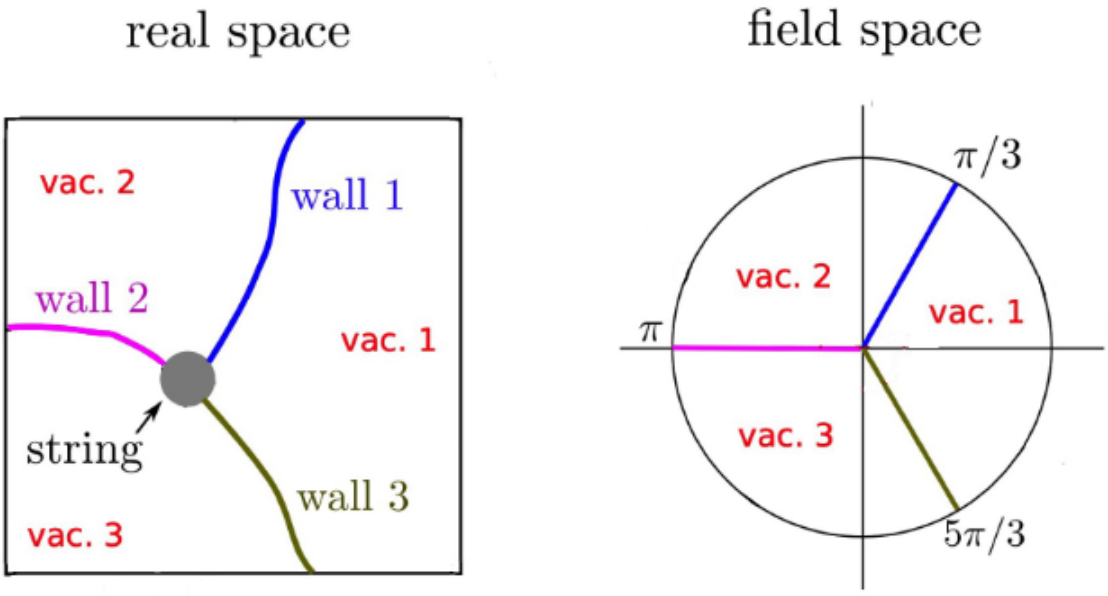

Figure 1.2: A diagram of the configuration of the field Φ after the formation of the string-wall network for $N = 3$. In real space, the energy density of the field is concentrated in domain walls at angles away from one another corresponding to the separations between the global minima of the potential, with cosmic strings lying at their intersections. Each of the individual domains occupy different vacua in field space, which have slightly different energy densities thanks to the presence of a bias term in the potential.

In general, then, the surface tension of a domain wall is

$$\sigma = f_\sigma v^2 V/N \tag{1.5.10}$$

where f_σ is a model-dependent constant. In this case, $f_\sigma \simeq 5.7$, while for the QCD axion $f_\sigma \simeq 6.5$ [HS85]. For all of the subsequent calculations where specific values are needed, we will take $N = 6$ and $f_\sigma \simeq N$.

As with strings, the length scale of the walls will quickly approach the cosmic time t. A convoluted wall with radius of curvature R will experience a force per unit area $F_T \simeq \sigma/R$. This will cause closed walls with $R \ll t$ to shrink and disappear

[VS00]. Numerical simulations done by e.g. [PRS89] have confirmed this, and have also shown that in general wall annihilation and recombination will sweep away any sub-horizon scale defects, leaving behind one horizon-scale wall per horizon volume. This means that we may therefore treat the walls as being in the scaling solution for the purpose of our calculations.

Once walls enter the scaling regime, their energy density becomes $\rho_w \simeq \sigma/t$. The energy density of an RD universe is given by equation (1.3.5). We may also use equation (1.3.7) to show that $\rho_{rad} \sim t^{-2}$. The wall energy density would exceed the radiation energy density at a time corresponding to

$$\rho_w \simeq \rho_{rad} \simeq \frac{\sigma A}{t} \simeq \frac{3}{32\pi G}\frac{1}{t^2} \ . \tag{1.5.11}$$

Explicitly, this is

$$t_{wd} \simeq \frac{3m_{Pl}^2}{4A\sigma} = 4.47 \times 10^{36}\ \text{GeV}^{-1}\frac{N}{f_\sigma A}\left(\frac{v}{GeV}\right)^{-2}\left(\frac{V}{GeV}\right)^{-1}, \tag{1.5.12}$$

where m_{Pl} is the reduced Planck constant. This corresponds to a temperature

$$T_{wd} = 3.61 \times 10^{-10}\ \text{GeV}\left(\frac{10}{g_*(T_{wd})}\right)^{1/4}\left(\frac{f_\sigma A}{N}\right)^{1/2}\left(\frac{V}{GeV}\right)^{1/2}\left(\frac{v}{GeV}\right) \tag{1.5.13}$$

and a Hubble parameter of

$$H(T_{wd}) = \frac{16\pi}{3}\frac{\sqrt{2}f_\sigma}{N^2}\left(\frac{V}{M_P}\right)^2 m_a \simeq 2.7 \times 10^{-6}\left(\frac{V}{10^{16}\ \text{GeV}}\right)^2 m_a. \tag{1.5.14}$$

The evolution of the resulting network of walls bounded by strings after this depends on N. If N=1 (i.e. if there is only one true vacuum in our model) then the string wall network will consist of "ribbons" which will annihilate when the surface tension of

the walls overcomes the tension of the strings [al12]. However, if $N > 1$, the resulting string-wall network is stable. As first noticed by Zel'dovich, Kobzarev, and Okun [ZKO74], the presence of a stable string wall network is cosmologically unacceptable if the discrete Z_N symmetry of the potential is exact. Per [ZKO74], we can solve equation (1.3.3) with $\rho \simeq \rho_w \simeq \sigma/R$ to find that in a wall-dominated universe $R(t) \sim t^2$. In other words, a string-wall network dominated universe will experience a period of power-law inflation inconsistent with cosmological observations.

To solve the problem of power-law inflation, Zel'dovich, Kobzarev, and Okun proposed making the Z_N symmetry approximate, such that one of the vacua has a lower energy density than the others [ZKO74]. To solve this issue in our case, we will use the Z_N breaking term first proposed by Pierre Sikivie in the context of the QCD axion [Sik82]

$$\mathcal{L}_{\text{bias}} = -\epsilon_b v^4 \frac{|\Phi|}{V} \cos(\theta - \delta) \tag{1.5.15}$$

where ϵ_b is a dimensionless constant, δ is the orientation of the bias term relative to the rest of the potential, and the energy scale of the explicit breaking is

$$V_{bias} \simeq \epsilon_b v^4 \ . \tag{1.5.16}$$

Once the resulting bias between the other vacua and the unique true vacuum becomes dynamically relevant, it drives the subsequent annihilation of the string-wall network [HKS11b].

The process of wall annihilation is further discussed in [GNY83b]. The difference in energy density between adjacent vacua exerts a pressure $P_V \simeq \epsilon_b v^4$ on the walls between them. We assume that this is initially much smaller than the surface tension

of the walls $P_T \simeq \sigma A/t$. P_T decreases over time until it becomes comparable with P_V, at which point the walls begin to annihilate. The time at which this happens is

$$t_{ann} \simeq \frac{\sigma}{V_{bias}} \simeq \frac{\sigma A}{\epsilon_b v^4} \simeq \frac{f_\sigma A V}{N \epsilon_b v^2} \tag{1.5.17}$$

After this, the volume pressure dominates, and the walls are accelerated away from regions where the field is in the true vacuum into regions of false vacuum. The vacuum energy released by this process drives the wall motion that leads to the annihilation of the domain walls. The corresponding temperature at which this happens is

$$T_{ann} = 1.08 \times 10^9 \text{ GeV } \epsilon_b^{1/2} \left(\frac{g_*(T_{ann})}{10}\right)^{-1/4} \left(\frac{f_\sigma A}{N}\right)^{-1/2} \left(\frac{V}{GeV}\right)^{-1/2} \left(\frac{v}{GeV}\right), \tag{1.5.18}$$

and the Hubble parameter at this time is

$$H(T_{ann}) = \frac{1}{2t_{ann}} \simeq \frac{V_{bias}}{2\sigma} \simeq \frac{\epsilon_b m_a}{\sqrt{2} f_\sigma} \ . \tag{1.5.19}$$

In addition to ALP production, the annihilation of the string-wall network leads to the production of gravitational waves and possibly primordial black holes [HKS13]. Constraints on the bias term in the QCD axion Lagrangian mean that these gravitational waves are not detectable by current searches. However, ALPs are not subject to these constraints, and therefore it is fruitful to investigate the possibility of the production of gravitational waves via the collapse of the string-wall network.

Notice that, in total, our model is governed by three independent parameters, which we can choose to be the scale of the SSB V, the mass of the axion m_a, and the scale of the bias term ϵ_b, or V, the scale of the explicit symmetry breaking v,

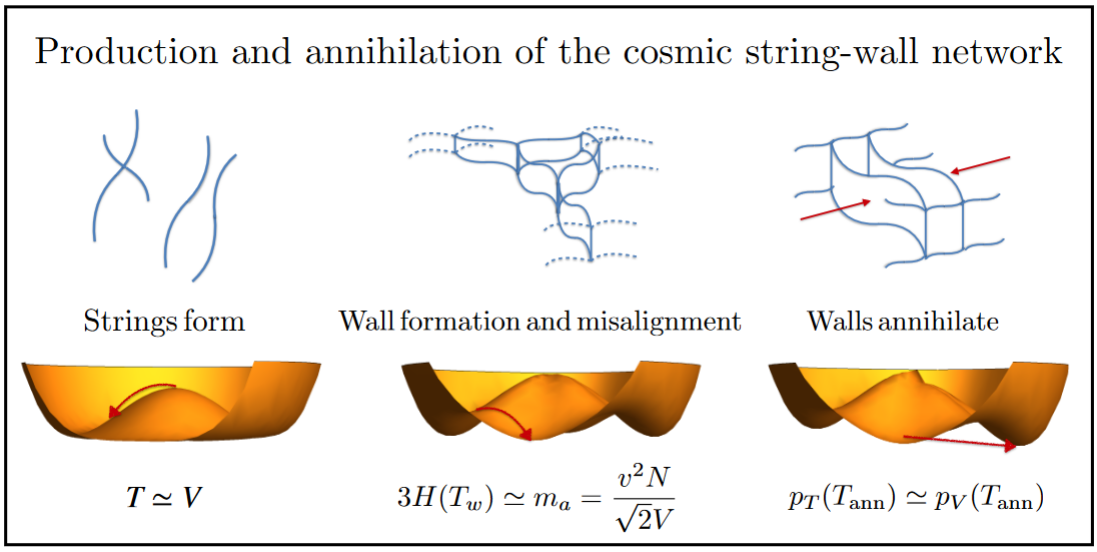

Figure 1.3: A graphical representation of the ALP cosmology we will be studying. When the temperature becomes of the order of the length scale of the symmetry breaking, the Kibble mechanism leads to the formation of cosmic strings. This is followed by the formation of domain walls connecting these strings together when the Hubble parameter is on the order of the mass of the axion, allowing for coherent oscillations and for the axion to pick up a mass. Finally, the string-wall network annihilates when the pressure from the bias term overcomes the tension of the domain walls, tearing them apart and leading to "catastrogenesis."

and ϵ_b. In addition, quantities related to the annihilation of the string-wall network such as those given in equations (1.5.17) and (1.5.18) only depend on the surface energy density of the walls σ and the scale of the bias V_{bias}, which are given in equations (1.5.10) and (1.5.16), respectively. Because we have assumed that interactions between ALPs and the SM are negligible, the constraints that remain on our model are those that come from its implications for the standard ΛCDM cosmology and other astrophysical phenomena, as well as due to the need for the model to be self-consistent.

1.6 Gravitational Waves

The existence of gravitational waves (GWs) was first discussed by Oliver Heaviside by analogy with electrodynamics [Hea93]. In 1905, Henri Poincaré also proposed their existence as a requirement of the validity of the Lorentz transformation [Poi07], and Albert Einstein showed that the Einstein field equations admit a wave solution that propagates at the speed of light [CGS16]. The first indirect observations of GWs were from the decay of the orbital periods of neutron star and black hole binary systems [Bon57, TM75], but they were not directly detected until 2016 via interferometry by the LIGO-VIRGO Collaborations [Abb16]. Since then they have been a fruitful probe into the physics of our universe as well as a new tool to test particle physics models [VS00, Mag07, Mag18, SS09, Bar19]. As I will show in this thesis, GWs that are produced by catastrogenesis are also an excellent probe into models of ALP DM candidates. Here in this thesis we will focus on stochastic GW backgrounds emitted by objects in the early universe, following [Mag01] and then [HKS10]. For a more complete review of the theory of GWs, see e.g. [Mag07] and [Mag18].

In general, particles in the early universe decouple from the primordial plasma when the interaction rate Γ that maintains equilibrium becomes smaller than the Hubble parameter $H(t)$, i.e.

$$\Gamma(T)/H(T) \ll 1. \tag{1.6.1}$$

For gravitons, the interaction in question is graviton-graviton four-point interactions, which are discussed in more detail in e.g. [ZBC09, Gio20]; the interaction rate can

be estimated without much effort as $\Gamma \sim T^5/M_P^4$. This means that for GWs,

$$\frac{\Gamma}{H} = \left(\frac{T}{M_P}\right)^3 \tag{1.6.2}$$

meaning that GWs decouple below the Planck scale $M_P \sim 10^{19}$ GeV. GWs produced below this temperature will therefore still encode all of the information about the conditions under which they were created, making them an excellent probe of the physics of the early universe.

We may characterize the intensity of a given stochastic GW background by its differential spectrum, which is equal to

$$\Omega_{gw}(f) = \frac{1}{\rho_c}\frac{d\rho_{gw}}{d\log f} \tag{1.6.3}$$

where ρ_{gw} is the energy density of the GWs in question, f is the frequency, and ρ_c is the critical density of the universe at present, which per equation (1.3.3) can be written as

$$\rho_c = \frac{3H_0^2}{8\pi G}. \tag{1.6.4}$$

where $H_0 = h_0 \times$ 100 km/sec-Mpc is the Hubble parameter at present. It is generally more convenient to calculate $h_0^2\Omega_{gw}(f)$ to avoid having to deal directly with this parameter; we refer to the quantity Ωh^2 as the density parameter.

To demonstrate how to calculate the quantity in equation (1.6.3) in practice, we will follow the discussion in [HKS10], which itself is derived from the calculations done in [Duf07]. Assuming the metric given in equation (1.3.2), any perturbation

$h_{ij}dx^i dx^j$ will induce a metric

$$ds^2 = dt^2 - R^2(t)(\delta_{ij} + h_{ij})dx^i dx^j \tag{1.6.5}$$

where h_{ij} obeys the conservation law $\partial_i h_{ij} = h^i_i = 0$. Plugging this ansatz into the Einstein field equations lets us obtain

$$\ddot{h}_{ij} + 3H\dot{h}_{ij} - \frac{\nabla^2}{R^2}h_{ij} = 16\pi G T^{TT}_{ij} \tag{1.6.6}$$

where T^{TT}_{ij} is the transverse traceless component of the stress energy tensor of the source of the GWs. If a source emits GWs within an interval $t_i \leq t \leq t_f$, then this equation can be solved using its Green's function, i.e.

$$\bar{h}_{ij}(\tau, \vec{k}) = A_{ij}(\vec{k})\sin[k(\tau - \tau_f)] + B_{ij}(\vec{k})\cos[k(\tau - \tau_f)] \tag{1.6.7}$$

where

$$A_{ij}(\vec{k}) = \frac{16\pi G}{k}\int_{\tau_i}^{\tau_f} d\tau' \cos|k(\tau_f - \tau')|a(\tau')T^{TT}_{ij}(\tau', \vec{k}),$$

$$B_{ij}(\vec{k}) = \frac{16\pi G}{k}\int_{\tau_i}^{\tau_f} d\tau' \sin|k(\tau_f - \tau')|a(\tau')T^{TT}_{ij}(\tau', \vec{k}), \tag{1.6.8}$$

τ is the conformal time defined by $d\tau = dt/R(t)$, $\vec{k}$ and k are the comoving momentum and its magnitude, respectively, and $\bar{h}_{ij} = R(t)h_{ij}$.

The GW energy density we are after is equal to the average of $\dot{h}_{ij}$ over all 3 spatial coordinates. Writing this out and then noting that the cross terms between $\bar{h}_{ij}$ and $\bar{h}'_{ij}$ vanish due to the requirement that h_{ij} be real as well as assuming that

$k/R_0 \gg H_0$ gives

$$\rho_{gw} = \frac{1}{32\pi G}\left\langle \dot{h}_{ij}(t,\vec{x})\dot{h}_{ij}(t,\vec{x})\right\rangle = \frac{1}{32\pi G R^4}\frac{1}{V_{com}}\int \frac{d^3k}{(2\pi)^3}\bar{h}'_{ij}(\tau,\vec{k})\bar{h}^{*}_{ij}{}' \tag{1.6.9}$$

where h'_{ij} is the derivative of h_{ij} with respect to the conformal time and $V_{com} \sim R^3$ is the comoving volume.

If necessary, we may calculate this explicitly by substituting equation (1.6.7) into the above expression. If we then substitute the resulting expression into equation (1.6.3), we find that

$$\Omega_{gw} = \left(\frac{g_*(T_0)}{g_*(T_i)}\right)^{1/3}\frac{\Omega_{rad}h^2}{\rho_{rad}(T_i)}\frac{Gk^3}{2\pi^2 V_{com}}I_k \tag{1.6.10}$$

where

$$I_k = \frac{R^4(t)V_{com}}{8\pi^2 G}\frac{d\rho_{gw}}{dk}\ , \tag{1.6.11}$$

$\Omega_{rad}h^2 = 4.15\times10^{-5}$ is the density parameter of radiation at present, and $\rho_{rad}(T_i)$ is the radiation energy density at the initial emission time t_i. Likewise, the frequency of emitted GWs at present is

$$f = \frac{k}{2\pi}\frac{R(t)}{R(t_0)} = \frac{k}{2\pi}\frac{g_*(T_0)}{g_*(T_i)}\frac{T_0}{T_i} \tag{1.6.12}$$

where we have used the method to calculate the redshift factor outlined in chapter 8.

To determine how the differential GW spectrum of a given source depends on k, we must then find the k-dependence of I_k; this is worked out for the string-wall network discussed in chapter 1.5 in chapter 9.

CHAPTER 2

Present Density of Stable ALPs

The formation and subsequent annihilation of the string-wall network produces cosmological relics in the form of ALPs, GWs, and possibly also PBHs. In this chapter, I will calculate the present energy density of ALPs in the case where they do not decay. There are three ways ALPs may be produced: via misalignment, emission from cosmic strings, and via catastrogenesis.

2.1 Production of ALPs via Misalignment

The first contribution to the present ALP density comes from the so-called misalignment mechanism. When the temperature of the universe reaches T_w and the ALP field begins to oscillate about the N vacua, different patches of the universe will initially be at phases $\theta_i = a_i/V$ that are displaced from the minima of the potential. Per [PWW83, AS83, DF83] the oscillations θ about the minima in these patches will produce an ALP energy density of

$$\rho_{mis} = \left\langle \frac{1}{2} m_a^2 V^2 \theta_i^2 \right\rangle = \frac{N^2 v^4}{4} \left\langle \theta^2 \right\rangle \tag{2.1.1}$$

where $\theta_i^2 = c_{anh}\pi^2/3$ is the naive average value of θ_i over the present horizon volume multiplied by an anharmonic coefficient $c_{anh} \simeq 2$ [Tur86, Lyt92, BHK08, OPR22].

At the present time, this results in an ALP energy density of

$$\Omega_a^{mis}h^2 = \left\langle \frac{1}{2}\theta_i^2 m_a^2 V^2 \left(\frac{R(T_w)}{R(t_0)}\right)^3 \frac{1}{\rho_c}h^2 \right\rangle \simeq 2.5\times 10^{-24}\left\langle \theta_i^2 \right\rangle \frac{V^2 m_a^{1/2}}{\mathrm{GeV}^2\mathrm{eV}^{1/2}} \frac{[g_*(T_w)]^{3/4}}{g_{s*}(T_w)} \tag{2.1.2}$$

where the redshift factor $R(T_w)/R(t_0)$ is taken from equation (8.0.4) in chapter 8.

2.2 Production of ALPs via Cosmic Strings

Once cosmic strings form, they will continuously emit ALPs until the formation of domain walls. Wall formation occurs when the mass of the ALPs becomes important, and thus at earlier times they may be treated as effectively massless. The majority of the energy lost by the strings contributes to the production of ALPs, which means that we may approximate the number density $dn_e(t)$ of massless ALPs emitted at time $t < t_w$ as

$$dn_e^{st}(t) \simeq -dt\left(\frac{d\rho_{st}(t)}{dt}\right)\frac{1}{\langle E_a\rangle} \tag{2.2.1}$$

where $\langle E_a\rangle$ is the average energy of a single ALP. Because the ALPs are relativistic, this should be equal to average momentum of a particle [HKS11b]

$$\langle E_a\rangle = \langle p\rangle = \frac{\langle p_{com}\rangle}{R(t)}\ . \tag{2.2.2}$$

Because the cosmic strings are in the scaling regime, the emission spectrum of the axions they emit should be peaked at $k \sim 2\pi/t$, which has also been confirmed via numerical simulations [HKS11b, DS89, YKY99]. Numerical simulations have also determined that the actual peak of the spectrum is at $k_{peak} \simeq \epsilon^{-1}2\pi/t$ where $\epsilon^{-1} \simeq 4$ is a dimensionless parameter that has been determined via numerical simulations.

Taking into account the redshift from the time of emission until the present, the number density of ALPs due to strings at present can be written as

$$n_a^{st}(t_0) \simeq -\int_{t_{st}}^{t_w} dt \left(\frac{R(t)}{R_0}\right)^3 \left(\frac{d\rho_{st}(t)}{dt}\right) \frac{t/4}{2\pi} \tag{2.2.3}$$

where t_{st} is the time at which strings first appear. We assume that $t_{st} \ll t_w$, and thus that the dominant contribution to this integral is due to the production of ALPs at the time of wall formation.

The resulting ALP energy density at present is $\rho_a^{st}(t_0) = m_a n_a^{st}(t_0)$. Taking $g_{s*}(T_0) = 3.93$ and $g_*(T_0) = 3.38$ to be the present values of the energy and entropy density degrees of freedom as well as using the result for the string energy density from equation (1.4.1), we find

$$\Omega_a^{st} \simeq 1 \times 10^{-23}\, \xi \left(\frac{V}{\text{GeV}}\right)^2 \left(\frac{m_a}{\text{eV}}\right)^{1/2} \frac{[g_*(T_w)]^{3/4}}{g_{s*}(T_w)} \ln\left(\frac{3V}{\sqrt{2\xi} m_a}\right) . \tag{2.2.4}$$

The value of ξ can be derived from numerical simulations; in our case, we assume that $\xi = 25$ [GHN21]. The contribution to the ALP density from strings always dominates over the contribution due to misalignment. However, there are large uncertainties in the evaluation of the ALP population due to strings [GHN21, OPR22] just as with the results for the QCD axion case [KSS15, KM17, BFH22].

If the bias parameter ϵ_b is sufficiently large, the contribution to the ALP density from strings alone can also dominate over the contribution due to string-wall annihilation given in equation (2.3.3) in chapter 2.3 (see the left panel of figure 2.1 for an example).

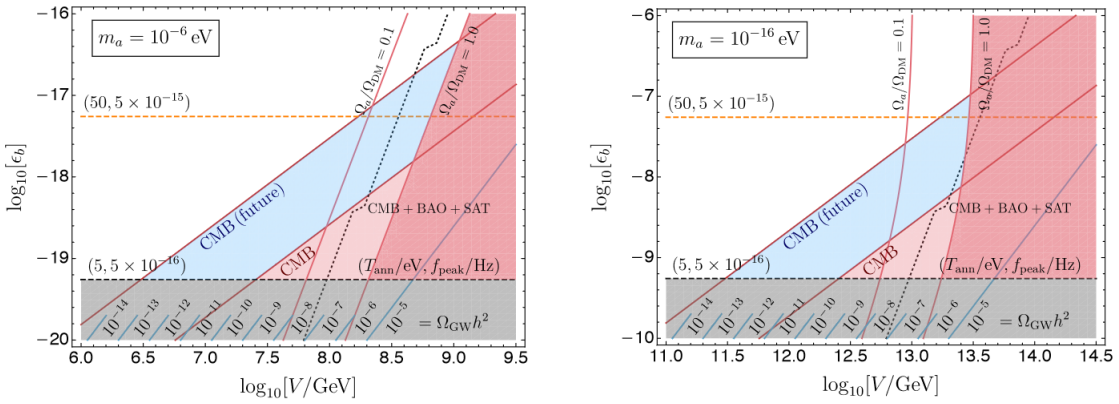

Figure 2.1: Regions of interest of the bias parameter ϵ_b as a function of the spontaneous symmetry breaking scale V, for ALP masses of $m_a = 10^{-6}$ eV in the left panel and $m_a = 10^{-16}$ eV in the right panel. The red region is excluded by either an ALP density larger than that of DM, or by current CMB limits on GWs (see figure 3.1). Lines corresponding to the fraction of the DM made up of ALPs $f_{ALP} = \Omega_a/\Omega_{DM} = 1$ and $f_{ALP} = 0.1$ are shown as well. The grey region is excluded by the requirement that ALPs be produced at $T_{ann} > 5$ eV. T_{ann} grows with ϵ_b as indicated by the $T_{ann} = 50$ eV orange dashed line. The blue region will be explored in the near future by CMB probes and astrometry, while we expect the region to the right of the black dotted lines to be subject to structure formation bounds.

2.3 Production of ALPs via Catastrogenesis

We may follow a similar argument to the one given in chapter 2.2 to determine the contribution to the present-day ALP density due to emission from the string-wall network. As with equation (2.2.3), the number density of ALPs from walls is

$$n_a^{wall}(t_0) \simeq -\int_{t_w}^{t_{ann}} dt \left(\frac{R(t)}{R_0}\right)^3 \left(\frac{d\rho_w(t)}{dt}\right) \frac{1}{\langle E_a \rangle}, \tag{2.3.1}$$

where in this case

$$\langle E_a \rangle = m_a \sqrt{1 + \epsilon_a^2} \tag{2.3.2}$$

is the average energy per emitted ALP and ϵ_a is the ratio of the comoving momentum of an ALP to its rest mass. According to numerical simulations (see e.g. [HKS13, KSS15]) the emitted ALPs are quasi-nonrelativistic, i.e. $\epsilon_a \simeq 1$ and $\langle E_a \rangle \simeq \sqrt{2} m_a$. Conservatively, we require that $T_{ann} \gtrsim 5$ eV, meaning that the ALP momentum at matter radiation equality (i.e. when $T \simeq 0.75$ eV) is of order $m_a/10$ and therefore ALPs produced in our model will make up a fraction of the CDM. As with strings, the ALP energy density at present is $\rho_a = n_a m_a$, and so

$$\Omega_a h^2 \simeq \frac{2 \times 10^{-42}\ \mathrm{eV}^2}{V_{bias}^{1/2}} \left(\frac{\sigma}{\mathrm{eV}}\right)^{3/2} \frac{[g_*(T_{ann})]^{3/4}}{g_{s*}(T_{ann})} \simeq \frac{2.4 \times 10^{-24}\ m_a^{1/2}}{\epsilon_b^{1/2} \mathrm{eV}^{1/2}} \left(\frac{f_\sigma^{3/4} V}{N \mathrm{GeV}}\right)^2 \tag{2.3.3}$$

Comparing equations (2.2.4) and (2.3.3), we see that the string-wall contribution to the present ALP density will dominate over that of the string system if $\epsilon_b \gtrsim 2 \times 10^{-9}$. Adding all three ALP density contributions together and requiring that they be less than 0.12 gives the overclosure bound shown in figure 2.2. The process of ALP cosmology is summarized in figure 1.3.

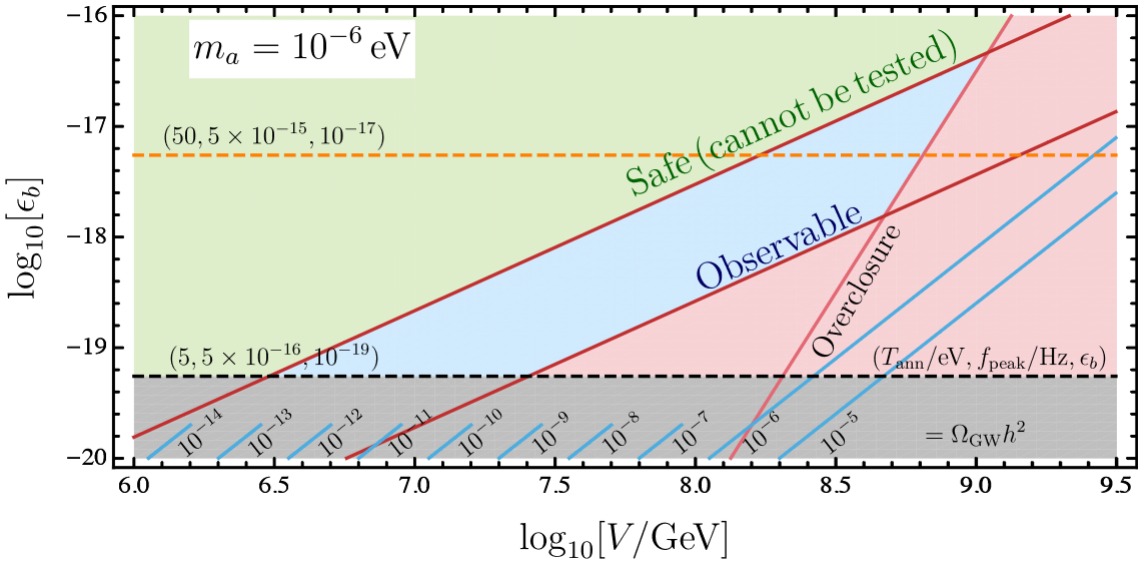

Figure 2.2: Regions of interest in $\{V, \epsilon_b\}$ space for $m_a = 10^6$ eV. The red regions correspond to either ALP densities larger than that of the DM at present or current CMB limits on GWs as displayed in figure 3.1. The grey region is excluded by the requirement that $T_{ann} < 5$ eV. The green region is allowed but not testable, while the blue region will be explored in the near future by CMB probes and astrometry.

CHAPTER 3

Present Density of Gravitational Waves for Stable ALPs

3.1 Present Energy Density Due to Catastrogenesis

In addition to the production of ALPs, gravitational waves are also produced during catastrogenesis [Mic07]. We may estimate the power emitted in the form of GWs using the quadrupole formula, i.e. $P \simeq G\dddot{Q}_{ij}\dddot{Q}_{ij}$. As discussed in chapter 1.5, the linear size of the walls during the scaling regime is $\sim t$, meaning that the quadrupole moment of the walls as a function of their energy $E_w \simeq \sigma t^2$ is $Q_{ij} \simeq E_w t^2$. Thus, $\dddot{Q}_{ij} \simeq \sigma t$, and the power emitted in the form of GWs is $P \simeq G\sigma^2 t^2$. The energy density $\Delta\rho_{GW}$ emitted during a time interval Δt is then

$$\Delta\rho_{GW} \simeq G\sigma^2 \frac{\Delta t}{t} \ . \tag{3.1.1}$$

In a time interval equal to the Hubble time $\Delta t \simeq t$, the emitted energy density is $G\sigma^2$, meaning that the GW emission by walls is independent of the emission time t. The contribution of the waves emitted at time t to the present-day GW energy density is redshifted by the ratio $(R(t)/R_0)^4$, where $R(t)$ is the scale factor of the universe at time t, and at present the scale factor is $R_0 = 1$. Therefore, the largest contribution to the present GW energy density spectrum, which also corresponds to the peak of the spectrum, will be from the GWs emitted at the latest emission time,

i.e. at t_{ann}. Thus,

$$\rho_{GW}|_{peak} \simeq G\sigma^2 \left(\frac{R(t_{ann})}{R_0}\right)^4 . \tag{3.1.2}$$

As usual, we define the density parameter $\Omega_{GW}h^2|_{peak} = \rho_{GW}|_{peak}h^2/\rho_c$, where ρ_c is the present critical density and h is the reduced Hubble constant. Combining this with the result from chapter 8 as well as taking the present number of entropic degrees of freedom to be $g_{s*}(t_0) \simeq 3.93$ [SS18] lets us obtain

$$\Omega_{GW}h^2|_{peak} \simeq \epsilon_{gw}\frac{1.2\times10^{-79}g_*(T_{ann})\sigma^4}{[g_{s*}(T_{ann})]^{4/3}V_{bias}^2\text{GeV}^4} = \epsilon_{gw}\frac{1.2\times10^{-79}g_*(T_{ann})}{\epsilon_b^2[g_{s*}(T_{ann})]^{4/3}}\left(\frac{f_\sigma V}{N\text{GeV}}\right)^4 . \tag{3.1.3}$$

This estimate has been confirmed by numerical simulations [HKS10, HKS14, KS11, HKS13]. The parameter ϵ_{gw} is a dimensionless factor derived from numerical simulations that parametrizes the efficiency of GW production (see e.g. figure 8 in [HKS13]). For $N = 6$, $\epsilon_{gw} \simeq 10 - 20$ [HKS13]. For our figures, we make the conservative estimate that $\epsilon_{gw} = 10$.

The result in equation (3.1.3) is also the maximum of the GW energy spectrum at time t as a function of the wavenumber at present k (which, if we define $R_0 = 1$, corresponds to the comoving wavenumber) or of the frequency $f = k/(2\pi)$, which can be written in general as

$$\Omega_{GW}h^2(k,t) = \left(\frac{h^2}{\rho_c(t)}\right)\left(\frac{d\rho_{GW}(t)}{d\ln k}\right) \tag{3.1.4}$$

(see e.g. [Mic07, GPV21]). In the scaling regime, the characteristic frequency of the GWs emitted at time t is the inverse of the horizon scale $H(t)$, and therefore the present-day frequency of waves emitted at time t is $f \simeq R(t)H(t)$. For GWs emitted

in the radiation dominated epoch (i.e. when $H(t) = 1/(2t)$, $d\ln f = (H(t) - t^{-1})dt$, and therefore $d\ln f = d\ln k = -(1/2)d\ln t$. Using the result from equation (3.1.1), we find that

$$\frac{d\rho_{GW}(t)}{d\ln k} \simeq G\sigma^2, \tag{3.1.5}$$

which is independent of t. Consequently, the peak amplitude of this spectrum at present for $t = t_0$ coincides with the result in equation (3.1.3).

Since the peak GW density is emitted at annihilation, the spectrum should be peaked at $f_{peak} \simeq R(t_{ann})H(t_{ann})$, namely

$$f_{peak} \simeq 0.76 \times 10^{-7}\text{Hz}\frac{T_{ann}}{\text{GeV}}\frac{[g_*(T_{ann})]^{1/2}}{[g_{s*}(T_{ann})]^{1/3}}. \tag{3.1.6}$$

The requirement that the ALPs be produced safely before matter-radiation equality, $T_{ann} \gtrsim 5$ eV, implies that $f_{peak} > 5 \times 10^{-16}$ Hz. As detailed below, we find that GWs observable in the near future in viable ALP models should have f_{peak} close to this lower limit.

The peak frequency estimated in equation (3.1.6) is insufficient to characterize the complete emission spectrum of GWs. The full spectrum has been computed numerically for axions for $N > 1$ in [HKS13]. Figure 6 of [HKS13] shows that the spectral slope changes at two scales: there is a peak at $k|_{peak} \simeq R(t_f)m_a$ and there is a bump at the scale $k \simeq R(t_f)H(t_f)$ where t_f is the final time in their simulation. Frequencies below the peak correspond to super-horizon wavelengths at t_{ann}. Causality requires that these be uncorrelated and therefore the spectrum behaves like a white noise spectrum that goes to zero as k^3 for $k < k_{peak}$ [CDK09].

The spectrum at frequencies above the peak is model-dependent. For a source

that is uncorrelated at different times, i.e. one that is produced by a series of short events, the spectrum should go as $1/k$ [CDK09]. The numerically obtained spectrum in [HKS13] has a roughly $1/k$ dependence for $k > k_{peak}$, although with an approximate slope and height of the secondary bump that depend on N. For a more detailed calcultion of the GW spectrum emitted by domain walls see chapter 9.

An example of the approximate GW spectrum just mentioned is shown in figure 3.1, together with several bounds and reaches of several future experiments. For $f > 10^{14}$ Hz, the most important bounds come from the Very Long Baseline Array (VLBA) astrometric catalog [DTP18], as GWs produce an apparent distortion of the position of background sources, and from the effective number of neutrino species during CMB emission N_{eff} [PSM16a], as GWs are one of the components of the radiation present in the early universe. In the near future, EUCLID will improve the bounds on N_{eff} by one order of magnitude [Lau11], and astrometry could reach as far as $\Omega \simeq 10^{-8}$ [ADG20]. At lower frequencies, measurements of the CMB polarization can be used to constrain GWs [KK99, SKC06, CCM20, Las16, CKP21]. Current bounds are obtained from Planck temperature [Agh20] and BICEP/Keck Array polarization data sets [Ade18], and could be improved by planned experiments such as LiteBIRD [Mat14], PICO [Han19], and CORE [Del18]. We also show constraints and projections from [NSY19], in which the authors relaxed the usual assumption of a power-law background and considered CMB constraints on monochromatic GWs, which may be closer to the peaked spectrum of our model. Notice that the constraints from [NSY19] are based on temperature anisotropies, while the projections for the future reach are obtained from the B-mode spectrum that optimistically assumes a full sky observation, i.e. 1 μK-arcmin white noise with a 1 arcmin Gaussian beam.

3.2 Present Energy Density Due to Strings

The dominant source of GW emission from the string network before the walls appear are loops continuously formed by string fragmentation. As with the string-wall network, we may estimate the emission from these loops via the quadrupole moment of the strings (see e.g. [CC20, GHN21, GSS20] and references therein). The energy of the string network is $E_s \simeq \mu H^{-1}$, where μ is the string mass per unit length. In this case, $\ddot{Q}_{ij} \simeq \mu$, and the power emitted in the form of GWs is $P \simeq G\mu^2$. Using the same assumptions as for walls, the GW energy density emitted by the string network over some time Δt is $\Delta\rho^{st}_{GW} \simeq G\mu^2(\Delta t)$.

We can fit an approximate simple expression to the numerical spectra of GWs emitted by strings during the RD era obtained in [CC20, GHN21, GSS20], namely

$$\Omega^{st}_{GW} \simeq 2 \times 10^{-15} \left(\frac{10^{-12}\ \text{Hz}}{f}\right)^{1/8} \left(\frac{V}{10^{14}\ \text{GeV}}\right)^4 . \tag{3.2.1}$$

This spectrum has a low frequency cutoff that corresponds to the largest scale at which loops could form, which is the horizon size when walls form. The $Ly-\alpha$ lower limit $m_a > 2 \times 10^{-20}$ eV [RP21] on the mass of an ALP constituting all of the DM imposes a limit $T_w > 5.3$ keV (see equation (1.5.6)) on the temperature at which walls appear. The frequency at present of GWs emitted at t_w by strings in the scaling regime can be computed by finding the frequency given in equation (3.1.6) for T_w instead of T_{ann}; explicitly, this is

$$f^{st}_{cut} \simeq \frac{T_w}{T_{ann}} f_{peak} \frac{[g_*(T_w)]^{1/2}}{[g_{s*}(T_w)]^{1/3}} \frac{[g_{s*}(T_{ann})]^{1/3}}{[g_*(T_{ann})]^{1/2}}, \tag{3.2.2}$$

which in terms of the ALP mass is

$$f_{cut}^{st} \simeq 82\ Hz \left(\frac{m_a}{GeV}\right)^{1/2} \left[\frac{g_*(T_w)}{105}\right]^{1/4} \left[\frac{105}{g_{s*}(T_{ann})}\right]^{1/3} \tag{3.2.3}$$

For $T_w = 5.3$ keV, this frequency is 4.7×10^{-11} Hz, with larger cutoff frequencies corresponding to wall formation at earlier times and larger values of m_a (see for example figure 4 of [GHN21]). Therefore, in our model the only source of GWs with $f < 10^{-12}$ Hz is the string-wall network.

3.3 Observability of Gravitational Waves

The region of the $\{\epsilon_b, V\}$ parameter space allowed by all present bounds and which could be explored by forthcoming measurements of low frequency GWs depends on m_a. In figure 2.1 we show this region for $m_a = 10^{-6}$ eV and $m_a = 10^{-16}$ eV, respectively.

The blue region in figure 2.1 will be explored in the near future by CMB and astrometry measurements. The GWs are observable at frequencies

$$5 \times 10^{-16}\ \text{Hz} < f_{obs} < 1 \times 10^{-14}\ \text{Hz} \tag{3.3.1}$$

corresponding to a bound on the annihilation temperature 5 eV $< T_{ann} < 10^2$ eV. Equations (1.5.18) and (3.1.6) imply that $f_{peak} \sim \epsilon_b^2$ as shown in the figure.

The red region in figure 2.1 is excluded by either requiring that the fraction of the DM made up of ALPs to be $f_{ALP} = \Omega_a/\Omega_{DM} \leq 1$, or by current CMB limits on GWs (see figure 3.1. The grey region corresponds to $T_{ann} \lesssim 5$ eV, which is excluded by the requirement that any produced ALPs be nonrelativistic by matter-radiation equality.

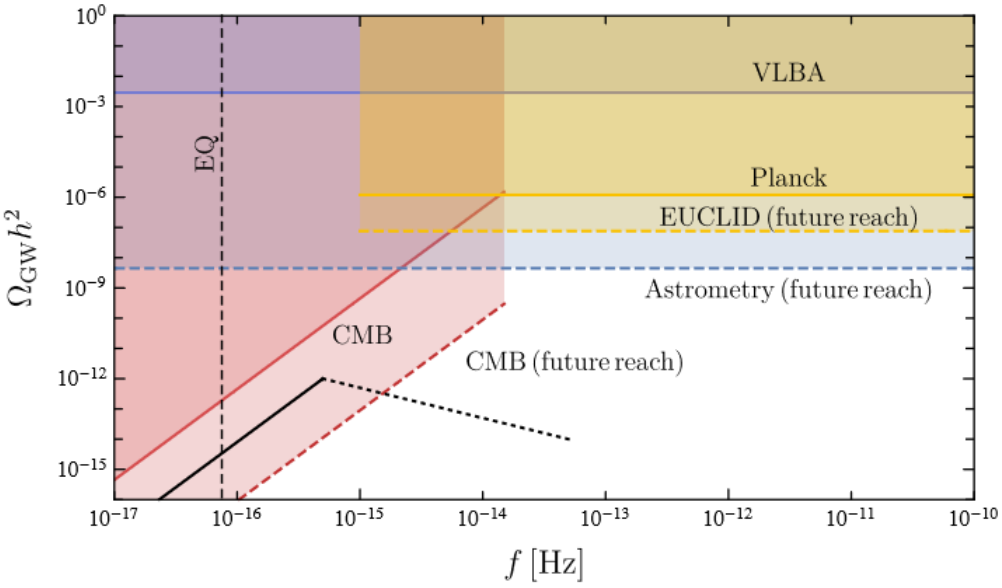

Figure 3.1: Regions of the density parameter of GWs from walls $\Omega_{GW}h^2$ vs. the peak frequency of the spectrum. The blue regions are probed by the current and future reach of astrometry [DTP18, ADG20], the yellow regions by measurements of the effective neutrino degrees of freedom [PSM16a, Lau11], and the red regions by CMB measurements [NSY19]. The connected black lines are an example of a differential GW spectrum from string-wall annihilation with $T_{ann} = 5$ eV and $\Omega_{GW}h^2|_{peak} \simeq 10^{-12}$. The solid black line is the low-frequency part of the spectrum predicted by causality, while the dotted black line is uncertain; these are proportional to f^3 and f^{-1}, respectively. The vertical dashed line indicates the frequency of GWs produced at matter-radiation equality.

The observable region in the $\{\epsilon_b, V\}$ plane translates with the ALP mass m_a as $V \sim m_a^{-1/2}$ and $\epsilon_b \sim m_a^{-1}$. For a fixed ALP abundance, equation (2.3.3) implies an expression for V which can be substituted into equation (3.1.3) to find that the GW amplitude depends on $(m_a\epsilon_b)^{-1} \sim \sigma/V_{bias}$. As shown in equation (1.5.18), the annihilation temperature and thus the peak GW frequency in equation (3.1.6) depend on the ratio $V_{bias}/\sigma \sim m_a\epsilon_b$ as well.

As m_a increases, the lowest value of V in the observable region of the parameter

space V_{obs} decreases as

$$V_{obs} \simeq 10^{6.5}\ \text{GeV} \left(\frac{10^{-6}\ \text{eV}}{m_a}\right)^{1/2}. \tag{3.3.2}$$

To ensure the hierarchy of the scales present in equation (1.3.1), we require that $v < 10^{-2}V$ and thus $m_a < 10^{-4}NV$. For $N = 6$, compatibility with this limit restricts the observable window to $V \gtrsim 2.5$ GeV and $m_a \lesssim 1.5$ MeV.

The scaling of the characteristic bias of the observable region

$$\epsilon_{b,\text{obs}} = 10^{-18} \left(\frac{10^{-6}\ \text{eV}}{m_a}\right) \tag{3.3.3}$$

shows that ALP production by walls dominates over the production by strings for

$$m_a \gtrsim 5 \times 10^{-16}\ \text{eV} \tag{3.3.4}$$

for which $\epsilon_b \lesssim 2 \times 10^{-9}$. Thus, the observable region in figure 2.1 just translates with the same shape for $m_a \gtrsim 10^{-16}$ eV, until the contribution to the ALP population from strings becomes comparable to the wall contribution as shown in the right panel.

In figure 2.1, the region to the right of the dotted black line is where we expect bounds from structure formation to become relevant. These bounds come specifically from measurements of the CMB and of baryon acoustic oscillations (BAOs) as well as from constraints on the number of Milky Way satellites. Bounds on the late production of DM can be roughly estimated as bounds on WDM. The allowable ratio of the density of WDM to the total DM density depends on the WDM mass m_{WDM}: the smaller the mass, the lower the temperature $T \simeq m_{WDM}/3$ at which WDM particles become non-relativistic and thus become CDM. Similarly, the late production of cold DM in our scenario possibly implies large effects on CMB, BAO,

and Milky Way satellite observations (for alternative realizations of late forming DM see e.g. [DW11, SDS15, DN21]). By taking $m_{WDM} = 3T_{ann}$ from figure 5 of [DAG17], we can obtain the region in figure 2.1 where bounds from structure formation become relevant. To obtain more accurate limits would require a specific analysis of structure formation in our scenario.

In the right panel of figure 2.1, the ALP mass is $m_a = 1\times10^{-16}$ eV. For this mass, as indicated in equation (3.3.4), ALPs are mostly produced via wall annihilation for $\epsilon_b \lesssim 2\times10^{-9}$. However, we can see in the change of the slopes of the fixed f_{ALP} lines that the ALP population emitted by strings dominates for larger values of ϵ_b.

Structure formation bounds are less stringent for ALPs with masses $m_a \lesssim 10^{-16}$ eV, which are dominantly produced by strings due to being produced earlier, mostly at wall formation. For these ALPs $T_w > 0.5$ MeV $\gg T_{ann}$. However, they are also subject to black hole superradiance limits (see e.g. [MDL20, UPL21]). These, together with structure formation bounds, are the only valid limits regardless of the strength of the couplings between the ALPs and SM particles unless the ALP quartic self-coupling is large enough to suppress superradiance (e.g. [BGL20]), in which case one can extend the observable window in figure 2.1 to lower ALP masses. Besides the bounds already mentioned, black hole superradiance also puts constraints on ALPs with masses in the range 10^{-13} eV $\lesssim m_a \lesssim 10^{-11}$ eV [BGL20].

The emission of GWs from the string-wall network does not depend on any couplings, including ALP-photon, ALP-electron, ALP-nucleon, and CP-violating couplings such as those listed in [Sik21, IR18, OV20]. Rather, the emission only depends on ϵ_b (for observability) and m_a. Consequently, GWs could probe very "dark" ALPs, which constitute a portal to the dark sector [KLY17, KKV19, AAJ20, CLM22]. If future laboratory searches detect a particle through any coupling that has a mass compatible with the QCD axion, the detection of GWs with a spectrum similar to

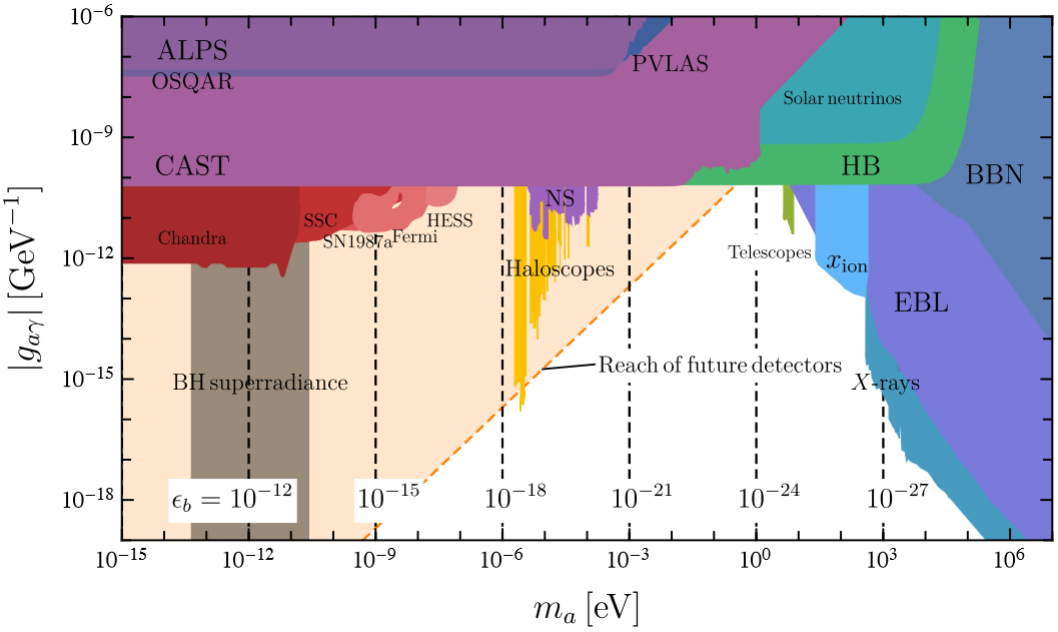

Figure 3.2: Current experimental bounds on the ALP mass due to a photon-axion coupling. The dotted lines are the centers of detection regions at given values of ϵ_b, whose width is of approximately two orders of magnitude. The current bounds on the mass of a possible ALP come from laboratory measurements [Bal15, DEG16, Ehr10], stellar measurements [ADG14, VSV15], helioscopes [And07, Ana17], other astrophysical measurements [PEF15, RMR20, DFS20, Abr13, FKM20, Aje16] (some of which assume an ALP DM [CR12, RTV21, GCK07]), and direct DM detection experiments [Asz10, Du18, Bra20, Bou18, LAC20, Zho18, Bac21a, HSS90, MFI17, Ale19]. The light orange region will be probed by future experiments, including [Oue19, SDS13, MFL19, LMP19, CDM17, BHL18, Ste16, ABD17].

the one we have described would challenge the attribution of this signal to a QCD axion, since GWs from QCD axions are not detectable [HKS13].

In addition to the already stated bounds on GW observation, we may also combine equations (3.1.3), (3.1.6), and (2.3.3) as well as the overclosure bound $\Omega_a h^2 < \Omega_{DM} h^2 \simeq 0.12$ to obtain the limit

$$\frac{\Omega_{GW} h^2|_{peak}}{10^{-17}} \left(\frac{f_{peak}}{10^{-9}\ \text{Hz}} \right)^2 < 10^{-2}\ , \tag{3.3.5}$$

which shows that our allowed observable window is at frequencies below the current range of direct GW detection, which goes from 10^{-9} to 10^{3} Hz for $\Omega_{GW}h^2 > 10^{-15}$. For example, this limit implies that for the reach of future astrometric data, which is $\Omega_{GW}h^2 \simeq 10^{-9}$, our observable window is at $f_{peak} < 10^{-14}$ Hz as shown in figure 3.1. The differential spectrum with $\Omega_{GW}h^2 = 1 \times 10^{-9}$ and $T_{ann} = 100$ eV that we show in figure 3.1, corresponding to $\sigma \simeq 200$ GeV^3 and $V_{bias} \simeq 1 \times 10^{-30}$ GeV^4 (realized e.g. by $m_a \simeq 6$ eV, $\epsilon_b \simeq 4 \times 10^{-24}$, $V \simeq 4 \times 10^5$ GeV) saturates this bound.

Recent results from the 15-year NANOGrav search [Afz23] have demonstrated the existence of a GW background that is consistent with cosmological models. However, at the time of the writing of this thesis it has not been resolved whether or not our model can explain this signal, nor whether or not there is a better explanation for it that does not involve physics beyond the Standard Model. Therefore, this signal is not taken to be evidence in favor of the models presented in this thesis.

CHAPTER 4

Primordial Black Hole Mass and DM Fraction for Stable ALPs

In addition to the direct production of dark matter and the indirect GW signal from a collapsing string-wall network, the existence of a U(1) ALP could also provide a mechanism for the formation of primordial black holes. The creation of these PBHs is due to the collapse of closed domain walls.

During the process of the annihilation of the string-wall network, some fraction of closed walls could shrink to their Schwarzschild radius $R_{Sch}(t) = 2M(t)/M_P^2$ and collapse into PBHs [FMP19a], where $M(t)$ is the mass within a closed wall at time t and $M_P = 1.22 \times 10^{19}$ GeV is the Planck mass. During the scaling regime, the typical linear size of the walls is the horizon size t, and so PBH formation will happen if the ratio

$$p(t) = \frac{R_{Sch}(t)}{t} = \frac{2M(t)}{tM_P^2}, \tag{4.0.1}$$

which we will also refer to as the quality factor, is close to one. As I will show, this could happen after the annihilation of the string-wall network has begun, i.e. when $T \lesssim T_{ann}$.

As discussed in chapter 1.5, annihilation begins when the contribution of the volume energy density to the mass within a closed wall of radius t due to the bias

term in equation (1.3.1) becomes comparable to the wall energy density. Shortly afterwards, the volume density term dominates over the surface term, and the volume pressure accelerates the walls towards one another. Close to annihilation, the mass within a closed wall as a function of the lifetime of the universe t is

$$M(t) \simeq \frac{4}{3}\pi t^3 V_{bias} + 4\pi t^2 \sigma. \tag{4.0.2}$$

This implies that $p(t)$ will increase over time. If p is close to one at t_{ann}, then PBHs will start to form as soon as annihilation begins. However, in our model $p(t_{ann}) \ll 1$, meaning that PBHs will form at a later time $t_* > t_{ann}$ corresponding to a temperature $T_* < T_{ann}$ for which $p(t_*) = 1$ at which only a fraction of the walls remain. We will derive these quantities explicitly by assuming that the universe is still RD at this time and thus the Hubble parameter is $H(t) = 1/(2t)$.

The volume energy density of a region of space bounded by a closed domain wall due to the bias $V_{bias} \simeq \epsilon_b v^4$ grows with time with respect to the surface energy density of the wall σ/t. These become comparable at T_{ann} and therefore

$$M(t_{ann}) \simeq \frac{16}{3}\pi t_{ann}^3 V_{bias} \ . \tag{4.0.3}$$

The quality factor at this time is

$$p(T_{ann}) \simeq \frac{30}{\pi^2} \frac{V_{bias}}{g_*(T_{ann}) T_{ann}} \ . \tag{4.0.4}$$

Note that $M(t_{ann})$ and $p(T_{ann})$ only depend on the parameters V_{bias} and σ. After t_{ann}, the volume contribution to the mass dominates over the surface contribution.

In terms of t and t_{ann}, the mass and quality factor are

$$M(t) \simeq \frac{4}{3}\pi t^3 V_{bias}(1+3\frac{t_{ann}}{t}) \tag{4.0.5}$$

and

$$p(T) \simeq \frac{p(T_{ann})}{4}\left(\frac{t}{t_{ann}}\right)^2\left(1+3\frac{t_{ann}}{t}\right). \tag{4.0.6}$$

When $t \gg t_{ann}$ we can neglect the second term in both equations to obtain

$$p(T) \simeq \frac{p(T_{ann})}{4}\frac{g_*(T_{ann})}{g_*(T)}\left(\frac{T_{ann}}{T}\right)^4. \tag{4.0.7}$$

We may then use this equation to define T_* by writing

$$p(T_*) \simeq \frac{p(T_{ann})}{4}\frac{g_*(T_{ann})}{g_*(T_*)}\left(\frac{T_{ann}}{T_*}\right)^4 = 1, \tag{4.0.8}$$

which also implicitly defines the corresponding time at which PBHs form t_*. Note that we have assumed that the characteristic length scale of the walls is still t after annihilation begins. Larger deviations from the scaling regime are expected, but determining when and how this happens will require more detailed simulations. The mass of the resulting PBHs is then given by $M(t_*)$, which is

$$M_{PBH} = M(t_*) \simeq \frac{4\pi}{3}V_{bias}t_*^3 \simeq \frac{2}{[p(T_{ann})]^{3/2}}M(t_{ann}) \simeq \left(\frac{3}{32\pi}\right)^{1/2}\frac{M_P^3}{V_{bias}^{1/2}}. \tag{4.0.9}$$

Equations (4.0.9) and (4.0.8) show that the PBH formation temperature T_* only

depends on V_{bias} (or, equivalently, M_{PBH}) as

$$T_* \simeq 0.9 \text{ GeV} \left[\frac{V_{bias}}{\text{GeV}^4 \ g_*(T_*)}\right]^{1/4} \simeq \frac{0.5 \text{ GeV}}{[g_*(T_*)]^{1/4}} \left(\frac{M_\odot}{M_{PBH}}\right)^{1/2} . \tag{4.0.10}$$

By inverting equations (4.0.1) and (4.0.9), we then obtain

$$p(T_{ann}) \simeq \frac{t_{ann}^2 M_P^4}{M_{PBH}^2} = \frac{90}{32\pi^3} \frac{1}{g_*(T_{ann})} \frac{M_P^6}{T_{ann}^4 M_{PBH}^2} = \frac{0.24}{g_*(T_{ann})} \left(\frac{10 \text{ eV}}{T_{ann}}\right)^4 \left(\frac{10^{16} M_\odot}{M_{PBH}}\right)^2 . \tag{4.0.11}$$

It is likely that closed domain walls during this time will have nonzero angular momentum and will also not be entirely spherical. This means that the probability of forming a PBH at temperature T may be smaller than $p(T)$. We take this into account by defining the formation probability $P_{formation} = p(T)^\beta$, where $\beta \geq 1$ is a real dimensionless coefficient. If the degree of asphericity of a closed domain wall is high enough, this could prevent the formation of a PBH, as its degree of asphericity will decrease initially but will increase again in the late stages of the collapse [Wid89]. If $p(T_{ann}) \ll 1$, however, this may not be the case, since walls will need to evolve longer before p reaches 1. In this case, [FMP19b] suggests that energy loss or angular momentum might impede the process of PBH formation. Still, highly aspherical closed walls are unlikely, as shown in the context of the collapse of a vacuum bubble produced via inflation [DV17]. We will thus assume that there will be some portion of the walls for which the degree of asphericity is small enough that collapse is still possible. With this in mind, the PBH density at formation is

$$\rho_{PBH} \simeq p^\beta(T_*) \rho_w(T_*). \tag{4.0.12}$$

Making use of the fact that at the production temperature the quality factor is

$p(T_*) = 1$, the fraction f_{PBH} of the total DM that is made up of PBHs is

$$f_{PBH} = \frac{\rho_{PBH}(T_*)}{\rho_{CDM}(T_*)} \simeq p^{\beta}(T_*)\frac{\rho_w(T_*)}{\rho_{CDM}(T_*)} = \frac{\rho_w(T_*)}{\rho_w(T_{ann})}\frac{\rho_w(T_{ann})}{\rho_{CDM}(T_*)}. \tag{4.0.13}$$

The bulk of the energy density of the string-wall network is used up in the production of ALPs at annihilation, and thus $\rho_w(T_{ann}) \simeq \rho_a(T_{ann}) = f_{ALP} \times \rho_{CDM}(T_{ann})$, where f_{ALP} is the fraction of the DM made up of ALPs. We may approximate the evolution of the wall energy density after T_{ann} as

$$\frac{\rho_w(T)}{\rho_w(T_{ann})} = \left(\frac{T}{T_{ann}}\right)^{\alpha}. \tag{4.0.14}$$

We can derive α from table VI and figure 4 of [KSS15], which display the times $t(10\%)$ and $t(1\%)$ at which the string-wall network has reached 10% and 1% of its original density after annihilation has started, which correspond respectively to temperatures $T(10\%)$ and $T(1\%)$. Note that this ratio is the same in comoving (as given in [KSS15]) and physical coordinates. Note here that per [KSS15] we still assume that the area parameter $A(t)$ is approximately 1. Under varying assumptions, the ratio $t(1\%)/t(10\%)$ ranges from 1.7 to 1.5, which corresponds to values of α between 7 and 12, meaning that $(\alpha - 3)/4$ is between 1 and 2. If the energy of the string-wall network is still dominated by the contribution of the walls until $t(1\%)$, then $\rho_{tot} \simeq \rho_w = A\sigma/V$ and

$$\left(\frac{T(10\%)}{T(1\%)}\right)^{\alpha} \simeq \frac{\rho_w(T(10\%))}{\rho_w(T(1\%))} = \frac{A/V|_{t(10\%)}}{A/V|_{t(1\%)}} = 10\left(\frac{t(1\%)}{t(10\%)}\right) \tag{4.0.15}$$

Fitting this to the aforementioned figure gives values of α roughly between 9 and 14, although we also choose to include $\alpha = 7$ as mentioned in [FMP19b]. Taking into account the systematic errors quoted in Table VI of [KSS15], however, we see

that α could be as large as 19. However, the volume contribution to the energy density of the string-wall network may not be negligible, which introduces further uncertainty when determining α. To get an estimate of this uncertainty, we proceed assuming that the volume energy of the string-wall network is dominant and thus the density is proportional to $A^{3/2}$. In fact, since the simulation volume in [KSS15] is the same whether or not there is a bias present, the ratio of the area densities is also the ratio between the area A of the walls in the biased case and the characteristic area $\sim t^2$ of walls that are perfectly in the scaling regime. Thus, $[A(t(10\%))]^{1/2} \simeq \sqrt{0.10}t(10\%)$ and $[A(t(1\%))]^{1/2} \simeq \sqrt{0.01}t(1\%)$. Moreover, if the volume density due to V_{bias} dominates over the surface energy density, the energy density of the walls is $\rho_w \simeq V_{bias}A(t)^{3/2}/t^3$, which means that

$$\left(\frac{T(10\%)}{T(1\%)}\right)^{\alpha} \simeq \frac{\rho_w(T(10\%))}{\rho_w(T(1\%))} \simeq 10^{3/2}, \tag{4.0.16}$$

which means that the value of α actually ranges from (3/2)7 to (3/2)19, suggesting that α could be as large as 28.

Combining the assumption from equation (4.0.14) with equation (4.0.8) and the fact that the axion number density redshifts as T^3, we find that

$$f_{PBH} \simeq f_{ALP}\left[\frac{p(T_{ann})}{4}\right]^{(\alpha-3)/4}\left[\frac{g_*(T_{ann})}{g_*(T_*)}\right]^{(\alpha-3)/4}\frac{g_{s*}(T_{ann})}{g_{s*}(T_*)}\ . \tag{4.0.17}$$

Neglecting the possible change in degrees of freedom between T_{ann} and T_*, this implies that f_{PBH} sits within the range

$$f_{PBH}\left(f_{ALP}\left[\frac{p(T_{ann})}{4}\right], f_{ALP}\left[\frac{p(T_{ann})}{4}\right]^{25/4}\right)\ . \tag{4.0.18}$$

We may also calculate f_{PBH} in terms of fixed α explicitly by noting that equations (4.0.14) and (4.0.13) imply that

$$f_{PBH} \simeq \left(\frac{T_*}{T_{ann}}\right)^{\alpha} \frac{\rho_w(T_{ann})}{\rho_{DM}(T_*)} \,. \tag{4.0.19}$$

In this equation, $\rho(T_*)$ can be easily related via a redshift factor to the present DM density. Meanwhile, $\rho_w(T_{ann})$ can be related to the present radiation density by noting that, since $\rho_w \sim 1/t$, it is related to the the wall energy density at the time at which walls would have dominated the universe had they not annihilated t_{wd} by the equation

$$\rho_w(t_{ann}) = \frac{t_{wd}}{t_{ann}} \rho_{rad}(t_{wd}) = \frac{H(T_{ann})}{H(T_{wd})} \rho_{rad}(t_{wd}). \tag{4.0.20}$$

Using equations (1.5.10), (4.0.10), and (1.5.18) we may also rewrite T_{wd} in terms of σ and in terms of T_* and T_{ann} as

$$T_{wd} \simeq \frac{0.9 \times 10^{-6} \text{ GeV}}{[g_*(T_{wd})]^{1/4}} \left(\frac{\sigma}{\text{GeV}}\right)^{1/2} \simeq \frac{2.0 \text{ GeV}[g_*(T_*)]^{1/2}}{[g_*(T_{wd}) g_*(T_{ann})]^{1/4}} \left(\frac{T_*}{\text{GeV}}\right)^2 \left(\frac{\text{GeV}}{T_{ann}}\right) \tag{4.0.21}$$

as well as

$$T_{wd} \simeq \frac{3.4 \text{ GeV}}{[g_*(T_{wd})]^{1/4}} \frac{f_\sigma^{1/2}}{N} \left(\frac{V}{10^9 \text{ GeV}}\right) \left(\frac{m_a}{10 \text{ GeV}}\right)^{1/2} \,. \tag{4.0.22}$$

Incorporating the redshift of the radiation density to the present day, equation (4.0.19) becomes

$$f_{PBH} \simeq \frac{4.0 \; g_{s*}(T_0)}{g_*(T_0)} \frac{[g_*(T_{ann}) g_*(T_{wd})]^{1/2}}{g_{s*}(T_*)} \frac{T_*^{(\alpha-3)} T_{wd}^2}{T_0 T_{ann}^{(\alpha-2)}} \left(\frac{\rho_{rad}}{\rho_{DM}}\right)_0 , \tag{4.0.23}$$

or, using equation (4.0.21),

$$f_{PBH} \simeq \frac{3.9\ g_{s*}(T_0)}{g_*(T_0)} \frac{g_*(T_*)}{g_{s*}(T_*)} \frac{T_*^{(\alpha+1)}}{T_0 T_{ann}^{\alpha}} \left(\frac{\rho_{rad}}{\rho_{DM}}\right)_0 . \tag{4.0.24}$$

Using equation (4.0.10) and the values of the present entropy and energy degrees of freedom written in the previous equation, we find

$$f_{PBH} \simeq 1.1 \times 10^{14} \times 1.5^{\alpha} \times 10^{-2\alpha} \left(\frac{10^{-10}\ M_\odot}{M_{PBH}}\right)^{(\alpha+1)/2} \left(\frac{10^6\ \text{GeV}}{T_{ann}}\right)^{\alpha} \left(\frac{105}{g_*(T_*)}\right)^{(\alpha-3)/4} \left(\frac{105}{g_{s*}(T_*)}\right), \tag{4.0.25}$$

where we have assumed that T_* and T_{ann} are close enough that we may neglect the change in energy degrees of freedom between them.

The relic ALP density $\Omega_a h^2$ from equation (2.3.3) can be written as a function of the annihilation temperature T_{ann} and the PBH mass M_{PBH},

$$\Omega_a h^2 = \frac{3.5 \times 10^7}{g_{s*}(T_{ann})} \left(\frac{\text{GeV}}{T_{ann}}\right)^3 \left(\frac{M_\odot}{M_{PBH}}\right)^2 . \tag{4.0.26}$$

Combining this with equation (4.0.11) also lets us write this in terms of M_{PBH} and $p(T_{ann})$,

$$\Omega_a h^2 = 3.2\ [p(T_{ann})]^{3/4} \left(\frac{10^{15} M_\odot}{M_{PBH}}\right)^{1/2} \frac{[g_*(T_{ann})]^{3/4}}{g_{s*}(T_{ann})}. \tag{4.0.27}$$

Likewise, we may also rewrite equation (3.1.3) as

$$\Omega_{GW} h^2 \simeq 1.4 \times 10^{-9}\ \frac{105\ [g_*(T_{ann})]^3}{[g_{s*}(T_{ann})]^4} \left(\frac{M_\odot}{M_{PBH}}\right)^4 \left(\frac{10^{-7}\ \text{Hz}}{f_{peak}}\right) . \tag{4.0.28}$$

Requiring that ALPs constitute a fraction of the DM, i.e. $\Omega_a h^2 = f_{ALP} \times 0.12$, leads

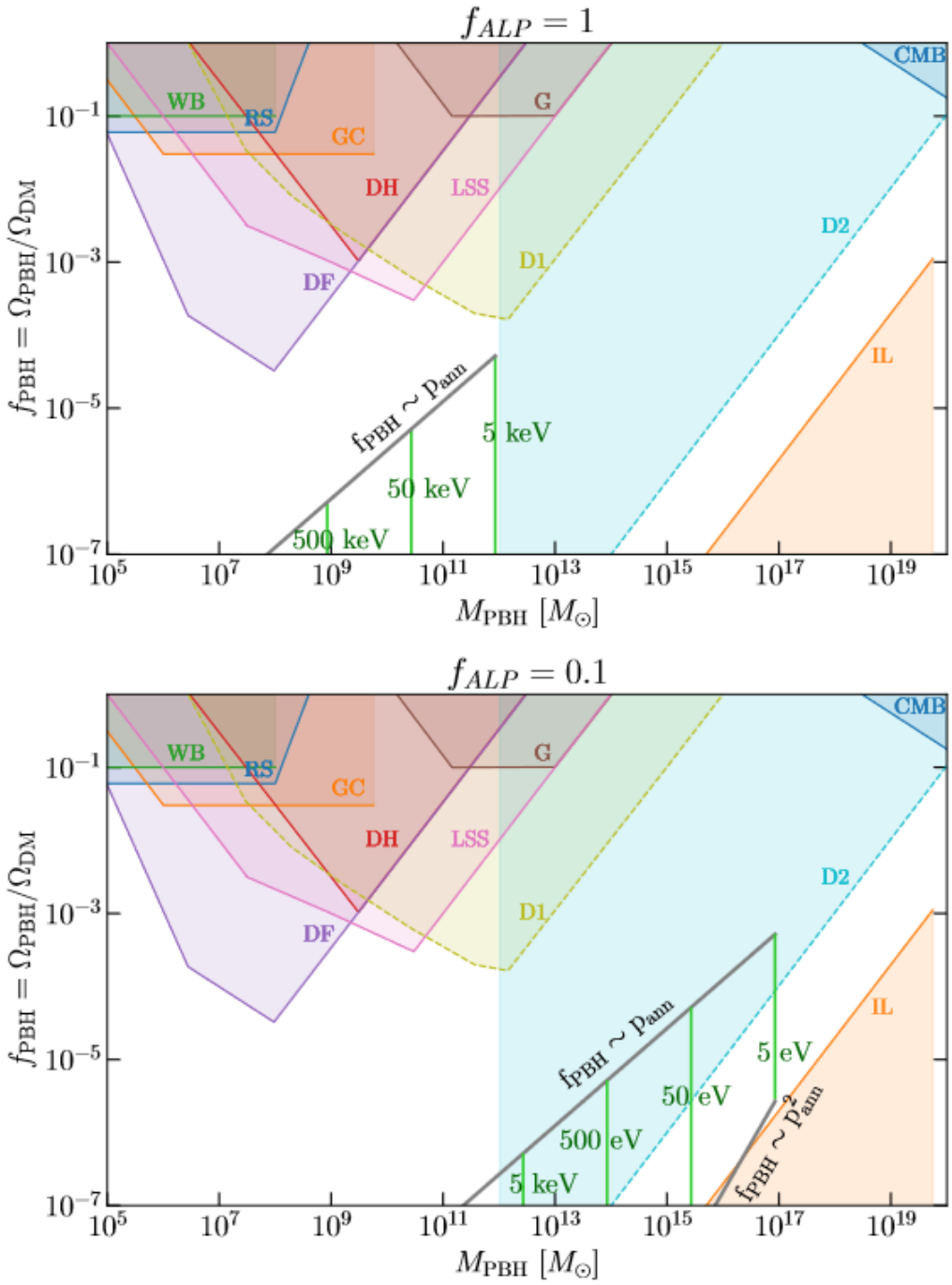

Figure 4.1: Plots of the mass fraction f_{PBH} and mass M_{PBH} of PBHs produced by the stable U(1) ALP model for the case where ALPs constitute all of the DM and where they constitute only 10%. The green lines correspond to different values of T_{ann}, while the black lines correspond to different values of α, which determine the relationship between f_{PBH} and $p(T_{ann})$. Shown bounds are due to millilensing of compact radio sources (RS), dynamical limits from disruption of wide binary stars (WB) and globular clusters (GC), heating of stars in the Galactic disk (DH), dynamical friction (DF), disruption of galaxies (G), and the CMB dipole (CMB). The incredulity limit (IL) corresponds to one PBH per Hubble volume. All of these limits are taken from [Den21a].

to the following expressions for $p(T_{ann})$ and M_{PBH},

$$p(T_{ann}) = 0.27\ f_{ALP}^{4/3} \left(\frac{M_{PBH}}{10^{17} M_\odot}\right)^{2/3} \frac{[g_{s*}(T_{ann})]^{4/3}}{g_*(T_{ann})} \tag{4.0.29}$$

$$\frac{M_{PBH}}{M_\odot} = \frac{1.7 \times 10^4}{[g_{s*}(T_{ann})]^{1/2}} \left(\frac{\text{GeV}}{T_{ann}}\right)^{3/2} f_{ALP}^{-1/2}. \tag{4.0.30}$$

In other words, an upper limit on f_{ALP} implies an upper limit on the PBH DM fraction f_{PBH} and a lower limit on the PBH mass.

In figure 4.1 we show f_{PBH} for $f_{ALP} = 1$ and $f_{ALP} = 0.1$ in the upper and lower panels, respectively. All displayed bounds are taken from [CKS20] and references therein, including mililensing of compact radio sources (RS), dynamical limits from the disruption of wide binaries (WB) and globular clusters (GC), heating of stars in the galactic disk (DH), dynamical friction constraints (DF), disruption of galaxies (G), and the CMB dipole bound (CMB). The incredulity limit (IL) is derived from the assumption that there is at least one PBH per Hubble volume. Projected realistic (D1) and optimistic (D2) discovery limits through μ-distortion of the CMB spectrum correspond to the regions contoured by dashed lines and are taken from [Den21b]. For a fixed ALP density, our predicted PBH population could fall within the indicated black funnel corresponding to the range in equation (4.0.18), where p_{ann} as a function of M_{PBH} is given in equation (4.0.29). The green vertical lines within each funnel show the PBH mass that corresponds to each indicated value of the annihilation temperature given in equation (4.0.30).

Due to structure formation constraints, the scenario in which $f_{ALP} = 1$ is likely only possible if $T_{ann} \gtrsim 1$ keV. Because of this, we cut off the allowed region displayed in the upper panel to the right of $T_{ann} = 5$ keV. In this case, the collapse of closed

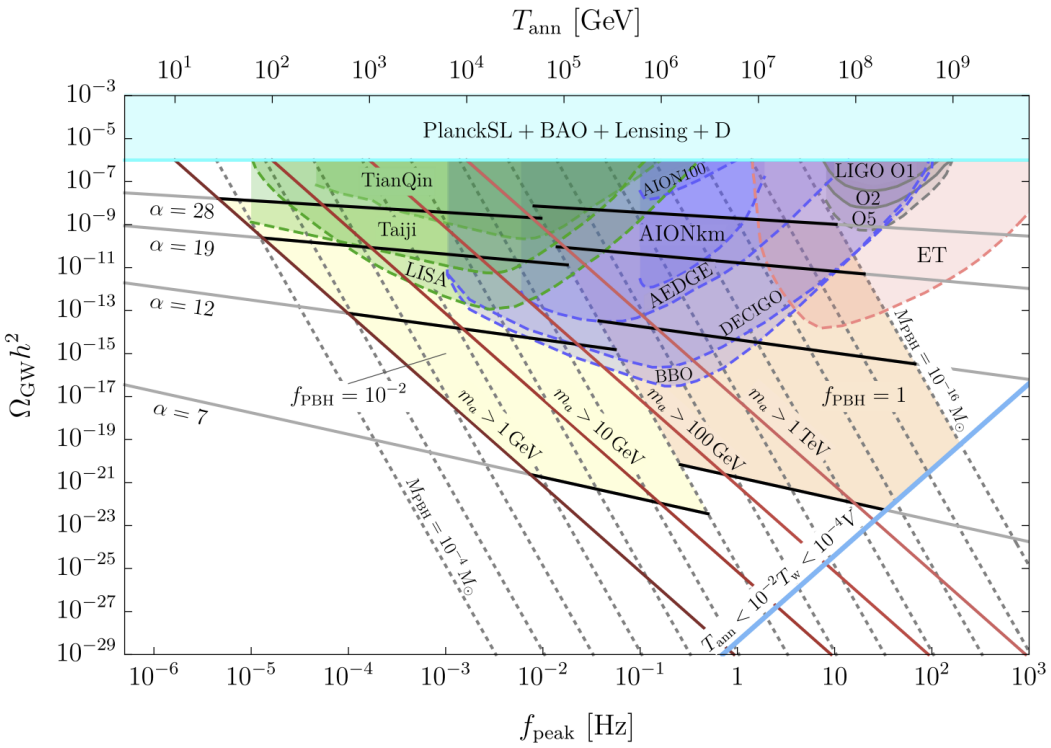

Figure 4.2: The present GW density $\Omega_{GW}h^2$ predominantly emitted by the string-wall network at annihilation as a function of f_{peak} or T_{ann} as shown on the upper and lower horizontal axes, respectively, for $f_{PBH} = 1$, as shown in the orange region, and $f_{PBH} = 10^{-2}$, as shown in the yellow region. The solid black lines correspond to f_{PBH} at fixed values of α ranging from 7 to 28. We also show the upper limits and expected reach of existing and future GW detectors as solid and dashed colored contours, respectively. The quoted lower limits on m_a exclude the regions below and to the left of the respective slanted red lines if $T_w/V = 10^{-2}$; for smaller values of this ratio, the allowed regions shrink. Grey dotted lines correspond to constant values of M_{PBH}. The consistency condition $T_{ann} < 10^{-2}\ T_w < 10^{-4}\ V$ excludes the region below and to the right of the thick blue line.

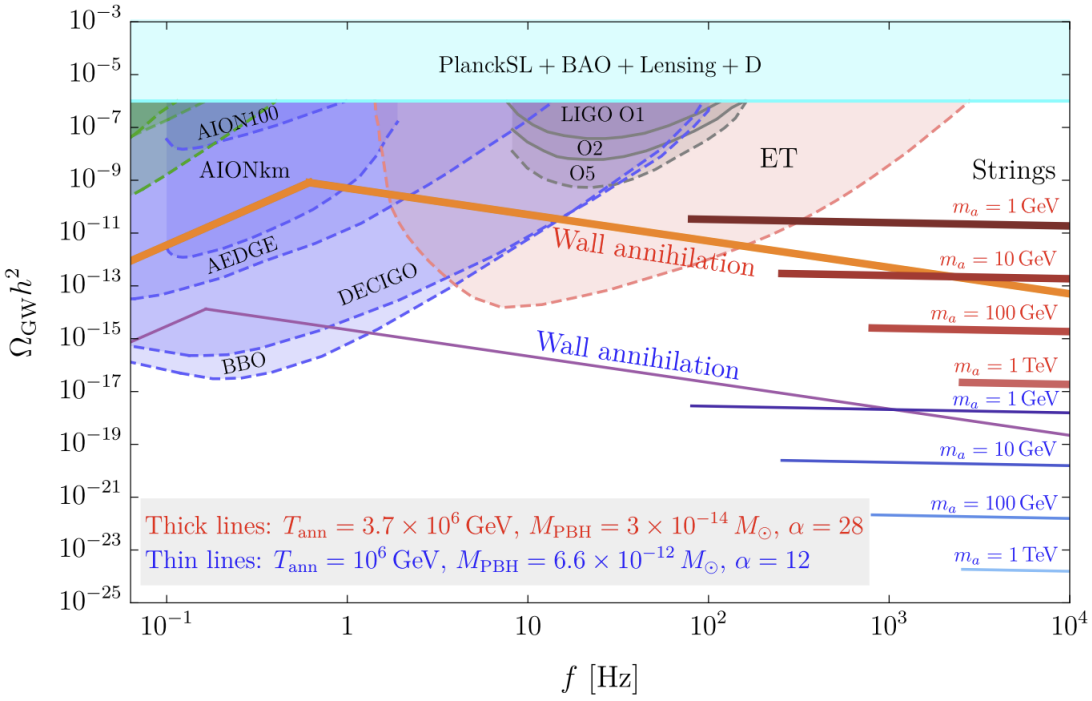

Figure 4.3: Plots of possible combined spectra from both wall annihilation and string annihilation for different values of m_a. The thick, red, solid lines correspond to a model with $\alpha = 28$, and show a spectrum that is observable by several future GW detectors, while the corresponding spectrum from strings shown as dark red lines would only be observable by the ET for $m_a \simeq 1$ GeV. For a more typical model where $\alpha = 12$, the GWs from wall annihilation, which are shown in violet, are observable, but the corresponding spectrum from strings, shown in blue, is not.

spherical domain walls could produce "stupendously" large black holes [CKV21] with masses of up to 10^{12} $M_\odot$. If wall annihilation happens at temperatures above 500 keV, supermassive black holes (SMBHs) could be produced with masses up to 10^9 $M_\odot$, on the order of those found at the centers of large galaxies. These black holes are observed at large redshifts [HL01, WYF21] and their production through accretion and mergers of smaller black holes from Pop III stars is generally complicated, and requires either a large initial seed or an increased growth rate (for a full review, see

[IVH20]), though turbulent cold flows may help the process along [LWK22].

An SMBH production mechanism relying on a first order phase transition has recently been proposed [DDG22], which is in tension which heavy quasar superradiance bounds [UPL21]. Our model avoids these bounds for large enough m_a. An alternative scenario invoking physics beyond the SM is that of the gravothermal collapse of self-interacting DM halos (see e.g. [BS02, BSI02, PSS15]). However, since the cross sections needed for gravothermal collapse are ruled out by observations of galaxy cluster collisions, more complicated models need to be built, including totally dissipative DM (i.e. with "hit-and-stick" collisions [XSH21]) or mixed DM (in which the DM has two components, and one component has a large self-interaction cross section, e.g. [CCC19]). Finally, SMBHs might be produced through PBH mergers [Due04], as well as via the collapse of domain walls [KRS05] or vacuum bubbles [DV17, KSS20] nucleated during inflation. The PBH formation scenario discussed in this thesis is much less complicated, since both the ALP DM density and the PBH population depend on only two macroscopic parameters, σ and V_{bias}. The expected mass of the SMBHs can reach up to $10^9\ M_\odot$, which corresponds via equation (4.0.30) to annihilation temperatures larger than $0.66\ f_{ALP}^{-1/3}$ MeV, and via equation (4.0.9) to a lower limit on V_{bias}. equation (2.3.3) shows that these limits translate to limits on σ for each value of f_{ALP}. However, these limits cannot be directly translated into bounds on the ALP mass, since the dynamics of the string-wall network depend on 2 macroscopic parameters, σ and V_{bias}, but there are three parameters in the Lagrangian in equation (1.3.1), ϵ_b, v, and V.

The lower panel of figure 4.1 presents our results for $f_{ALP} = 0.1$, which is compatible with $T_{ann} \gtrsim 5$ eV, since structure formation bounds do not apply to a subdominant component of the DM, leading to a corresponding cutoff in the allowable region shown. In this case, "stupendously" large black holes [CKV21, Den21a] with

masses up to 10^{17} $M_\odot$ and densities as large as 10^{-4} of the DM density could be produced. These black holes will necessarily not reside in galaxies [CKV21]. It is not clear if they can exist at all, and we will remain agnostic about the mechanism that keeps them from forming outside of galaxies. The existence of these PBHs will be potentially probed by measurements of the CMB spectral μ-distortions in future experiments [Den21a]. If the annihilation temperature is above 500 keV, SMBHs will again be produced, although with a lower density than for larger values of f_{ALP}.

CHAPTER 5

Signatures from Catastrogenesis for Unstable ALPs

In the previous chapters, we dealt with models in which the produced ALPs are light and are stable up until the present day. However, heavier bosons could decay

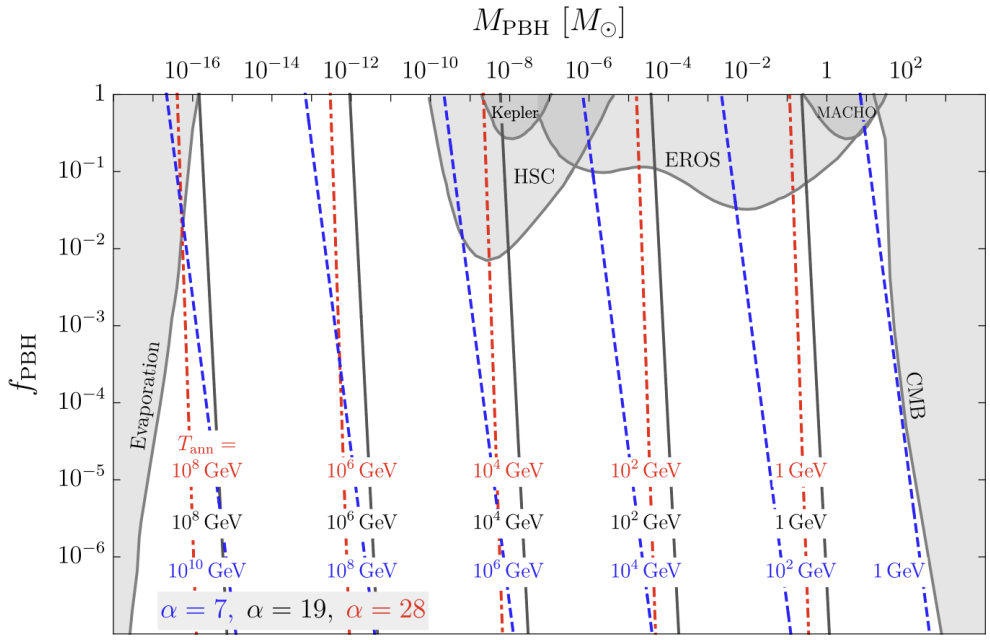

Figure 5.1: A plot of the PBH DM fraction as a function of PBH mass, assuming a monochromatic mass function, for different values of T_{ann} as given in equation (4.0.25). Different colored lines correspond to different values of α, with dashed blue lines for $\alpha = 7$, solid grey lines for $\alpha = 19$, and dashed dotted red lines for $\alpha = 28$. Observational upper limits on f_{PBH} are shown in grey. See main text for more details.

very early into SM products which then rapidly thermalize. There are many ways in which a heavy pNGB could decay into SM particles. For example, axions would decay into photons and charged fermions. Majorons could mostly decay into two relatively heavy right-handed neutrinos, which in turn decay very fast into pions, charged fermion pairs, and active neutrinos. This means that pGBs of these types cannot be the DM in the models we consider, but catastrogenesis could still produce DM in the form of light PBHs. As mentioned at the end of chapter 1.2, heavy ALPs below 1 GeV are subject to numerous experimental and observational constraints. As a result, we will only deal with models where the ALP mass is greater than 1 GeV and the DM is not constituted by ALPs, which are unstable, but instead by light PBHs.

5.1 Gravitational Wave Density for Unstable ALPs

Given that we only consider ALPs with masses $m_a \gtrsim 1$ GeV, in our unstable ALP models the cutoff frequency of the string GW spectrum given in equation (3.2.3) will be $\gtrsim 82$ Hz. In addition, I will show in the following chapter that equations (3.2.1) and (3.1.3) imply that for the unstable model there is a restricted parameter space in which GWs from strings could be observable by the upcoming Einstein GW Telescope [Sat12].

As stated previously, the present GW abundance due to the annihilation of the string-wall network only depends on σ and V_{bias}. In this case, it is convenient to rewrite our equations in terms of the peak frequency f_{peak} and the PBH DM fraction f_{PBH}, which are previously given in equations (3.1.6) and (4.0.25). In terms of these

parameters, $\Omega_{GW}h^2$ is

$$\Omega_{GW}h^2 \simeq (7.6\times10^{-5})^{\alpha/(\alpha+1)}(1.4\times10^{-7})^{20/(\alpha+1)}\left(\frac{1\text{ Hz}}{f_{peak}}f_{PBH}\right)^{8/(\alpha+1)}$$

$$\times\left[\frac{105}{g_*(T_{ann})}\left(\frac{g_*(T_*)}{105}\right)^2\right]^{(\alpha-3)/(\alpha+1)}\left(\frac{105}{g_{s*}(T_{ann})}\right)^{4(\alpha+3)/3(\alpha+1)}\left(\frac{g_{s*}(T_*)}{105}\right)^{8/(\alpha+1)}. \tag{5.1.1}$$

Figure 4.2 shows the expected present GW density produced by the string-wall network as a function of f_{peak} on the lower horizontal axis and as a function of T_{ann} on the upper horizontal axis. The regions where $f_{PBH}=1$ and where $f_{PBH}=10^{-2}$ are shown in orange and yellow, respectively. The black solid lines correspond to a range of values of α between 7 and 28. Predictions are compared to the current upper limits and expected reach of several GW detectors, which are shown in figure 4.2 as solid and dashed contour lines, respectively. We include the projected sensitivities of the space-based experiments TianQin [Luo16], Taiji [RGC20], and the Laser Interferometry Space Antenna (LISA) [Ama17] in green, the reach of the Atom Interferometry Observatory and Network (AION) [Bad20], the Atomic Experiment for Dark Matter and Gravity Exploration in Space (AEDGE) [El 20], the Deci-hertz Interferometer Gravitational Wave Observatory (DECIGO) [SKN01], and the Big Bang Observer (BBO) [CC06] in blue. Finally, the projected reach of the Einstein Telescope (ET) project [Sat12] is shown in red and the projected and current reach of the Laser Interferometer Gravitational-Wave Observatory (LIGO) [Col19] is shown in grey. The cyan band corresponds to the 95% C.L. upper limit from Planck on the effective number of degrees of freedom during CMB emission, as well as other data

[PSM16b] which imposes a bound of $\Omega_{GW}h^2 < 10^{-6}$.

Also shown in figure 4.2 are dotted grey lines of constant PBH mass that range from 10^{-16} to 10^{-4} $M_\odot$, which are derived from equation (4.0.28). As explained in chapter 6, the quoted lower limits on the ALP mass only allow the regions above and to the right of the respective slanted red line, meaning that m_a cannot be larger than the quoted limit to the left, if $T_w/V = 10^{-2}$. The allowed regions shrink (i.e. the slanted red lines move to the right) for smaller values of T_w/V.

Figure 4.2 clearly demonstrates that a GW signal due to domain wall annihilation is within the reach of several experiments for $\alpha \gtrsim 12$, both if PBHs constitute the whole of the DM or just a small fraction of it.

Unlike the GW signal from wall annihilation, the GW signal emitted by strings before the appearance of walls depends on the ALP mass. Therefore, we do not include the signal from strings in 4.2. equation (3.2.3) shows that the cutoff frequency moves rapidly to higher frequencies $\sim m_a^{1/2}$, moving from the LIGO frequency range to the range which will be probed by ET. However, equation (3.2.1) shows that the GW energy density due to cosmic strings is always below 10^{-9}. Since we only consider $V < 10^{16}$ GeV, this means that the GW signal from strings is out of the reach of LIGO. However, this signal is potentially within the reach of ET, although only for models with very high values of α. Figure 4.3 shows two examples of GW spectra from wall annihilation and from string emission. One of them, with $\alpha = 28$, has a large peak amplitude from wall annihilation, with a spectrum $\sim f^3$ below the peak and $\sim 1/f$ above it as shown by the thick red lines that would be largely observable in several future GW detectors. The corresponding spectrum from strings, shown in dark red for several values of m_a, would be observable by ET only for $m_a \simeq 1$ GeV. The other spectra shown correspond to $\alpha = 12$. In this case, the GWs from wall annihilation (shown in violet) could still be observed by DECIGO and BBO, but the

GWs from strings (shown in blue) could not.

Similar predictions for GWs from wall annihilation were found in [Fer22] for the high-quality QCD axion. Because our consistency conditions are tighter and we include the production of asteroid-mass PBHs, we find a less prominent GW signal. Assuming that, for example, $\alpha = 7$, we find that above 1 Hz the GW amplitude cannot be larger than $\Omega_{GW}h^2 \simeq 10^{-19}$.

5.2 Primordial Black Hole Production and DM Fraction for Unstable ALPs

For the unstable ALP model we have discussed, the resulting contribution to the DM is in the form of light PBHs. Figure 5.1 shows upper limits on f_{PBH} as a function of M_{PBH}. The constraints correspond to Hawking radiation bounds [CKS10, BC19a, DG19, Lah19, LMS20, CDG17, MRK22], microlensing bounds [Tis07, Nii19b, KSS20, GCL14, All01], and CMB bounds [SPI20]. All bounds on the PBH abundance are taken from [Kav19], except for the ones from the Subaru Hyper Suprime-Cam (HSC) data [Nii19b, KSS20]. The lines of constant annihilation temperature T_{ann} implied by equation (4.0.25) for different values of α are shown in dashed blue for $\alpha = 7$, solid grey for $\alpha = 19$, and in dashed dotted red for $\alpha = 28$. We can clearly see in the figure that there are annihilation temperatures corresponding to the PBH mass range $10^{-16}\ M_\odot < M_{PBH} < 10^{-10}\ M_\odot$, for which all of the DM could be made up of PBHs.

The range of annihilation temperatures T_{ann} for which PBHs could constitute 100% of the DM can be seen more clearly in figure 5.2. The yellow band in the same figure shows the range of temperatures for which $f_{PBH} = 10^{-2}$, which is a DM fraction that is just below all of the observational bounds for $10^{-10}\ M_\odot < M_{PBH} <$

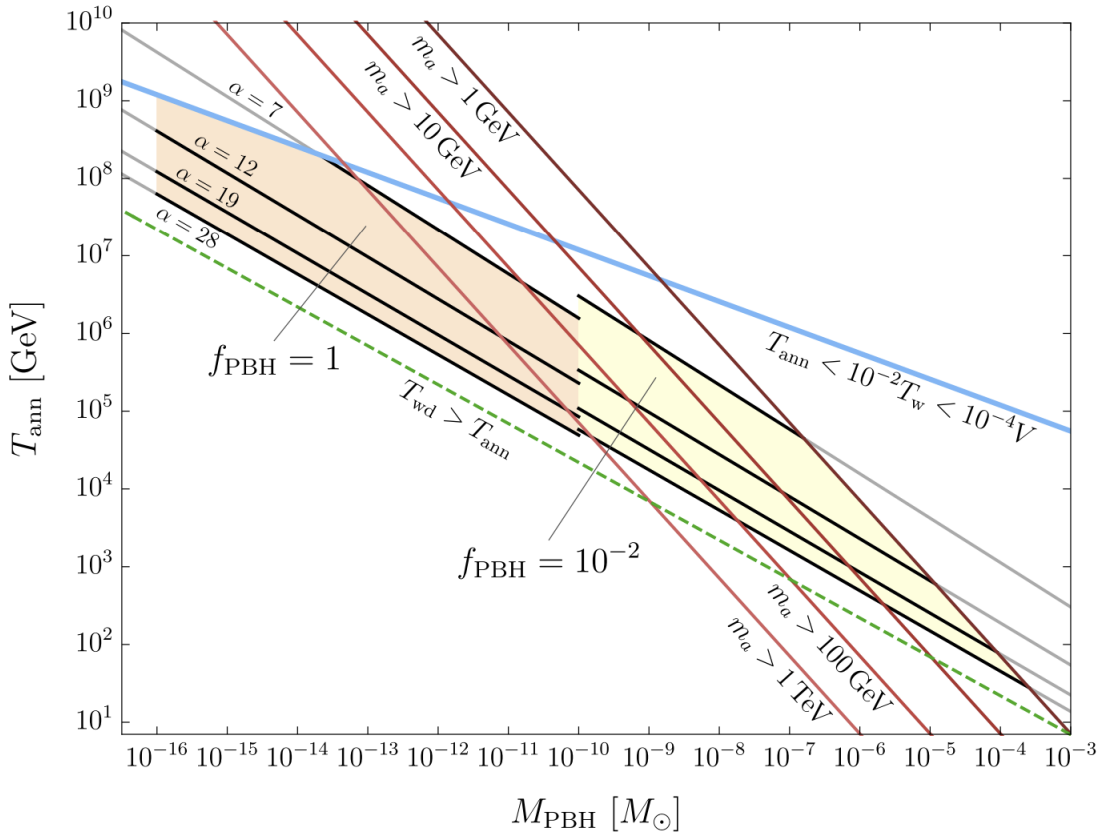

Figure 5.2: Regions of T_{ann} as a function of the PBH mass for which the PBH DM fraction given in equation (4.0.25) is 1, in orange, or 10^{-2}, in yellow which are allowed by the upper limits shown in (figure 1). Each lower limit on m_a excludes the region above and to the right of the corresponding red line under the condition that $T_w < 10^{-2}V$. Other consistency conditions, $T_{ann} < 10^{-2}\ T_w < 10^{-4}\ V$ and $T_w < T_{ann}$, reject the regions above the thick blue line and below the dashed green line, respectively.

1 $M_\odot$. PBHs in this range could potentially account for some observed events, such as those found by HSC [Nii19b] as well as other microlensing observations [Tis07] and observations made by LIGO [Sas16].

As we explain in the chapter on self-consistency bounds, the requirement that walls form well after strings appear, i.e. $T_w \ll V$, implies a lower limit on m_a that

translates into a region in figure 5.2 being excluded. Writing this assumption more precisely as $T_w < 10^{-2}\ V$ lets us obtain the limits shown in figure 5.2 as red lines. Each lower limit on the ALP mass (from 1 GeV to 1 TeV) excludes the region above and to the right of the corresponding red line, meaning that larger values of m_a are only possible to the left of the corresponding line. These limits exclude values of M_{PBH} lower than $10^{-2}\ M_\odot$ for $f_{PBH} = 10^{-2}$. The consistency conditions $T_{ann} < 10^{-2}$ and $T_w < 10^{-2}$ combine to reject the regions above the thick blue line in figure 5.2. Finally, requiring that the string-wall network does not dominate the energy density of the universe, i.e. $T_{wd} < T_{ann}$, rejects the region below the green dashed line and thus does not affect any of the regions of interest.

Notice that some of the above mentioned consistency conditions depend on T_w and thus on m_a. Therefore, changing the assumption that m_a does not depend on temperature may also change these conditions. However, the results that depend only on wall annihilation, i.e. those that contribute to the present density of PBHs and GWs due to catastrogenesis, are independent of this assumption, since annihilation happens late enough for $m_a(T)$ to have reached its asymptotic value.

CHAPTER 6

Additional Limits and Bounds

The main relics from string-wall annihilation that we discuss in this paper are cold dark matter, gravitational waves, and primordial black holes. However, there are other phenomenological bounds that do not additionally constrain our models but are still worth noting here. For example, The string-wall network would be present during Big Bang Nucleosynthesis, thus it contributes to the effective number of neutrino species [HKS11a],

$$\Delta N_{eff}^{walls} \simeq 2.1 \times 10^{-21} \left(\frac{f_\sigma m_a}{N^2 \ eV} \right) \left(\frac{V}{GeV} \right)^2 . \tag{6.0.1}$$

In the range of interest of our parameters N_{eff} is always much smaller than present upper limits (which are close to 0.5 [Agh20]).

For self-consistency, walls must form before annihilating, i.e. $T_{ann} < T_w$, which implies a weak upper limit on the bias,

$$\epsilon_b < 0.5 f_\sigma \left[\frac{g_\star(T_{ann})}{g_\star(T_w)} \right]^{1/2} . \tag{6.0.2}$$

The string-wall network would eventually dominate the energy density of the

Universe at a temperature T_{wd} (assuming radiation domination),

$$T_{wd} = \left[\frac{40}{\pi^2 g_*(T_{wd})}\right]^{1/4} \left(\frac{\sigma}{m_P}\right)^{1/2} = \frac{3.4\times10^{-14}\,GeV}{[g_\star(T_{wd})]^{1/4}} \left(\frac{V}{N\ GeV}\right) \left(\frac{f_\sigma\ m_a}{eV}\right)^{1/2}. \tag{6.0.3}$$

We require that the string-wall network annihilated before, i.e. $T_{ann} > T_{wd}$, which implies a lower limit on the bias,

$$\frac{V_{bias}}{GeV^4} > 2.4\times10^{-37} \left(\frac{\sigma}{GeV^3}\right)^2 \left[\frac{g_*(T_{ann})}{g_\star(T_{wd})}\right]^{1/2}. \tag{6.0.4}$$

or

$$\epsilon_b > 2.39\times10^{-37} \left[\frac{g_*(T_{ann})}{g_*(T_{wd})}\right]^{1/2} \left(\frac{f_\sigma\ V}{N\ GeV}\right)^2. \tag{6.0.5}$$

In total, the self-consistency limits described above can be summarized along with the need for strings to form after inflation as the requirement that 10^{16} GeV $> V \gg T_w \gg T_{ann} > T_{wd}$. Conservatively, we require that $T_w/V \lesssim 10^{-2}$ and $T_{ann} \lesssim 10^{-2}$.

Our model has three independent parameters, which at the level of the Lagrangian in equation (1.3.1) are V, v, and $\epsilon_b \ll 1$. We may also choose m_a to be an independent parameter instead of v using the relationship in equation (1.5.3) as long as we assume $m_a \ll V$. In our case, however, the most convenient choice of parameters is the annihilation temperature T_{ann}, the PBH mass M_{PBH}, and m_a. In terms of these parameters,

$$V \simeq \frac{3}{16\pi}\left(\frac{10}{\pi}\right)^{1/4} \frac{N M_P^{7/2}}{f_\sigma^{1/2}[g_*(T_{ann})]^{1/4} m_a^{1/2} T_{ann} M_{PBH}}, \tag{6.0.6}$$

or alternatively

$$V \simeq 1.4 \times 10^{12}\ \text{GeV} \frac{N}{f_\sigma^{1/2}} \left(\frac{105}{g_*(T_{ann})}\right)^{1/4} \left(\frac{1\ \text{GeV}}{m_a}\right)^{1/2} \left(\frac{10^6\ \text{GeV}}{T_{ann}}\right) \left(\frac{10^{-10}\ M_\odot}{M_{PBH}}\right). \tag{6.0.7}$$

Likewise, we may also write the scale of the bias term as

$$\epsilon_b = 1.2 \times 10^{-5} \left(\frac{g_*(T_{ann})}{105}\right)^{1/2} \left(\frac{T_{ann}}{10^6\ \text{GeV}}\right)^2 \left(\frac{1\ \text{GeV}}{m_a}\right). \tag{6.0.8}$$

As shown in equation (1.5.6), T_w only depends on m_a. We may then write m_a in terms of the ratio T_w/V,

$$m_a \simeq 29\ \text{GeV} \frac{(T_w/V)}{10^{-2}} \frac{N}{f_\sigma^{1/2}} \left(\frac{g_*(T_w)}{g_*(T_{ann})}\right)^{1/4} \left(\frac{10^6\ \text{GeV}}{T_{ann}}\right) \left(\frac{10^{-10} M_\odot}{M_{PBH}}\right) \tag{6.0.9}$$

from which a lower limit on m_a for fixed T_w/V imposes a limit in the T_{ann}, M_{PBH} plane. These limits are shown in figure 5.2 as red lines for $m_a > 1$ GeV, 10 GeV, 100 GeV, and 1 TeV, where they reject the regions above and to the right of each line, and in figure 4.2 where the regions below and to the left of each line are rejected. As T_w/V decreases, these limits become stronger, rejecting larger regions of the parameter space.

Using equation (1.3.6), we may write the Hubble parameter at the temperature at which strings appear $T \sim V$ as

$$H(V) = 1.4 \times 10^{-2} \left[\frac{V}{10^{16}\ \text{GeV}}\right] V \left[\frac{g_*(V)}{105}\right]^{1/2}. \tag{6.0.10}$$

Requiring that $H(T_w) < H(V)$, i.e. that walls appear sufficiently after strings,

implies

$$m_a < 4.2 \times 10^{-2} \left[\frac{V}{10^{16}\text{GeV}}\right] V \left[\frac{g_*(V)}{105}\right]^{1/2} < 4.2 \times 10^{-2}\ V \left[\frac{g_*(V)}{105}\right]^{1/2} . \quad (6.0.11)$$

Combining this with the upper limit due to inflation $V < 10^{16}$ GeV implies that $m_a \lesssim 10^{-2}\ V$.

Making use of equation (1.5.19) and our assumption that $f_\sigma = 6$ allows us to estimate $H(T_{ann}) \simeq \epsilon_b m_a/8.46$, meaning that the condition that $H(T_{ann})/H(T_w) \ll 1$ is equivalent to requiring that ϵ_b be sufficiently small. Since $H(T_w) \simeq m_a/3$ and $H(T_{ann})/H(T_w) = (T_{ann}/T_w)^2$, we may write

$$\epsilon_b = 2.8 \left(\frac{T_{ann}}{T_w}\right)^2 . \quad (6.0.12)$$

This means that a small value of ϵ_b naturally implies that $T_{ann} \ll T_w$.

If we extract m_a from the ratio T_{ann}/T_w we find that

$$m_a \simeq 4.2 \times 10^{-2}\ \text{GeV} \left(\frac{10^{-2}}{T_{ann}/T_w}\right)^2 \left(\frac{g_*(T_w)}{105}\right)^{1/2} \left(\frac{T_{ann}}{10^6\ \text{GeV}}\right)^2 . \quad (6.0.13)$$

Setting this equal to the expression for m_a in equation (6.0.9) lets us obtain the relation

$$\frac{T_{ann}}{10^6\ \text{GeV}} \simeq 8.9 \frac{N^{1/3}}{f_\sigma^{1/6}} \left(\frac{105}{g_*(T_w)} \frac{105}{g_*(T_{ann})}\right)^{1/12} \left(\frac{10^{-10} M_\odot}{M_{PBH}}\right)^{1/3} \left(\frac{(T_w/V)}{10^{-2}}\right)^{2/3} \left(\frac{(T_{ann}/T_w)}{10^{-2}}\right)^{1/3} . \quad (6.0.14)$$

If we require that $T_w/V < 10^{-2}$ and $T_{ann}/T_w < 10^{-2}$, this last expression imposes an M_{PBH}-dependent upper limit on T_{ann}, which is the thick blue line in figure 5.2 and figure 4.2.

The last bound on our model is the requirement that wall domination does not occur before annihilation. The Hubble parameter when this occurs is given in equation (1.5.14). Combining this with the requirement that $H(T_{wd}) < H(T_{ann}) \simeq 0.33(T_{ann}/T_w)^2 m_a$ gives the relation

$$\frac{V}{10^{16}\text{ GeV}} < 3.5 \times 10^2 \left(\frac{T_{ann}}{T_w}\right). \tag{6.0.15}$$

This condition is automatically fulfilled if $T_{ann}/T_w = 10^{-2}$ since the need for strings to form after inflation requires that $V < 10^{16}$ GeV. For smaller values of this ratio, the condition in equation (6.0.15) can also be written as

$$\frac{T_{wd}}{T_{ann}} \simeq 4.8 \times 10^{-4} \left(\frac{105}{g_*(T_{ann})}\right)^{1/4} \left(\frac{105}{g_*(T_{wd})}\right)^{1/4} \left(\frac{10^6\text{ GeV}}{T_{ann}}\right)^2 \left(\frac{10^{-10} M_\odot}{M_{PBH}}\right) < 1. \tag{6.0.16}$$

This limit rejects the region below and to the left of the dashed green line in figure 5.2, and thus does not constrain any of the regions of interest.

Recent arguments made by Gorghetto and Hardy have suggested that there are constraints on the SSB scale V due to isocurvature fluctuations that come from stable ALPs [GH23]. In particular, if axions are produced late enough then their energy density could exhibit significant inhomogeneities in tension with the upper bounds given by CMB observations (see e.g. [Cro03, Fei20, Bal21]). However, because of the large uncertainties involved in calculating these limits as well as the relatively high annihilation temperatures in our models, we neglect to include this bound in our discussion or in any of our figures.

CHAPTER 7

Bias from Planck Scale Physics

Both models presented in this thesis are agnostic as to the bias term in the potential in equation (1.3.1). However, it is worth exploring where it might come from. As stated previously, quantum gravity should break any global symmetry at some energy scale, since classical black holes have no global charge [HO21]. Thus, we expect that for a global U(1) symmetry there should be a series of Planck-suppressed

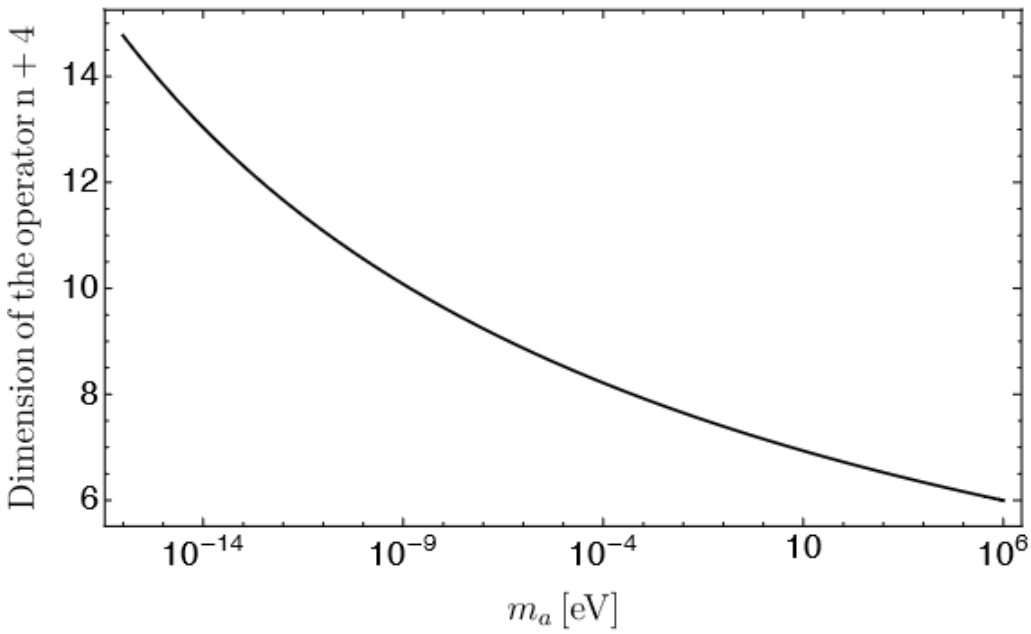

Figure 7.1: A plot of the required dimensionality of the bias term as a function of the ALP mass. We can see that theories with lower ALP masses will require significantly more fine-tuning than those where the ALP mass is greater than 1 GeV.

terms of dimension $n+4$ terms that break it, i.e.

$$\mathcal{L}_I^{QG} \sim \sum_{n=1}^{\infty} g_P^{(n)} \phi^3 (\phi e^{-i\delta} + \phi^* e^{i\delta}) \frac{\phi^n}{m_P^n}. \tag{7.0.1}$$

In the case of the QCD axion, the bias term is necessary for the string-wall network to annihilate when $N > 1$ in the post-inflationary scenario [Sik82]. However, similar operators can spoil the solution to the strong CP problem [GHW81], which is known as the "axion quality problem" [Sik21, DGN20b]. In particular, this spoiling happens for Planck suppressed operators of dimension $n+4 < 10$, meaning that any explicit breaking should be due to an operator of dimension $n+4 \geq 10$. Note that operators of dimension 10, 11, and 12 efficiently annihilate the string-wall network [BS92, KM92].

Therefore, we expect that the bias in the general ALP scenario would be produced by a Planck-suppressed operator whose scale is

$$V_{bias} = \epsilon_b v^4 = g_P V^4 \frac{V^n}{m_P^n}. \tag{7.0.2}$$

where $|\phi| \sim V$ after SSB. If we assume that g_P is of order one, we can also take the logarithm of this expression to find

$$\log \epsilon_b \frac{v^4}{V^4} = n \log \frac{V}{m_P}. \tag{7.0.3}$$

Although the production of heavier ALPs requires small biases to produce observable GWs, we find that the dimension n required decreases with m_a. We may write equation (7.0.3) in terms of m_a using equations (1.5.16) and (1.5.3). The results of this are shown in figure 7.1. We see that the dimension of this operator goes down for heavier ALP masses, and therefore the theory requires less fine-tuning for the

unstable case than for the stable case.

CHAPTER 8

Calculation of the Redshift Factor due to Cosmological Expansion

Due to the expansion of the universe, all of the density parameters calculated in this paper are redshifted by different powers of the ratio of the scale factor at the time of production and the scale factor at the present day $R(t_{production})/R(t_0)$. It is possible to calculate this for a given production time by solving the Friedmann equations under the proper initial conditions. However, it is often easier to calculate this quantity in terms of corresponding temperatures instead, i.e. $R(T_{production})/R(T_0)$. To do so, we assume that the entropy per comoving volume $R^3 s(T)$ is conserved, where $s(T)$ is the entropy density of the background, given by

$$s(T) = \frac{2g_{s*}(T)\pi^2}{45}T^3 \tag{8.0.1}$$

where $g_{s*}(T)$ is the number of effective entropy degrees of freedom due to the number of particle species that are present in the universe at a temperature T.

Equation (8.0.1) and conservation of entropy per comoving volume imply that

$$R^3(T)g_{s*}(T)\ T^3 = R^3(T_0)g_{s*}(T_0)\ T_0^3 \tag{8.0.2}$$

where $T_0 = 2.35 \times 10^{-4}$ eV is the temperature of the photon background of the universe and $g_{s*}(T_0) \approx 3.93$ is the current number of entropy degrees of freedom.

This then implies that

$$\left(\frac{R(T)}{R(T_0)}\right)^3 = \frac{g_{s*}(T_0)\ T_0^3}{g_{s*}(T)\ T^3}. \tag{8.0.3}$$

The energy density of ALPs from wall annihilation given in equation (2.3.3) is multiplied by this factor for $T = T_{ann}$; plugging equation (1.5.18) into equation (8.0.3) gives a redshift factor of

$$\left(\frac{R(T_{ann})}{R(T_0}\right)^3 = 3.38 \times 10^{-66} \left(\frac{f_\sigma A}{\epsilon_b N}\right)^{3/2} \left(\frac{v}{GeV}\right)^{-3} \left(\frac{V}{GeV}\right)^{3/2} \left(\frac{g_*(T_{ann})}{10}\right)^{-1/4}. \tag{8.0.4}$$

While this equation is in terms of three parameters, it can be written more efficiently in terms of two, i.e. σ and V_{bias}, which are given in equations (1.5.10) and (1.5.16), respectively. The result is

$$\left(\frac{R(T_{ann})}{R(T_0}\right)^3 = 3.38 \times 10^{-66}\ A^{3/2} \left(\frac{\sigma}{V_{bias}}\right)^{3/2} \left(\frac{g_*(T_{ann})}{10}\right)^{-1/4}. \tag{8.0.5}$$

CHAPTER 9

Estimation of the GW Spectrum Emitted by Walls

The power dependence of the approximate GW spectrum shown in figure 3.1 has been calculated exactly by numerical simulations [HKS10, HKS14, KS11, HKS13]. However, it is also possible to estimate it by treating the sub- and super-horizon scales approximately, i.e. finding the power-dependence of Ω_{gw} as given in equation (1.6.10). To do so, we will sketch the derivation given in [CDK09].

For convenience, let us introduce the dimensionless stress tensor, which is defined as

$$\Pi_{ij} = \frac{T_{ij}}{R^2 \rho_X} \tag{9.0.1}$$

where ρ_X is the energy density of the source and T_{ij} is its stress tensor as written in equation (1.6.6). For cosmological sources, we may always assume that this tensor is anisotropic and homogeneous, and therefore the average power of the source $P_s(\vec{x}, \vec{x}', t, t')$ can be written as

$$\langle \Pi_{ij}(\vec{x}, t) \Pi_{ij}(\vec{x}', t') \rangle = P_s(|\vec{x} - \vec{x}'|, t, t'). \tag{9.0.2}$$

In momentum space where we define $\vec{z} = \vec{x} - \vec{x}'$ and $z = |\vec{z}|$, we have

$$\left\langle \Pi_{ij}(\vec{k}, t) \Pi_{ij}(\vec{k}', t') \right\rangle = (2\pi)^3 \delta^3(\vec{k} - \vec{k}') \int d^3\vec{z} e^{i\vec{k}\cdot\vec{z}} P_s(z, t, t') \tag{9.0.3}$$

and

$$P_s(k,t,t') = 4\pi \int_0^\infty z^2 dz \frac{\sin(kz)}{kz} P_s(z,t,t'). \tag{9.0.4}$$

Per [CDK09], we also assume that the equal time anisotropic power spectrum is separable, i.e.

$$P_s(k,t,t) = |F(k)|^2 |g(t)|^2. \tag{9.0.5}$$

A causal source will have a correlation function that is zero for values of z greater than some given correlation scale R, meaning that at large enough scales (i.e. as k approaches 0) the spectrum should approach a white noise spectrum. In addition, we note that this quantity is proportional to the quantity given in equation (1.6.11), meaning that for the GW energy given in equation (1.6.9) to be finite we need $k^3|F(k)|^2$ to decay as k approaches infinity. An example spectrum that has these properties and is also dimensionally correct is

$$|F(k)|^2 = \frac{R^3}{1+(kR)^4} \tag{9.0.6}$$

where R is the characteristic length scale of the source.

For domain walls, we may simplify equation (9.0.3) by assuming that GWs are generated by a series of short, totally uncorrelated events. For a single event that begins at time t_* and ends at another time $t_* + 1/\beta$, this is equivalent to assuming that $1/\beta$ is much smaller than the Hubble time H^{-1} and that each event is causally

disconnected from the others. In this case, the correlation function becomes

$$\left\langle \Pi_{ij}(\vec{k},t)\Pi_{ij}(\vec{k}',t')\right\rangle = (2\pi)^3\delta(\vec{k}-\vec{k}')\frac{\delta(t-t')}{\beta}|F(k)|^2|g(t)|^2. \tag{9.0.7}$$

The anisotropic stress power spectrum can then be obtained,

$$P_s(k,t,t') = \frac{\delta(t-t')}{\beta}|F(k)|^2|g(t)|^2$$

$$P_s(k,k,k) = \frac{|F(k)|^2}{\beta}\int_{-\infty}^{\infty} dt|g(t)|^2. \tag{9.0.8}$$

By comparing equations (1.6.11) and the above equations, we see that

$$\Omega_{gw} \simeq \frac{4\Omega_{rad}}{3\pi^2}\left(\frac{\Omega_X}{\Omega_{rad}}\right)^2 H_* k^3 P_s(k,k,k) \tag{9.0.9}$$

and thus the power dependence of the spectrum is also the power dependence of $k^3P_s(k,k,k)$. From equation (9.0.8), we see that for uncorrelated sources this only depends on $|F(k)|^2$, from which we immediately can tell that the spectrum has a k^3 dependence for low frequencies and a k^{-1} dependence for high frequencies, which results in the approximate spectrum shown in 3.1.

CHAPTER 10

Conclusions

ALPs are a viable dark matter candidate. In addition to direct detection, there are several ways of probing models of both stable and unstable ALPs, which are Pseudo-Nambu Goldstone bosons associated with a spontaneously and explicitly broken U(1) symmetry. In these models, a string-wall network forms that then annihilates due to an energy bias between the vacua of the theory. We refer to the production of ALPs, GWs, and PBHs as a result of this process as "catastrogenesis." A cosmological probe of these models is the produced gravitational wave spectrum. In the case of stable ALPs, the GW spectrum could be observable with peak frequencies between 5×10^{-17} and 10^{-15} Hz and density parameters between 10^{-15} and 10^{-12}, which lie within the reach of future CMB measurements. For the case of unstable ALPs, they would be observable between frequencies of 5×10^{-5} and 500 Hz and density parameters anywhere between 10^{-22} and 10^{-9}, which is within the reach of future interferometry experiments. Another indirect probe of ALP models is the formation of primordial black holes. Unstable ALPs where the ALP mass is above 1 GeV will result in small black holes of masses between 10^{-16} all the way up to 1 $M_\odot$, and for masses up to 10^{-10} $M_\odot$ PBHs could constitute all of the DM. In contrast, stable ALPs will produce supermassive PBHs that between masses of 10^8 to 10^{12} $M_\odot$. In either case, there are significant windows of the parameter space that could be excluded by future observations.

BIBLIOGRAPHY

[AAJ20] Paola Arias, Ariel Arza, Joerg Jaeckel, and Diego Vargas-Arancibia. "Hidden Photon Dark Matter Interacting via Axion-like Particles." 7 2020.

[Abb16] B. P. Abbott et al. "Observation of Gravitational Waves from a Binary Black Hole Merger." *Phys. Rev. Lett.*, **116**(6):061102, 2016.

[ABD17] David Alesini, Danilo Babusci, Daniele Di Gioacchino, Claudio Gatti, Gianluca Lamanna, and Carlo Ligi. "The KLASH Proposal." 7 2017.

[ABK10] Bobby Samir Acharya, Konstantin Bobkov, and Piyush Kumar. "An M Theory Solution to the Strong CP Problem and Constraints on the Axiverse." *JHEP*, **11**:105, 2010.

[Abr02] Matthew E. Abroe et al. "Frequentist estimation of cosmological parameters from the MAXIMA-1 cosmic microwave background anisotropy data." *Mon. Not. Roy. Astron. Soc.*, **334**:11, 2002.

[Abr13] A. Abramowski et al. "Constraints on axionlike particles with H.E.S.S. from the irregularity of the PKS 2155-304 energy spectrum." *Phys. Rev. D*, **88**(10):102003, 2013.

[ADD10] Asimina Arvanitaki, Savas Dimopoulos, Sergei Dubovsky, Nemanja Kaloper, and John March-Russell. "String Axiverse." *Phys. Rev. D*, **81**:123530, 2010.

[Ade18] P. A. R. Ade et al. "BICEP2 / Keck Array x: Constraints on Primordial Gravitational Waves using Planck, WMAP, and New BICEP2/Keck Observations through the 2015 Season." *Phys. Rev. Lett.*, **121**:221301, 2018.

[ADG14] Adrian Ayala, Inma Domínguez, Maurizio Giannotti, Alessandro Mirizzi, and Oscar Straniero. "Revisiting the bound on axion-photon coupling from Globular Clusters." *Phys. Rev. Lett.*, **113**(19):191302, 2014.

[ADG20] Asimina Arvanitaki, Savas Dimopoulos, Marios Galanis, Luis Lehner, Jedidiah O. Thompson, and Ken Van Tilburg. "Large-misalignment mechanism for the formation of compact axion structures: Signatures from the QCD axion to fuzzy dark matter." *Phys. Rev. D*, **101**(8):083014, 2020.

[Afz23] Adeela Afzal et al. "The NANOGrav 15 yr Data Set: Search for Signals from New Physics." *Astrophys. J. Lett.*, **951**(1):L11, 2023.

[Agh20] N. Aghanim et al. "Planck 2018 results. VI. Cosmological parameters." *Astron. Astrophys.*, **641**:A6, 2020.

[Aje16] M. Ajello et al. "Search for Spectral Irregularities due to Photon–Axionlike-Particle Oscillations with the Fermi Large Area Telescope." *Phys. Rev. Lett.*, **116**(16):161101, 2016.

[al12] T. Hiramatsu et. al. "Production of dark matter axions from collapse of string-wall systems." *Phys. Rev. D*, **86**, 2012.

[Ale19] D. Alesini et al. "Galactic axions search with a superconducting resonant cavity." *Phys. Rev. D*, **99**(10):101101, 2019.

[All01] R. A. Allsman et al. "MACHO project limits on black hole dark matter in the 1-30 solar mass range." *Astrophys. J. Lett.*, **550**:L169, 2001.

[Ama17] Pau Amaro-Seoane et al. "Laser Interferometer Space Antenna.", 2017.

[Ana17] V. Anastassopoulos et al. "New CAST Limit on the Axion-Photon Interaction." *Nature Phys.*, **13**:584–590, 2017.

[And07] S. Andriamonje et al. "An Improved limit on the axion-photon coupling from the CAST experiment." *JCAP*, **04**:010, 2007.

[AS83] L. F. Abbott and P. Sikivie. "A Cosmological Bound on the Invisible Axion." *Phys. Lett. B*, **120**:133–136, 1983.

[Asz10] S. J. Asztalos et al. "A SQUID-based microwave cavity search for dark-matter axions." *Phys. Rev. Lett.*, **104**:041301, 2010.

[Bac21a] K. M. Backes et al. "A quantum-enhanced search for dark matter axions." *Nature*, **590**(7845):238–242, 2021.

[Bac21b] D. Backhouse. *The Phenomenological Motivation of Axions: A Review.* PhD thesis, University of Oxford, 2021.

[Bad20] L. Badurina et al. "AION: an atom interferometer observatory and network." *Journal of Cosmology and Astroparticle Physics*, **2020**(05):011–011, may 2020.

[Bak06] C. A. Baker et al. "Improved Experimental Limit on the Electric Dipole Moment of the Neutron." *Phys. Rev. Lett.*, 2006.

[Bal15] R. Ballou et al. "New exclusion limits on scalar and pseudoscalar axionlike particles from light shining through a wall." *Phys. Rev. D*, **92**(9):092002, 2015.

[Bal21] Guillermo Ballesteros et al. "Revisiting isocurvature bounds in models unifying the axion with the inflaton." *Journal of Cosmology and Astroparticle Physics*, **2021**(09):036, 2021.

[Ban20] D Banerjee et al. "Search for axionlike and scalar particles with the NA64 experiment." *Physical Review Letters*, **125**(8):081801, 2020.

[Bar19] Leor Barack et al. "Black holes, gravitational waves and fundamental physics: a roadmap." *Class. Quant. Grav.*, **36**(14):143001, 2019.

[BC19a] Mathieu Boudaud and Marco Cirelli. "Voyager 1 $e^{\pm}$ Further Constrain Primordial Black Holes as Dark Matter." *Phys. Rev. Lett.*, **122**(4):041104, 2019.

[BC19b] Mathieu Boudaud and Marco Cirelli. "Voyager 1 e±further constrain

primordial black holes as dark matter." *Physical Review Letters*, **122**(4):041104, 2019.

[BCS57] J. Bardeen, L. N. Cooper, and J. R. Schrieffer. "Theory of Superconductivity." *Phys. Rev.*, **108**:1175–1204, Dec 1957.

[BD06] P Battinelli and S Demers. "The C star population of DDO 190." *Astronomy & Astrophysics*, **447**(2):473–480, 2006.

[Ber85] F Bergsma et al. "Search for axion-like particle production in 400 GeV proton-copper interactions." *Physics Letters B*, **157**(5-6):458–462, 1985.

[Ber00] L. Bergstrom. "Non-Baryonic Dark Matter - Observational Evidence and Detection Methods." *Rept. Prog. Phys.*, **63**(793), 2000.

[Ber18] Jeffrey M. Berryman et al. "Lepton-Number-Charged Scalars and Neutrino Beamstrahlung." *Phys. Rev. D*, **97**(7):075030, 2018.

[BES80] J. R. Bond, G. Efstathiou, and J. Silk. "Massive Neutrinos and the Large-Scale Structure of the Universe." *Phys. Rev. Lett.*, **45**:1980–1984, Dec 1980.

[BFH22] Malte Buschmann, Joshua W. Foster, Anson Hook, Adam Peterson, Don E. Willcox, Weiqun Zhang, and Benjamin R. Safdi. "Dark matter from axion strings with adaptive mesh refinement." *Nature Commun.*, **13**(1):1049, 2022.

[BGL20] Masha Baryakhtar, Marios Galanis, Robert Lasenby, and Olivier Simon. "Black hole superradiance of self-interacting scalar fields." 11 2020.

[BHK08] Kyu Jung Bae, Ji-Haeng Huh, and Jihn E. Kim. "Update of axion CDM energy." *JCAP*, **09**:005, 2008.

[BHL18] Masha Baryakhtar, Junwu Huang, and Robert Lasenby. "Axion and hidden photon dark matter detection with multilayer optical haloscopes." *Phys. Rev. D*, **98**(3):035006, 2018.

[BHS05] Gianfranco Bertone, Dan Hooper, and Joseph Silk. "Particle dark matter: Evidence, candidates and constraints." *Physics reports*, **405**(5-6):279–390, 2005.

[Blo30] Felix Bloch. "Zur theorie des ferromagnetismus." *Zeitschrift für Physik*, **61**(3-4):206–219, 1930.

[Blu91] J. Blümlein et al. "Limits on neutral light scalar and pseudoscalar particles in a proton beam dump experiment." *Zeitschrift für Physik C Particles and Fields*, **51**:341–350, 1991.

[BN92] R. D. Blandford and R. Narayan. "Cosmological Applications of Gravitational Lensing." *Annual Review of Astronomy and Astrophysics*, **30**(1):311–358, 1992.

[BNT17] Martin Bauer, Matthias Neubert, and Andrea Thamm. "Collider Probes of Axion-Like Particles." *JHEP*, **12**:044, 2017.

[Bon57] Hermann Bondi. "Plane gravitational waves in general relativity." *Nature*, **179**(4569):1072–1073, 1957.

[Bou18] C. Boutan et al. "Piezoelectrically Tuned Multimode Cavity Search for Axion Dark Matter." *Phys. Rev. Lett.*, **121**(26):261302, 2018.

[BPP82] George R. Blumenthal, Heinz Pagels, and Joel R. Primack. "GALAXY FORMATION BY DISSIPATIONLESS PARTICLES HEAVIER THAN NEUTRINOS." *Nature*, **299**:37–38, 1982.

[Bra20] T. Braine et al. "Extended Search for the Invisible Axion with the Axion Dark Matter Experiment." *Phys. Rev. Lett.*, **124**(10):101303, 2020.

[Brd20] Vedran Brdar et al. "Revisiting neutrino self-interaction constraints from Z and τ decays." *Physical Review D*, **101**(11):115001, 2020.

[BS92] Stephen M. Barr and D. Seckel. "Planck scale corrections to axion models."

Phys. Rev. D, **46**:539–549, 1992.

[BS02] Shmuel Balberg and Stuart L. Shapiro. "Gravothermal collapse of selfinteracting dark matter halos and the origin of massive black holes." *Phys. Rev. Lett.*, **88**:101301, 2002.

[BSI02] Shmuel Balberg, Stuart L. Shapiro, and Shogo Inagaki. "Selfinteracting dark matter halos and the gravothermal catastrophe." *Astrophys. J.*, **568**:475–487, 2002.

[BST82] J. R. Bond, A. S. Szalay, and M. S. Turner. "Formation of Galaxies in a Gravitino-Dominated Universe." *Phys. Rev. Lett.*, **48**:1636–1639, Jun 1982.

[BT18] Guillermo Ballesteros and Marco Taoso. "Primordial black hole dark matter from single field inflation." *Physical Review D*, **97**(2):023501, 2018.

[Cap22] A. Caputo et al. "Low-Energy Supernovae Severely Constrain Radiative Particle Decays." *Phys. Rev. Lett.*, **128**(22):221103, 2022.

[Car75] Bernard J Carr. "The Primordial black hole mass spectrum.", 1975.

[CC06] Vincent Corbin and Neil J Cornish. "Detecting the cosmic gravitational wave background with the big bang observer." *Classical and Quantum Gravity*, **23**(7):2435, 2006.

[CC20] Chia-Feng Chang and Yanou Cui. "Stochastic Gravitational Wave Background from Global Cosmic Strings." *Phys. Dark Univ.*, **29**:100604, 2020.

[CCC19] Jeremie Choquette, James M. Cline, and Jonathan M. Cornell. "Early formation of supermassive black holes via dark matter self-interactions." *JCAP*, **07**:036, 2019.

[CCM20] Thomas J. Clarke, Edmund J. Copeland, and Adam Moss. "Constraints on primordial gravitational waves from the Cosmic Microwave Background." *JCAP*, **10**:002, 2020.

[CDG17] Steven Clark, Bhaskar Dutta, Yu Gao, Louis E. Strigari, and Scott Watson. "Planck Constraint on Relic Primordial Black Holes." *Phys. Rev. D*, **95**(8):083006, 2017.

[CDK09] Chiara Caprini, Ruth Durrer, Thomas Konstandin, and Geraldine Servant. "General Properties of the Gravitational Wave Spectrum from Phase Transitions." *Phys. Rev. D*, **79**:083519, 2009.

[CDM17] Allen Caldwell, Gia Dvali, Béla Majorovits, Alexander Millar, Georg Raffelt, Javier Redondo, Olaf Reimann, Frank Simon, and Frank Steffen. "Dielectric Haloscopes: A New Way to Detect Axion Dark Matter." *Phys. Rev. Lett.*, **118**(9):091801, 2017.

[CGS16] Jorge L. Cervantes-Cota, Salvador Galindo-Uribarri, and George F. Smoot. "A Brief History of Gravitational Waves." *Universe*, **2**(3), 2016.

[Chk80] Dzh. L. Chkareuli. "Quark-lepton families: from SU(5) to SU(8) symmetry[1)]." *Soviet Journal of Experimental and Theoretical Physics Letters*, **32**(11):671–674, December 1980.

[CK17] Eric Cotner and Alexander Kusenko. "Primordial black holes from supersymmetry in the early universe." *Physical Review Letters*, **119**(3):031103, 2017.

[CK22] Bernard Carr and Florian Kühnel. "Primordial black holes as dark matter candidates." *SciPost Physics Lecture Notes*, p. 048, 2022.

[CKP21] Paolo Campeti, Eiichiro Komatsu, Davide Poletti, and Carlo Baccigalupi. "Measuring the spectrum of primordial gravitational waves with CMB, PTA and Laser Interferometers." *JCAP*, **01**:012, 2021.

[CKS10] B. J. Carr, Kazunori Kohri, Yuuiti Sendouda, and Jun'ichi Yokoyama. "New cosmological constraints on primordial black holes." *Phys. Rev. D*, **81**:104019, 2010.

[CKS20] Bernard Carr, Kazunori Kohri, Yuuiti Sendouda, and Jun'ichi Yokoyama. "Constraints on Primordial Black Holes." 2 2020.

[CKV21] Bernard Carr, Florian Kuhnel, and Luca Visinelli. "Constraints on Stupendously Large Black Holes." *Mon. Not. Roy. Astron. Soc.*, **501**(2):2029–2043, 2021.

[CLM22] Andrea Caputo, Hongwan Liu, Siddharth Mishra-Sharma, Maxim Pospelov, and Joshua T. Ruderman. "A Stimulating Explanation of the Extragalactic Radio Background." 6 2022.

[CMP81] Y. Chikashige, Rabindra N. Mohapatra, and R. D. Peccei. "Are There Real Goldstone Bosons Associated with Broken Lepton Number?" *Phys. Lett. B*, **98**:265–268, 1981.

[CMP21] Adam Coogan, Logan Morrison, and Stefano Profumo. "Direct detection of Hawking radiation from asteroid-mass primordial black holes." *Physical Review Letters*, **126**(17):171101, 2021.

[Col19] LIGO Scientific Collaboration. "Search for the isotropic stochastic background using data from Advanced LIGO's second observing run." *Physical Review D*, **100**(6):061101, 2019.

[CR12] Davide Cadamuro and Javier Redondo. "Cosmological bounds on pseudo Nambu-Goldstone bosons." *JCAP*, **02**:032, 2012.

[Cro03] Patrick Crotty et al. "Bounds on isocurvature perturbations from cosmic microwave background and large scale structure data." *Physical Review Letters*, **91**(17):171301, 2003.

[CRV22a] Andrea Caputo, Georg Raffelt, and Edoardo Vitagliano. "Muonic boson limits: Supernova redux." *Physical Review D*, **105**(3):035022, 2022.

[CRV22b] Andrea Caputo, Georg Raffelt, and Edoardo Vitagliano. "Muonic boson

limits: Supernova redux." *Phys. Rev. D*, **105**(3):035022, 2022.

[CRV22c] Andrea Caputo, Georg Raffelt, and Edoardo Vitagliano. "Radiative transfer in stars by feebly interacting bosons." *JCAP*, **08**(08):045, 2022.

[DAG17] Roberta Diamanti, Shin'ichiro Ando, Stefano Gariazzo, Olga Mena, and Christoph Weniger. "Cold dark matter plus not-so-clumpy dark relics." *JCAP*, **06**:008, 2017.

[DB09] L. Duffy and K. van Bibber. "Axions as dark matter particles." *New J. Phys.*, **11**, 2009.

[DBD17] JG De Swart, Gianfranco Bertone, and Jeroen van Dongen. "How dark matter came to matter." *Nature Astronomy*, **1**(3):0059, 2017.

[DDG22] Hooman Davoudiasl, Peter B. Denton, and Julia Gehrlein. "Supermassive Black Holes, Ultralight Dark Matter, and Gravitational Waves from a First Order Phase Transition." *Phys. Rev. Lett.*, **128**(8):081101, 2022.

[DEG16] Federico Della Valle, Aldo Ejlli, Ugo Gastaldi, Giuseppe Messineo, Edoardo Milotti, Ruggero Pengo, Giuseppe Ruoso, and Guido Zavattini. "The PVLAS experiment: measuring vacuum magnetic birefringence and dichroism with a birefringent Fabry–Perot cavity." *Eur. Phys. J. C*, **76**(1):24, 2016.

[Del18] J. Delabrouille et al. "Exploring cosmic origins with CORE: Survey requirements and mission design." *JCAP*, **04**:014, 2018.

[Den21a] Heling Deng. "μ-distortion around stupendously large primordial black holes." *JCAP*, **11**(11):054, 2021.

[Den21b] Heling Deng. "μ-distortion around stupendously large primordial black holes." , **2021**(11):054, November 2021.

[DF83] Michael Dine and Willy Fischler. "The Not So Harmless Axion." *Phys. Lett. B*, **120**:137–141, 1983.

[DFB87] Alan Dressler, SM Faber, David Burstein, Roger L Davies, Donald Lynden-Bell, RJ Terlevich, and Gary Wegner. "Spectroscopy and photometry of elliptical galaxies-A large-scale streaming motion in the local universe." *The Astrophysical Journal*, **313**:L37–L42, 1987.

[DFK11] Michael Dine, Guido Festuccia, John Kehayias, and Weitao Wu. "Axions in the Landscape and String Theory." *JHEP*, **01**:012, 2011.

[DFS81a] Michael Dine, Willy Fischler, and Mark Srednicki. "A Simple Solution to the Strong CP Problem with a Harmless Axion." *Phys. Lett. B*, **104**:199–202, 1981.

[DFS81b] Michael Dine, Willy Fischler, and Mark Srednicki. "A simple solution to the strong CP problem with a harmless axion." *Physics Letters B*, **104**(3):199–202, 1981.

[DFS20] Christopher Dessert, Joshua W. Foster, and Benjamin R. Safdi. "X-ray Searches for Axions from Super Star Clusters." *Phys. Rev. Lett.*, **125**(26):261102, 2020.

[DG19] William DeRocco and Peter W. Graham. "Constraining Primordial Black Hole Abundance with the Galactic 511 keV Line." *Phys. Rev. Lett.*, **123**(25):251102, 2019.

[DGN20a] Luca Di Luzio, Maurizio Giannotti, Enrico Nardi, and Luca Visinelli. "The landscape of QCD axion models." *Physics Reports*, **870**:1–117, 2020. The landscape of QCD axion models.

[DGN20b] Luca Di Luzio, Maurizio Giannotti, Enrico Nardi, and Luca Visinelli. "The landscape of QCD axion models." *Phys. Rept.*, **870**:1–117, 2020.

[DGV17] Heling Deng, Jaume Garriga, and Alexander Vilenkin. "Primordial black hole and wormhole formation by domain walls." *Journal of Cosmology and Astroparticle Physics*, **2017**(04):050, 2017.

[DHS21] Paul Frederik Depta, Marco Hufnagel, and Kai Schmidt-Hoberg. "Updated BBN constraints on electromagnetic decays of MeV-scale particles." *JCAP*, **04**:011, 2021.

[Dia23a] Melissa Diamond et al. "Axion-sourced fireballs from supernovae." *Phys. Rev. D*, **107**(10):103029, 2023.

[Dia23b] Melissa Diamond et al. "Multimessenger Constraints on Radiatively Decaying Axions from GW170817." 5 2023.

[DMP09] A. De Angelis, O. Mansutti, M. Persic, and M. Roncadelli. "Photon propagation and the VHE gamma-ray spectra of blazars: how transparent is really the Universe?" *Mon. Not. Roy. Astron. Soc.*, **394**:L21–L25, 2009.

[DN21] Subinoy Das and Ethan O. Nadler. "Constraints on the epoch of dark matter formation from Milky Way satellites." *Phys. Rev. D*, **103**(4):043517, 2021.

[Dol17] Matthew J Dolan et al. "Revised constraints and Belle II sensitivity for visible and invisible axion-like particles." *Journal of High Energy Physics*, **2017**(12):1–29, 2017.

[DRM07] Alessandro De Angelis, Marco Roncadelli, and Oriana Mansutti. "Evidence for a new light spin-zero boson from cosmological gamma-ray propagation?" *Phys. Rev. D*, **76**:121301, 2007.

[DS89] R. L. Davis and E. P. S. Shellard. "DO AXIONS NEED INFLATION?" *Nucl. Phys. B*, **324**:167–186, 1989.

[DTP18] Jeremy Darling, Alexandra E. Truebenbach, and Jennie Paine. "Astrometric Limits on the Stochastic Gravitational Wave Background." *Astrophys. J.*, **861**(2):113, 2018.

[Du18] N. Du et al. "A Search for Invisible Axion Dark Matter with the Axion Dark Matter Experiment." *Phys. Rev. Lett.*, **120**(15):151301, 2018.

[Due04] Norbert Duechting. "Supermassive black holes from primordial black hole seeds." *Phys. Rev. D*, **70**:064015, 2004.

[Duf07] Jean-Fran çois Dufaux et al. "Theory and numerics of gravitational waves from preheating after inflation." *Phys. Rev. D*, **76**:123517, Dec 2007.

[DV17] Heling Deng and Alexander Vilenkin. "Primordial black hole formation by vacuum bubbles." *JCAP*, **12**:044, 2017.

[DW11] Subinoy Das and Neal Weiner. "Late Forming Dark Matter in Theories of Neutrino Dark Energy." *Phys. Rev. D*, **84**:123511, 2011.

[Ehr10] Klaus Ehret et al. "New ALPS Results on Hidden-Sector Lightweights." *Phys. Lett. B*, **689**:149–155, 2010.

[El 20] Yousef Abou El-Neaj et al. "AEDGE: Atomic Experiment for Dark Matter and Gravity Exploration in Space." *EPJ Quantum Technology*, **7**(1), mar 2020.

[Fei20] Martin Feix et al. "Post-inflationary axion isocurvature perturbations facing CMB and large-scale structure." *Journal of Cosmology and Astroparticle Physics*, **2020**(11):046, 2020.

[Fer22] Ricardo Z Ferreira et al. "High Quality QCD Axion at Gravitational Wave Observatories." *Physical Review Letters*, **128**(14):141101, 2022.

[FG79] S. M. Faber and J. S. Gallagher. "Masses and Mass-To-Light Ratios of Galaxies." *Annual Review of Astronomy and Astrophysics*, **17**(1):135–187, 1979.

[FK18] Alexander Franklin and Eleanor Knox. "Emergence without limits: The case of phonons." *Studies in History and Philosophy of Science Part B: Studies in History and Philosophy of Modern Physics*, **64**:68–78, 2018.

[FK21] Marcos M Flores and Alexander Kusenko. "Primordial black holes from

long-range scalar forces and scalar radiative cooling." *Physical Review Letters*, **126**(4):041101, 2021.

[FKM20] Joshua W. Foster, Yonatan Kahn, Oscar Macias, Zhiquan Sun, Ralph P. Eatough, Vladislav I. Kondratiev, Wendy M. Peters, Christoph Weniger, and Benjamin R. Safdi. "Green Bank and Effelsberg Radio Telescope Searches for Axion Dark Matter Conversion in Neutron Star Magnetospheres." *Phys. Rev. Lett.*, **125**(17):171301, 2020.

[FMM22] Ricardo Z. Ferreira, M. C. David Marsh, and Eike Müller. "Strong supernovae bounds on ALPs from quantum loops." *JCAP*, **11**:057, 2022.

[FMP19a] F. Ferrer, E. Masso, G. Panico, O. Pujolas, and F. Rompineve. "Primordial Black Holes from the QCD Axion." *Phys. Rev. Lett.*, **122**:10301, 2019.

[FMP19b] Francesc Ferrer, Eduard Masso, Giuliano Panico, Oriol Pujolas, and Fabrizio Rompineve. "Primordial Black Holes from the QCD axion." *Phys. Rev. Lett.*, **122**(10):101301, 2019.

[FN79] C.D. Froggatt and H.B. Nielsen. "Hierarchy of quark masses, cabibbo angles and CP violation." *Nuclear Physics B*, **147**(3):277–298, 1979.

[Fri79] Aleksandr Friedmann. "On the curvature of space." In *A Source Book in Astronomy and Astrophysics, 1900–1975*, pp. 838–843. Harvard University Press, 1979.

[FRV22] Damiano F. G. Fiorillo, Georg G. Raffelt, and Edoardo Vitagliano. "Strong Supernova 1987A Constraints on Bosons Decaying to Neutrinos." 9 2022.

[G 05] J. Silk G. Bertone, D. Hooper. "Particle dark matter: evidence, candidates, and constraints." *Phys. Rep.*, **405**:279–390, 2005.

[GCK07] Daniel Grin, Giovanni Covone, Jean-Paul Kneib, Marc Kamionkowski, Andrew Blain, and Eric Jullo. "A Telescope Search for Decaying Relic

Axions." *Phys. Rev. D*, **75**:105018, 2007.

[GCL14] Kim Griest, Agnieszka M. Cieplak, and Matthew J. Lehner. "Experimental Limits on Primordial Black Hole Dark Matter from the First 2 yr of Kepler Data." *Astrophys. J.*, **786**(2):158, 2014.

[GH23] Marco Gorghetto and Edward Hardy. "Post-inflationary axions: a minimal target for axion haloscopes." *JHEP*, **05**:030, 2023.

[GHN21] Marco Gorghetto, Edward Hardy, and Horia Nicolaescu. "Observing Invisible Axions with Gravitational Waves." 1 2021.

[GHW81] Howard M Georgi, Lawrence J Hall, and Mark B Wise. "Grand unified models with an automatic Peccei-Quinn symmetry." *Nuclear Physics B*, **192**(2):409–416, 1981.

[Gio20] Massimo Giovannini. "Primordial backgrounds of relic gravitons." *Prog. Part. Nucl. Phys.*, **112**:103774, 2020.

[GLW96] Juan Garcia-Bellido, Andrei Linde, and David Wands. "Density perturbations and black hole formation in hybrid inflation." *Physical Review D*, **54**(10):6040, 1996.

[GNY83a] G. B. Gelmini, S. Nussinov, and T. Yanagida. "Does Nature Like Nambu-Goldstone Bosons?" *Nucl. Phys. B*, **219**:31–40, 1983.

[GNY83b] Graciela B Gelmini, S Nussinov, and T Yanagida. "Does nature like Nambu-Goldstone bosons?" *Nuclear Physics B*, **219**(1):31–40, 1983.

[Gol61] Jeffrey Goldstone. "Field theories with Superconductor solutions." *Il Nuovo Cimento (1955-1965)*, **19**:154–164, 1961.

[Gou20] André de Gouvêa et al. "Leptonic Scalars at the LHC." *JHEP*, **07**:142, 2020.

[GPV21] Graciela B. Gelmini, Silvia Pascoli, Edoardo Vitagliano, and Ye-Ling Zhou.

"Gravitational wave signatures from discrete flavor symmetries." *JCAP*, **02**:032, 2021.

[GS89] Steven B. Giddings and Andrew Strominger. "String wormholes." *Physics Letters B*, **230**(1):46–51, 1989.

[GSS20] Yann Gouttenoire, Géraldine Servant, and Peera Simakachorn. "Beyond the Standard Models with Cosmic Strings." *JCAP*, **07**:032, 2020.

[GVZ16] Jaume Garriga, Alexander Vilenkin, and Jun Zhang. "Black holes and the multiverse." *Journal of Cosmology and Astroparticle Physics*, **2016**(02):064, 2016.

[Hal02] N. W. Halverson et al. "DASI first results: A Measurement of the cosmic microwave background angular power spectrum." *Astrophys. J.*, **568**:38–45, 2002.

[Han19] Shaul Hanany et al. "PICO: Probe of Inflation and Cosmic Origins." 3 2019.

[Haw71] Stephen Hawking. "Gravitationally collapsed objects of very low mass." *Monthly Notices of the Royal Astronomical Society*, **152**(1):75–78, 1971.

[Haw74a] "Black Holes in the Early Universe." *Mon. Not. Roy. Astron. Soc.*, **168**(399), 1974.

[Haw74b] Stephen W Hawking. "Black hole explosions?" *Nature*, **248**(5443):30–31, 1974.

[Haw75] Stephen W Hawking. "Particle creation by black holes." *Communications in mathematical physics*, **43**(3):199–220, 1975.

[Haw89] Stephen William Hawking. "Black holes from cosmic strings." *Physics Letters B*, **231**(3):237–239, 1989.

[HBG00] Wayne Hu, Rennan Barkana, and Andrei Gruzinov. "Fuzzy Cold Dark

Matter: The Wave Properties of Ultralight Particles." *Phys. Rev. Lett.*, **85**:1158–1161, Aug 2000.

[Hea93] Oliver Heaviside. "A gravitational and electromagnetic analogy." *The Electrician*, **31**(Part I):281–282, 1893.

[HKL20] Anson Hook, Soubhik Kumar, Zhen Liu, and Raman Sundrum. "High Quality QCD Axion and the LHC." *Phys. Rev. Lett.*, **124**(22):221801, 2020.

[HKS10] Takashi Hiramatsu, Masahiro Kawasaki, and Ken'ichi Saikawa. "Gravitational Waves from Collapsing Domain Walls." *JCAP*, **05**:032, 2010.

[HKS11a] Takashi Hiramatsu, Masahiro Kawasaki, and Kenichi Saikawa. "Evolution of String-Wall Networks and Axionic Domain Wall Problem." *Jour. Cosm. Astr. Phys.*, **2011**:030–056, 2011.

[HKS11b] Takashi Hiramatsu, Masahiro Kawasaki, Toyokazu Sekiguchi, Masahide Yamaguchi, and Jun'ichi Yokoyama. "Improved estimation of radiated axions from cosmological axionic strings." *Phys. Rev. D*, **83**:123531, 2011.

[HKS13] Takashi Hiramatsu, Masahiro Kawasaki, Ken'ichi Saikawa, and Toyokazu Sekiguchi. "Axion cosmology with long-lived domain walls." *JCAP*, **01**:001, 2013.

[HKS14] Takashi Hiramatsu, Masahiro Kawasaki, and Ken'ichi Saikawa. "On the estimation of gravitational wave spectrum from cosmic domain walls." *JCAP*, **02**:031, 2014.

[HL01] Zoltan Haiman and Abraham Loeb. "What is the highest plausible redshift of luminous quasars?" *Astrophys. J.*, **552**:459, 2001.

[HMS82] Stephen William Hawking, IG Moss, and JM Stewart. "Bubble collisions in the very early universe." *Physical Review D*, **26**(10):2681, 1982.

[HO21] Daniel Harlow and Hirosi Ooguri. "Symmetries in quantum field theory and

quantum gravity." *Commun. Math. Phys.*, **383**(3):1669–1804, 2021.

[Hoo] Anson Hook. "TASI Lectures on the Strong CP Problem and Axions.".

[HS85] M. C. Huang and P. Sikivie. "The Structure of Axionic Domain Walls." *Phys. Rev. D*, **32**:1560, 1985.

[HS23] Sebastian Hoof and Lena Schulz. "Updated constraints on axion-like particles from temporal information in supernova SN1987A gamma-ray data." *Journal of Cosmology and Astroparticle Physics*, **2023**(03):054, 2023.

[HSS90] C. Hagmann, P. Sikivie, N. S. Sullivan, and D. B. Tanner. "Results from a search for cosmic axions." *Phys. Rev. D*, **42**:1297–1300, Aug 1990.

[IR18] Igor G. Irastorza and Javier Redondo. "New experimental approaches in the search for axion-like particles." *Prog. Part. Nucl. Phys.*, **102**:89–159, 2018.

[IVH20] Kohei Inayoshi, Eli Visbal, and Zoltán Haiman. "The Assembly of the First Massive Black Holes." *Ann. Rev. Astron. Astrophys.*, **58**:27–97, 2020.

[J 03] F. Takayama J. Feng, A. Rajaraman. "Superweakly Interacting Massive Particles." *Phys. Rev. Lett.*, **91**, 2003.

[JMR18] J Jaeckel, PC Malta, and J Redondo. "Decay photons from the axionlike particles burst of type II supernovae." *Physical Review D*, **98**(5):055032, 2018.

[JR10] Joerg Jaeckel and Andreas Ringwald. "The Low-Energy Frontier of Particle Physics." *Ann. Rev. Nucl. Part. Sci.*, **60**:405–437, 2010.

[Kav19] BJ Kavanagh. "bradkav/PBHbounds: Release version.", 2019.

[Kav20] Bradley J. Kavanagh. "bradkav / PBHbounds." https://github.com/bradkav/PBHbounds, July 2020.

[Kib76] T. W. B. Kibble. "Topology of cosmic domains and strings." *J. Phys. A: Math. Gen.*, **09**:1387, 1976.

[Kim79a] Jihn E. Kim. "Weak Interaction Singlet and Strong CP Invariance." *Phys. Rev. Lett.*, **43**:103, 1979.

[Kim79b] Jihn E. Kim. "Weak-Interaction Singlet and Strong CP Invariance." *Phys. Rev. Lett.*, **43**:103–107, Jul 1979.

[KK99] Marc Kamionkowski and Arthur Kosowsky. "The Cosmic microwave background and particle physics." *Ann. Rev. Nucl. Part. Sci.*, **49**:77–123, 1999.

[KKV19] Oleg E. Kalashev, Alexander Kusenko, and Edoardo Vitagliano. "Cosmic infrared background excess from axionlike particles and implications for multimessenger observations of blazars." *Phys. Rev. D*, **99**(2):023002, 2019.

[KLY17] Kunio Kaneta, Hye-Sung Lee, and Seokhoon Yun. "Portal Connecting Dark Photons and Axions." *Phys. Rev. Lett.*, **118**(10):101802, 2017.

[KM92] Marc Kamionkowski and John March-Russell. "Planck scale physics and the Peccei-Quinn mechanism." *Phys. Lett. B*, **282**:137–141, 1992.

[KM17] Vincent B. . Klaer and Guy D. Moore. "The dark-matter axion mass." *JCAP*, **11**:049, 2017.

[KMZ85] M Yu Khlopov, BA Malomed, and Ya B Zeldovich. "Gravitational instability of scalar fields and formation of primordial black holes." *Monthly Notices of the Royal Astronomical Society*, **215**(4):575–589, 1985.

[Kna17] Simon Knapen et al. "Searching for Axionlike Particles with Ultraperipheral Heavy-Ion Collisions." *Phys. Rev. Lett.*, **118**(17):171801, 2017.

[KRS05] Maxim. Yu. Khlopov, Sergei G. Rubin, and Alexander S. Sakharov. "Primordial structure of massive black hole clusters." *Astropart. Phys.*, **23**:265, 2005.

[KS11] Masahiro Kawasaki and Ken'ichi Saikawa. "Study of gravitational radiation

from cosmic domain walls." *JCAP*, **09**:008, 2011.

[KSS15] Masahiro Kawasaki, Ken'ichi Saikawa, and Toyokazu Sekiguchi. "Axion dark matter from topological defects." *Phys. Rev. D*, **91**(6):065014, 2015.

[KSS20] Alexander Kusenko, Misao Sasaki, Sunao Sugiyama, Masahiro Takada, Volodymyr Takhistov, and Edoardo Vitagliano. "Exploring Primordial Black Holes from the Multiverse with Optical Telescopes." *Phys. Rev. Lett.*, **125**:181304, 2020.

[KSZ21] Kevin J. Kelly, Manibrata Sen, and Yue Zhang. "Intimate Relationship between Sterile Neutrino Dark Matter and ΔNeff." *Phys. Rev. Lett.*, **127**(4):041101, 2021.

[LAC20] S. Lee, S. Ahn, J. Choi, B. R. Ko, and Y. K. Semertzidis. "Axion Dark Matter Search around 6.7 μeV." *Phys. Rev. Lett.*, **124**(10):101802, 2020.

[Lah19] Ranjan Laha. "Primordial Black Holes as a Dark Matter Candidate Are Severely Constrained by the Galactic Center 511 keV γ -Ray Line." *Phys. Rev. Lett.*, **123**(25):251101, 2019.

[Las16] Paul D. Lasky et al. "Gravitational-wave cosmology across 29 decades in frequency." *Phys. Rev. X*, **6**(1):011035, 2016.

[Lau11] R. Laureijs et al. "Euclid Definition Study Report." 10 2011.

[Lee01] A. T. Lee et al. "A High spatial resolution analysis of the MAXIMA-1 cosmic microwave background anisotropy data." *Astrophys. J. Lett.*, **561**:L1–L6, 2001.

[Lin19] Tongyan Lin. "Dark matter models and direct detection." *PoS*, **333**:009, 2019.

[LM02] M. Loewenstein and R. Mushotzky. "The nature of dark matter in elliptical galaxies: chandra x-ray observatory observations of ngc 4636." 8 2002.

[LMO47] Celso MG LATTES, Hugh Muirhead, Giuseppe PS Occhialini, and Cecil Frank Powell. "Processes involving charged mesons." *Nature*, **159**(4047):694–697, 1947.

[LMP19] Matthew Lawson, Alexander J. Millar, Matteo Pancaldi, Edoardo Vitagliano, and Frank Wilczek. "Tunable axion plasma haloscopes." *Phys. Rev. Lett.*, **123**(14):141802, 2019.

[LMS20] Ranjan Laha, Julian B. Muñoz, and Tracy R. Slatyer. "INTEGRAL constraints on primordial black holes and particle dark matter." *Phys. Rev. D*, **101**(12):123514, 2020.

[LR99] David H. Lyth and Antonio Riotto. "Particle physics models of inflation and the cosmological density perturbation." *Phys. Rept.*, **314**:1–146, 1999.

[Luc20] G. Lucente et al. "Heavy axion-like particles and core-collapse supernovae: constraints and impact on the explosion mechanism." *Journal of Cosmology and Astroparticle Physics*, **2020**(12):008, 2020.

[Luo16] Jun Luo et al. "TianQin: a space-borne gravitational wave detector." *Classical and Quantum Gravity*, **33**(3):035010, 2016.

[LV20] Marek Lewicki and Ville Vaskonen. "On bubble collisions in strongly supercooled phase transitions." *Physics of the Dark Universe*, **30**:100672, 2020.

[LW77] B. W. Lee and S. Weinberg. "Cosmological Lower Bound on Heavy Neutrino Masses." *Phys. Rev. Lett.*, **39**:165, 1977.

[LWK22] M. A. Latif, D. J. Whalen, S. Khochfar, N. P. Herrington, and T. E. Woods. "Turbulent cold flows gave birth to the first quasars." *Nature*, **607**(7917):48–51, 2022.

[Lyt92] D. H. Lyth. "Axions and inflation: Sitting in the vacuum." *Phys. Rev. D*,

45:3394–3404, 1992.

[M 08] A. Masiero M. Taoso, G. Bertone. "Dark Matter Candidates: A Ten-Point Test." *JCAP*, **22**, 2008.

[Mag01] Michele Maggiore. "Stochastic backgrounds of gravitational waves." *ICTP Lect. Notes Ser.*, **3**:397–414, 2001.

[Mag07] Michele Maggiore. *Gravitational Waves. Vol. 1: Theory and Experiments.* Oxford Master Series in Physics. Oxford University Press, 2007.

[Mag18] Michele Maggiore. *Gravitational Waves. Vol. 2: Astrophysics and Cosmology.* Oxford University Press, 3 2018.

[Mat14] T. Matsumura et al. "Mission design of LiteBIRD." *J. Low Temp. Phys.*, **176**:733, 2014.

[MDL20] Viraf M. Mehta, Mehmet Demirtas, Cody Long, David J. E. Marsh, Liam Mcallister, and Matthew J. Stott. "Superradiance Exclusions in the Landscape of Type IIB String Theory." 11 2020.

[Mel99] Yannick Mellier. "Probing the Universe with Weak Lensing." *Annual Review of Astronomy and Astrophysics*, **37**(1):127–189, 1999.

[MFI17] Ben T. McAllister, Graeme Flower, Eugene N. Ivanov, Maxim Goryachev, Jeremy Bourhill, and Michael E. Tobar. "The ORGAN Experiment: An axion haloscope above 15 GHz." *Phys. Dark Univ.*, **18**:67–72, 2017.

[MFL19] David J. E. Marsh, Kin-Chung Fong, Erik W. Lentz, Liboř Smejkal, and Mazhar N. Ali. "Proposal to Detect Dark Matter using Axionic Topological Antiferromagnets." *Phys. Rev. Lett.*, **123**(12):121601, 2019.

[Mic07] Maggiore Michele. "Gravitational Waves. Vol. 1: Theory and Experiments." 2007.

[MRK22] Shikhar Mittal, Anupam Ray, Girish Kulkarni, and Basudeb Dasgupta.

"Constraining primordial black holes as dark matter using the global 21-cm signal with X-ray heating and excess radio background." *JCAP*, **03**:030, 2022.

[Net02] C. B. Netterfield et al. "A measurement by Boomerang of multiple peaks in the angular power spectrum of the cosmic microwave background." *Astrophys. J.*, **571**:604–614, 2002.

[Nii19a] Hiroko Niikura et al. "Constraints on Earth-mass primordial black holes from OGLE 5-year microlensing events." *Physical Review D*, **99**(8):083503, 2019.

[Nii19b] Hiroko Niikura et al. "Microlensing constraints on primordial black holes with Subaru/HSC Andromeda observations." *Nature Astron.*, **3**(6):524–534, 2019.

[NSY19] Toshiya Namikawa, Shohei Saga, Daisuke Yamauchi, and Atsushi Taruya. "CMB Constraints on the Stochastic Gravitational-Wave Background at Mpc scales." *Phys. Rev. D*, **100**(2):021303, 2019.

[Oli03] Keith A. Olive. "TASI lectures on dark matter." In *Theoretical Advanced Study Institute in Elementary Particle Physics (TASI 2002): Particle Physics and Cosmology: The Quest for Physics Beyond the Standard Model(s)*, pp. 797–851, 1 2003.

[OPR22] Ciaran A. J. O'Hare, Giovanni Pierobon, Javier Redondo, and Yvonne Y. Y. Wong. "Simulations of axionlike particles in the postinflationary scenario." *Phys. Rev. D*, **105**(5):055025, 2022.

[Oue19] Jonathan L. Ouellet et al. "First Results from ABRACADABRA-10 cm: A Search for Sub-μeV Axion Dark Matter." *Phys. Rev. Lett.*, **122**(12):121802, 2019.

[OV20] Ciaran A. J. O'Hare and Edoardo Vitagliano. "Cornering the axion with CP-violating interactions." *Phys. Rev. D*, **102**:115026, 2020.

[Pee82] P. J. E. Peebles. "Large-scale background temperature and mass fluctuations

due to scale-invariant primeval perturbations." , **263**:L1–L5, December 1982.

[PEF15] Alexandre Payez, Carmelo Evoli, Tobias Fischer, Maurizio Giannotti, Alessandro Mirizzi, and Andreas Ringwald. "Revisiting the SN1987A gamma-ray limit on ultralight axion-like particles." *JCAP*, **02**:006, 2015.

[Poi07] Henri Poincaré. "On the dynamics of the electron (Excerpts)." *The Genesis of General Relativity*, pp. 1179–1198, 2007.

[PQ77] R. D. Peccei and Helen R. Quinn. "CP Conservation in the Presence of Pseudoparticles." *Phys. Rev. Lett.*, **38**:1440–1443, Jun 1977.

[Pre80] William H Press. "Spontaneous Production of the Zel'dovich Spectrum of Cosmological Fluctuations." *Physica Scripta*, **21**(5):702, jan 1980.

[PRS89] William H. Press, Barbara S. Ryden, and David N. Spergel. "Dynamical Evolution of Domain Walls in an Expanding Universe." *Astrophys. J.*, **347**:590–604, 1989.

[PSM16a] Luca Pagano, Laura Salvati, and Alessandro Melchiorri. "New constraints on primordial gravitational waves from Planck 2015." *Phys. Lett. B*, **760**:823–825, 2016.

[PSM16b] Luca Pagano, Laura Salvati, and Alessandro Melchiorri. "New constraints on primordial gravitational waves from Planck 2015." *Physics Letters B*, **760**:823–825, 2016.

[PSS96] Massimo Persic, Paolo Salucci, and Fulvio Stel. "The Universal rotation curve of spiral galaxies: 1. The Dark matter connection." *Mon. Not. Roy. Astron. Soc.*, **281**:27, 1996.

[PSS15] Jason Pollack, David N. Spergel, and Paul J. Steinhardt. "Supermassive Black Holes from Ultra-Strongly Self-Interacting Dark Matter." *Astrophys. J.*, **804**(2):131, 2015.

[PWW83] John Preskill, Mark B. Wise, and Frank Wilczek. "Cosmology of the Invisible Axion." *Phys. Lett. B*, **120**:127–132, 1983.

[Raf99] G. Raffelt. "Particle Physics from Stars." *Ann. Rev. Nucl. Part. Sci.*, **49**:163–216, 1999.

[Rei82] David B. Reiss. "Can the Family Group Be a Global Symmetry?" *Phys. Lett. B*, **115**:217–220, 1982.

[RGC20] Wen-Hong Ruan, Zong-Kuan Guo, Rong-Gen Cai, and Yuan-Zhong Zhang. "Taiji program: Gravitational-wave sources." *International Journal of Modern Physics A*, **35**(17):2050075, 2020.

[Rio87] EM Riordan et al. "Search for short-lived axions in an electron-beam-dump experiment." *Physical Review Letters*, **59**(7):755, 1987.

[RMR20] Christopher S. Reynolds, M. C. David Marsh, Helen R. Russell, Andrew C. Fabian, Robyn Smith, Francesco Tombesi, and Sylvain Veilleux. "Astrophysical Limits on Very Light Axion-like Particles from Chandra Grating Spectroscopy of NGC 1275." , **890**(1):59, February 2020.

[RP21] Keir K. Rogers and Hiranya V. Peiris. "Strong bound on canonical ultra-light axion dark matter from the Lyman-alpha forest." *Phys. Rev. Lett.*, **126**:071302, 2021.

[RTV21] Marco Regis, Marco Taoso, Daniel Vaz, Jarle Brinchmann, Sebastiaan L. Zoutendijk, Nicolas F. Bouché, and Matthias Steinmetz. "Searching for light in the darkness: Bounds on ALP dark matter with the optical MUSE-faint survey." *Phys. Lett. B*, **814**:136075, 2021.

[S 93a] A. Masiero S. A. Bonometto, F. Gabbiani. "Mixed Dark Matter from Axino Distribution." *Phys. Rev. D.*, **49**:3918–3922, 1993.

[S 93b] L. Widrow S. Dodelson. "Sterile Neutrinos as Dark Matter." 1993.

[Sas16] Misao Sasaki et al. "Primordial black hole scenario for the gravitational-wave event GW150914." *Physical review letters*, **117**(6):061101, 2016.

[Sat12] Bangalore Sathyaprakash et al. "Scientific objectives of Einstein telescope." *Classical and Quantum Gravity*, **29**(12):124013, 2012.

[SDS13] I. Shilon, A. Dudarev, H. Silva, and H. H. J. ten Kate. "Conceptual Design of a New Large Superconducting Toroid for IAXO, the New International AXion Observatory." *IEEE Trans. Appl. Supercond.*, **23**(3):4500604, 2013.

[SDS15] Abir Sarkar, Subinoy Das, and Shiv K. Sethi. "How Late can the Dark Matter form in our universe?" *JCAP*, **03**:004, 2015.

[Sik82] P. Sikivie. "Of Axions, Domain Walls and the Early Universe." *Phys. Rev. Lett.*, **48**:1156–1159, 1982.

[Sik21] Pierre Sikivie. "Invisible Axion Search Methods." *Rev. Mod. Phys.*, **93**(1):015004, 2021.

[SKC06] Tristan L. Smith, Marc Kamionkowski, and Asantha Cooray. "Direct detection of the inflationary gravitational wave background." *Phys. Rev. D*, **73**:023504, 2006.

[SKN01] Naoki Seto, Seiji Kawamura, and Takashi Nakamura. "Possibility of direct measurement of the acceleration of the universe using 0.1 Hz band laser interferometer gravitational wave antenna in space." *Physical Review Letters*, **87**(22):221103, 2001.

[SPI20] Pasquale D. Serpico, Vivian Poulin, Derek Inman, and Kazunori Kohri. "Cosmic microwave background bounds on primordial black holes including dark matter halo accretion." *Phys. Rev. Res.*, **2**(2):023204, 2020.

[SS09] B. S. Sathyaprakash and B. F. Schutz. "Physics, Astrophysics and Cosmology with Gravitational Waves." *Living Rev. Rel.*, **12**:2, 2009.

[SS18] Ken'ichi Saikawa and Satoshi Shirai. "Primordial gravitational waves, precisely: The role of thermodynamics in the Standard Model." *JCAP*, **05**:035, 2018.

[Ste16] I. Stern. "ADMX Status." *PoS*, **ICHEP2016**:198, 2016.

[SV82] J. Schechter and J. W. F. Valle. "Neutrino Decay and Spontaneous Violation of Lepton Number." *Phys. Rev. D*, **25**:774, 1982.

[SVZ80a] M.A. Shifman, A.I. Vainshtein, and V.I. Zakharov. "Can confinement ensure natural CP invariance of strong interactions?" *Nuclear Physics B*, **166**(3):493–506, 1980.

[SVZ80b] Mikhail A. Shifman, A. I. Vainshtein, and Valentin I. Zakharov. "Can Confinement Ensure Natural CP Invariance of Strong Interactions?" *Nucl. Phys. B*, **166**:493–506, 1980.

[SW06] Peter Svrcek and Edward Witten. "Axions In String Theory." *JHEP*, **06**:051, 2006.

[T 94] M. Srednicki T. Falk, K. Olive. "Heavy Sneutrinos as Dark Matter." *Phys. Lett. B.*, **339**:248–251, 1994.

[Tis07] P. Tisserand et al. "Limits on the Macho Content of the Galactic Halo from the EROS-2 Survey of the Magellanic Clouds." *Astron. Astrophys.*, **469**:387–404, 2007.

[TM75] JH Taylor and RN Manchester. "Observed properties of 147 pulsars." *The Astronomical Journal*, **80**:794–806, 1975.

[Tur86] Michael S. Turner. "Cosmic and Local Mass Density of Invisible Axions." *Phys. Rev. D*, **33**:889–896, 1986.

[TVW90] J. Anthony Tyson, Francisco Valdes, and R. A. Wenk. "Detection of systematic gravitational lens galaxy image alignments - Mapping dark matter

in galaxy clusters." *The Astrophysical Journal*, **349**, 1990.

[UF00] Keiichi Umetsu and Toshifumi Futamase. "Detection of Dark Matter Concentrations in the Field of Cl 16044304 from Weak Lensing Analysis." *The Astrophysical Journal*, **539**(1):L5–L8, aug 2000.

[UPL21] Caner Ünal, Fabio Pacucci, and Abraham Loeb. "Properties of ultralight bosons from heavy quasar spins via superradiance." *JCAP*, **05**:007, 2021.

[VS00] A. Vilenkin and E. P. S. Shellard. *Cosmic Strings and Other Topological Defects*. Cambridge University Press, 7 2000.

[VSV15] Núria Vinyoles, Aldo Serenelli, Francesco L. Villante, Sarbani Basu, Javier Redondo, and Jordi Isern. "New axion and hidden photon constraints from a solar data global fit." *JCAP*, **10**:015, 2015.

[WBH13] Jonelle L. Walsh, Aaron J. Barth, Luis C. Ho, and Marc Sarzi. "THE M87 BLACK HOLE MASS FROM GAS-DYNAMICAL MODELS OF SPACE TELESCOPE IMAGING SPECTROGRAPH OBSERVATIONS*." *The Astrophysical Journal*, **770**(2):86, may 2013.

[Wei78] Steven Weinberg. "A New Light Boson?" *Phys. Rev. Lett.*, **40**:223–226, 1978.

[Wid89] Lawrence M. Widrow. "The Collapse of Nearly Spherical Domain Walls." *Phys. Rev. D*, **39**:3576, 1989.

[Wil78] Frank Wilczek. "Problem of Strong P and T Invariance in the Presence of Instantons." *Physical Review Letters*, **40**(5):279, 1978.

[Wil82] Frank Wilczek. "Axions and Family Symmetry Breaking." *Phys. Rev. Lett.*, **49**:1549–1552, 1982.

[WMR01] L. Van Waerbeke, Y. Mellier, M. Radovich, E. Bertin, M. Dantel-Fort, H. J. McCracken, O. Le Fè vre, S. Foucaud, J.-C. Cuillandre, T. Erben, B. Jain,

P. Schneider, F. Bernardeau, and B. Fort. "Cosmic shear statistics and cosmology." *Astronomy &amp Astrophysics*, **374**(3):757–769, aug 2001.

[Wri92] Edward L Wright et al. "Interpretation of the cosmic microwave background radiation anisotropy detected by the COBE Differential Microwave Radiometer." *Astrophysical Journal, Part 2-Letters (ISSN 0004-637X), vol. 396, no. 1, Sept. 1, 1992, p. L13-L18. Research supported by NASA.*, **396**:L13–L18, 1992.

[WYF21] Feige Wang, Jinyi Yang, Xiaohui Fan, Joseph F. Hennawi, Aaron J. Barth, Eduardo Banados, Fuyan Bian, Konstantina Boutsia, Thomas Connor, Frederick B. Davies, Roberto Decarli, Anna-Christina Eilers, Emanuele Paolo Farina, Richard Green, Linhua Jiang, Jiang-Tao Li, Chiara Mazzucchelli, Riccardo Nanni, Jan-Torge Schindler, Bram Venemans, Fabian Walter, Xue-Bing Wu, and Minghao Yue. "A Luminous Quasar at Redshift 7.642." , **907**(1):L1, January 2021.

[WZ79] F. Wilczek and A. Zee. "Horizontal Interaction and Weak Mixing Angles." *Phys. Rev. Lett.*, **42**:421–425, Feb 1979.

[XSH21] Huangyu Xiao, Xuejian Shen, Philip F. Hopkins, and Kathryn M. Zurek. "SMBH seeds from dissipative dark matter." *JCAP*, **07**:039, 2021.

[YKY99] Masahide Yamaguchi, M. Kawasaki, and Jun'ichi Yokoyama. "Evolution of axionic strings and spectrum of axions radiated from them." *Phys. Rev. Lett.*, **82**:4578–4581, 1999.

[Yok95] Jun'ichi Yokoyama. "Formation of MACHO-primordial black holes in inflationary cosmology." *arXiv preprint astro-ph/9509027*, 1995.

[ZBC09] Wen Zhao, D. Baskaran, and P. Coles. "Detecting relics of a thermal gravitational wave background in the early Universe." *Phys. Lett. B*, **680**:411–416, 2009.

[Zel72] Ya. B. Zeldovich. "A Hypothesis, Unifying the Structure and the Entropy of the Universe." *Monthly Notices of the Royal Astronomical Society*, **160**(1):1P–3P, 10 1972.

[Zhi80a] AR Zhitnitskij. "On possible suppression of the axion-hadron interactions." *Yadernaya Fizika*, **31**(2):497–504, 1980.

[Zhi80b] A. R. Zhitnitsky. "On Possible Suppression of the Axion Hadron Interactions. (In Russian)." *Sov. J. Nucl. Phys.*, **31**:260, 1980.

[Zho18] L. Zhong et al. "Results from phase 1 of the HAYSTAC microwave cavity axion experiment." *Phys. Rev. D*, **97**(9):092001, 2018.

[ZKO74] Ya.B. Zeldovich, I.Yu. Kobzarev, and L.B. Okun. "Cosmological Consequences of the Spontaneous Breakdown of Discrete Symmetry." *Zh. Eksp. Teor. Fiz.*, **67**:3–11, 1974.

[ZN66] Ya B Zel'dovich and ID Novikov. "The hypothesis of cores retarded during expansion and the hot cosmological model." *Astronomicheskii Zhurnal*, **43**:758, 1966.

[Zwi33] F. Zwicky. "The Redshift of Extragalactic Nebulae." *Helv. Phys. Acta*, **6**:110–127, 1933.